

Study of HIV-1 Reverse Transcriptase and Protease Inhibition by Mushroom Extracts



A Thesis Submitted in Partial Fulfillment of the Requirements
for the Degree of Master of Science in Clinical Biochemistry and Molecular Medicine

Department of Clinical Chemistry

Faculty of Allied Health Sciences

Chulalongkorn University

Academic Year 2018

Copyright of Chulalongkorn University

การศึกษาฤทธิ์ในการยับยั้งเชื้อไวรัส-1 รีเวอร์สทรานสคริปเทส และโปรตีเอส ของสารสกัดเห็ด



วิทยานิพนธ์นี้เป็นส่วนหนึ่งของการศึกษาตามหลักสูตรปริญญาวิทยาศาสตรมหาบัณฑิต

สาขาวิชาชีวเคมีคลินิกและอณูทางการแพทย์ ภาควิชาเคมีคลินิก

คณะสหเวชศาสตร์ จุฬาลงกรณ์มหาวิทยาลัย

ปีการศึกษา 2561

ลิขสิทธิ์ของจุฬาลงกรณ์มหาวิทยาลัย

Thesis Title Study of HIV-1 Reverse Transcriptase and Protease Inhibition by
Mushroom Extracts
By Mr. Chanin Sillapachaiyaporn
Field of Study Clinical Biochemistry and Molecular Medicine
Thesis Advisor Assistant Professor Siriporn Chuchawankul, Ph.D.
Thesis Co Advisor Associate Professor Alison T Ung, Ph.D.

Accepted by the Faculty of Allied Health Sciences, Chulalongkorn University in Partial
Fulfillment of the Requirement for the Master of Science

THESIS COMMITTEE

..... Dean of the Faculty of Allied Health
Sciences
(Assistant Professor Palanee Ammaranond, Ph.D.)

..... Chairman
(Assistant Professor Tewin Tencomnao, Ph.D.)

..... Thesis Advisor
(Assistant Professor Siriporn Chuchawankul, Ph.D.)

..... Thesis Co-Advisor
(Associate Professor Alison T Ung, Ph.D.)

..... Examiner
(Associate Professor Rachana Santiyanont, Ph.D.)

..... External Examiner
(Warunya Arunotayanun, Ph.D.)

ชรินทร์ ศิลป์ชัยพร : การศึกษาฤทธิ์ในการยับยั้งเอนไซม์เอชไอวี-1 รีเวอร์สทรานสคริปเทส และโปรตีเอส ของสารสกัดเห็ด. (Study of HIV-1 Reverse Transcriptase and Protease Inhibition by Mushroom Extracts) อ.ที่ปรึกษาหลัก : ผศ. ดร.ศิริพร ชื้อชวาลกุล, อ.ที่ปรึกษาร่วม : รศ. ดร.Alison T Ung

ไวรัสเอชไอวี-1 (Human Immunodeficiency Virus, HIV-1) เป็นไวรัสที่ก่อให้เกิดโรคภูมิคุ้มกันบกพร่อง (Acquired Immunodeficiency Syndrome, AIDS) ที่เป็นปัญหาที่สำคัญทางสาธารณสุข การพัฒนายาต้านไวรัสในปัจจุบันนิยมยับยั้งเอนไซม์เอชไอวี-1 รีเวอร์สทรานสคริปเทส (HIV-1 RT) และโปรตีเอส (HIV-1 PR) เป็นหลัก ผู้วิจัยจึงสนใจศึกษาฤทธิ์ในการยับยั้งเอนไซม์เอชไอวี-1 รีเวอร์สทรานสคริปเทส และโปรตีเอสของสารสกัดเห็ดจากเห็ดนมเสื่อ (*Lignosus rhinoceros*) เห็ดหูหนูขาว (*Auricularia polytricha*) และเห็ดเผาะ (*Astraeus spp.*) จากการศึกษาพบว่าสารสกัดเห็ดด้วยเฮกเซนจากเห็ดหูหนูขาว (APH) สามารถยับยั้งการทำงานของเอนไซม์เอชไอวี-1 รีเวอร์สทรานสคริปเทส และโปรตีเอส ได้ทั้งในการทดสอบในหลอดทดลอง และสามารถยับยั้งการสร้างโปรตีนแคปซิด (p24) และดีเอ็นเอของไวรัสในเซลล์ MOLT-4 ที่ติดเชื้อเอชไอวี-1 ได้ โดยนอกจากนี้ยังได้ทำการแยกองค์ประกอบ และวิเคราะห์องค์ประกอบของสารสกัดเห็ด APH ด้วยวิธีโครมาโตกราฟี (Chromatography) และสเปกโทรสโกปี (Spectroscopy) พบว่าสารสกัดเห็ด APH ประกอบด้วยไตรกลีเซอไรด์ (triacylglycerol) ที่แตกต่างกันสองชนิด กรดลิโนเลอิก (linoleic acid) และเออร์โกสเตอรอล (ergosterol) ซึ่งเมื่อทำการทดสอบฤทธิ์ของสารสกัดประกอบในเซลล์ที่ติดเชื้อเอชไอวี-1 พบว่าเออร์โกสเตอรอล กรดลิโนเลอิก กรดโอเลอิก และกรดปาล์มิติก สามารถยับยั้งการสร้างโปรตีนแคปซิดได้อย่างมีนัยสำคัญ จากการศึกษาความสามารถในการจับกันระหว่างสารสกัดประกอบและเอนไซม์เอชไอวี-1 โปรตีเอส โดยการวิเคราะห์ทางคอมพิวเตอร์ด้วยวิธี CDocker พบว่า สารสกัดประกอบสามารถจับได้ดีกับเอนไซม์เอชไอวี-1 โปรตีเอส ดังนั้น จากผลการวิจัยสรุปได้ว่า เห็ดหูหนูขาวเป็นแหล่งของกรดไขมัน และเออร์โกสเตอรอล ที่มีฤทธิ์ยับยั้งการทำงานของเอนไซม์เอชไอวี-1 โปรตีเอส อีกทั้งข้อมูลที่ได้จากการวิจัยนี้จะเป็นข้อมูลพื้นฐานที่สำคัญในการพัฒนายาต้านไวรัสที่มีประสิทธิภาพต่อไป

สาขาวิชา	ชีวเคมีคลินิกและอณูพันธุศาสตร์	ลายมือชื่อนิสิต
	การแพทย์	
ปีการศึกษา	2561	ลายมือชื่อ อ.ที่ปรึกษาหลัก
		ลายมือชื่อ อ.ที่ปรึกษาร่วม

5876652937 : MAJOR CLINICAL BIOCHEMISTRY AND MOLECULAR MEDICINE

KEYWORD: Human immunodeficiency virus type-1, *Lignosus rhinocerus*, *Auricularia polytricha*, *Astraeus spp.*, HIV-1 Protease inhibitor, HIV-1 Reverse transcriptase inhibitor

Chanin Sillapachaiyaporn : Study of HIV-1 Reverse Transcriptase and Protease Inhibition by Mushroom Extracts. Advisor: Asst. Prof. Siriporn Chuchawankul, Ph.D.
Co-advisor: Assoc. Prof. Alison T Ung, Ph.D.

Human immunodeficiency virus type-1 (HIV-1) can cause acquired immunodeficiency syndrome (AIDS), a world serious public health problem. HIV-1 protease (HIV-1 PR) and reverse transcriptase (HIV-1 RT) are necessary target enzymes which have been used for antiretroviral drugs development. Herein, *Lignosus rhinocerus* (LR), *Auricularia polytricha* (AP) and *Astraeus spp.* (AH) crude extracts were screened for inhibitory activities on both enzymes. Crude hexane extract of AP (APH) exhibited significant inhibition on both HIV-1 PR and RT activities not only in *an in vitro* non-cell based but also cell based assays. In HIV-1 infected MOLT-4 cell model, APH significantly reduced capsid protein (p24) and viral DNA synthesis. Furthermore, phytochemical compounds of APH was isolated and identified by chromatography and spectroscopy techniques. We found four major compounds, including two triacylglycerols, linoleic acid and ergosterol. Moreover, ergosterol, linoleic acid, oleic acid and palmitic acid showed significant inhibition of p24 production in the infected cells. *In silico* analysis by CDocker method supported that all candidate compounds displayed interaction with specific sites of HIV-1 PR. These results suggest that AP could be a good source of fatty acid and ergosterol which have anti-HIV-1 properties by blocking HIV-1 PR. These data would be a beneficial information for antiretroviral drug development furthermore.

Field of Study:	Clinical Biochemistry and Molecular Medicine	Student's Signature
Academic Year:	2018	Advisor's Signature
		Co-advisor's Signature

ACKNOWLEDGEMENTS

Firstly, I would like to express my very great appreciation to Asst. Prof. Dr. Siriporn Chuchawankul, my advisor. This work would not have been completed without her support, encouragement and assistance. She was always there when I was in a trouble or had a question about my research. I got a lot of wonderful opportunities from her.

I wish to extend my deep gratitude to Assoc. Prof. Dr. Alison T Ung, my co-advisor for her kindness, patient and guidance. I have been learnt many things from her, not only about lab works but also social life.

I am particularly grateful for the assistance given by the thesis committee and all lecturers in Program of Medical Technology, Faculty of Allied Health Sciences, Chulalongkorn University CU.

I would like to offer my thanks to Dr. Razauden Bin Mohamed Zulkifli of Department of Biosciences and Health Sciences, Faculty of Biosciences and Medical Engineering, Universiti Teknologi Malaysia and Dr. Low Chen Fei of Institute of Systems Biology (INBIOSIS), Universiti Kebangsaan Malaysia for inspiring me a molecular modelling idea.

My special thanks are extend to Szu Ting Ng of Ligno Biotech™ Sdn. Bhd for providing sclerotial powder L. rhinocerus (Tiger Milk mushroom); Assoc. Prof. Dr. Songyot Anuchapreeda of Faculty of Associated Medical Sciences, Chiang Mai University for MOLT-4 cells; Asst. Prof. Dr. Jitra Piapukiew and Miss Yanisa Punsung of Department of Botany, Faculty of Science, Chulalongkorn University for their helping in mushroom identification; Chulalongkorn Medical Research Center, Faculty of Medicine, Chulalongkorn University for supporting biosafety level 2 enhance facility and School of Mathematical and Physical Sciences, Faculty of Science, University of Technology Sydney for chemical laboratory support. Moreover, the following reagents were obtained through the NIH AIDS Reagent Program, Division of AIDS, NIAID, NIH: ACH-2 cells from Dr. Thomas Folks; darunavir (Cat# 11447) from Tibotec, Inc. and nevirapine.

I would like to gratefully acknowledge all scholarships from the Graduate School, Chulalongkorn University. There are comprised of the 72nd anniversary of his Majesty King Bhumibol Adulyadej, the 90th anniversary Chulalongkorn University Fund (Ratchadaphiseksomphot Endowment Fund), Overseas Research Experience Scholarship for Graduate Student and Support for the Overseas Presentations of Graduate Level Academic Thesis scholarships.

I would also like to thank all colleagues and technicians of the laboratories of Faculty of Allied Health Sciences, Chulalongkorn University and Faculty of Science, University of Technology Sydney for their helping in lab works.

Lastly but most importantly, I must express my very great profound thankfulness to my family for their support, encouragement and trusting me. This accomplishment would not have been possible without them. Thank you.

Chanin Sillapachaiyaporn

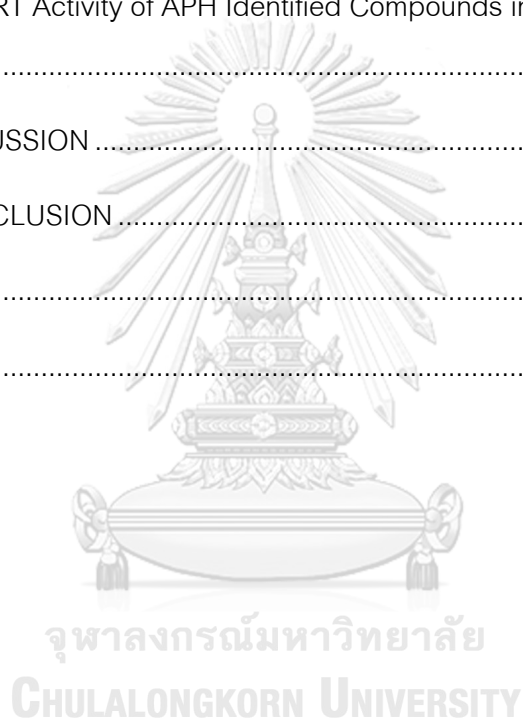
TABLE OF CONTENTS

	Page
ABSTRACT (THAI).....	iii
ABSTRACT (ENGLISH)	iv
ACKNOWLEDGEMENTS.....	v
TABLE OF CONTENTS.....	vi
LIST OF TABLES.....	x
LIST OF FIGURES	xii
CHAPTER I INTRODUCTION.....	15
1.1 Research objectives	16
1.2 Research hypothesis	17
1.3 Conceptual framework.....	17
CHAPTER II LITERATURE REVIEW.....	18
2.1 Human immunodeficiency virus (HIV)	18
2.2 Antiretroviral Drugs and Drug Targets.....	20
2.2.1 Antiretroviral drugs	20
2.2.2 Antiretroviral drugs targets.....	24
2.3 Natural products	26
2.4 Computer-Aided Molecular Modelling.....	38
2.5 <i>In vitro</i> HIV-1 PR and RT inhibitor Screening Kits	39
2.6 Cell Models	41
CHAPTER III MATERIALS AND METHODS	44
3.1 Laboratory Instruments and Equipment.....	44

3.2 Chemicals and Reagents.....	47
3.3 Mushroom Materials.....	49
3.4 Mushroom species identification	50
3.5 Extraction	50
3.6 <i>In Vitro</i> Non-Cell Based Assays for Anti-HIV-1 Activity	52
3.6.1 HIV-1 Protease Inhibition.....	52
3.6.2 HIV-1 Reverse Transcriptase Inhibition	53
3.7 <i>In Vitro</i> Cell-Based Assays for Anti-HIV-1 Activity.....	53
3.7.1 Cell culture.....	53
3.7.2 Cytotoxicity Assay	53
3.7.3 Virus expression	54
3.7.4 Infectivity Assay.....	54
3.7.5 Viral p24 determination	55
3.7.6 Viral DNA extraction and Real-Time PCR	55
3.8 Isolation and Purification.....	57
3.8.1 Thin Layer Chromatography (TLC)	57
3.8.2 Crystallization of fraction 4 (F4).....	58
3.8.3 Column Chromatography	58
3.8.4 Preparative Liquid Chromatography (prep LC)	58
3.9 Compound Identification.....	59
3.9.1 Fourier-Transform Infrared Spectroscopy (FTIR).....	59
3.9.2 Nuclear Magnetic Resonance Spectroscopy (NMR)	59
3.9.3 High-Resolution Mass Spectrometry (HRMS).....	59

3.9.4 Gas Chromatography-Mass Spectrometry (GC-MS).....	59
3.9.5 Base hydrolysis of fraction 1 (F1).....	59
3.9.6 Structural elucidation.....	60
3.10 Molecular Modelling.....	61
3.10.1 Protein Preparation.....	61
3.10.2 Ligand Preparation.....	62
3.10.3 Molecular Docking.....	62
3.11 Statistical Analysis.....	63
CHAPTER IV RESULTS.....	64
4.1 Extraction.....	64
4.2 HIV-1 PR Inhibitor Screening.....	64
4.3 HIV-1 RT Inhibitor Screening.....	65
4.4 Cytotoxicity of Crude Extracts.....	66
4.5 Virus expression.....	73
4.5 Infectivity Assay.....	74
4.6 Anti-HIV-1 PR Activity of Crude Extracts in HIV-1 Infected MOLT-4 Cells.....	76
4.7 Anti-HIV-1 RT Activity of Crude Extracts in HIV-1 Infected MOLT-4 Cells.....	77
4.8 Isolation and Purification.....	79
4.9 Identification.....	80
4.9.1 GC-MS analysis of pre-crystallisation of APH crude extract.....	80
4.9.2 The structure elucidation of fraction 1 (F1).....	84
Hydrolysis of fraction (F1).....	86
4.9.3 The structure elucidation of fraction (F2).....	89

4.9.4 The structure elucidation of fraction (F3)	89
4.9.5 The structure elucidation of fraction (F4)	90
4.10 Molecular Modelling.....	91
4.11 Cytotoxicity of APH Identified Compounds Against MOLT-4 Cells.....	102
4.12 Anti-HIV-1 PR Activity of APH Identified Compounds in HIV-1 Infected MOLT-4 Cells	105
4.13 Anti-HIV-1 RT Activity of APH Identified Compounds in HIV-1 Infected MOLT-4 Cells	106
CHAPTER V DISCUSSION	107
CHAPTER VI CONCLUSION	112
REFERENCES.....	113
VITA	162



LIST OF TABLES

	Page
Table 1 The list of compounds from mushroom extracts which possess HIV-1 RT inhibitory activity	27
Table 2 The list of compounds from mushroom extracts which possess HIV-1 PR inhibitory activity	29
Table 3 Chemical constituents found in <i>A. polytricha</i> extracts	31
Table 4 Phytochemical profile of <i>L.rhinocerus</i>	33
Table 5 CD4 ⁺ T lymphocytic cell lines used for HIV-1 infection and expression	42
Table 6 Primer pairs for viral DNA amplification (108)	56
Table 7 Solvent extractive values of crude extracts	64
Table 8 The fifty percent cytotoxic concentration (CC ₅₀) of crude extracts at 24, 48 and 72 hours after treatment	72
Table 9 Chromatograph yield of crude APH.....	80
Table 10 Chemical profile of APH from GC-MS analysis.....	81
Table 11 Quantitative of APH analysis by GC-MS	84
Table 12 List of hydrolysed products and their corresponding fatty acids of F1 hydrolysis from GC-MS analysis.....	88
Table 13 name, structure and molecular formula of constituent compounds of APH crude extract	90
Table 14 CDOCKER results at the active site of HIV-1 PR.....	94
Table 15 CDOCKER results at DNA polymerase domain of HIV-1 RT	98
Table 16 CDOCKER results at RNase H domain of HIV-1 RT	101

Table 17 The fifty percent cytotoxic concentration (CC_{50}) of APH identified compounds after 24, 48 and 72 hours treatment.....	103
--	-----



LIST OF FIGURES

	Page
Figure 1 Conceptual framework.....	17
Figure 2 HIV-1 replication cycle.....	19
Figure 3 Structure of maraviroc, co-receptor antagonists.....	20
Figure 4 Structure of enfuvirtide, fusion inhibitor.....	21
Figure 5 Structure of nucleoside-analogue reverse transcriptase inhibitors (NRTIs).....	22
Figure 6 Structure of nonnucleoside-analogue reverse transcriptase inhibitors (NNRTIs)	22
Figure 7 Structure of raltegravir, integrase inhibitor.....	22
Figure 8 Structure of protease inhibitors (PIs).....	23
Figure 9 The structure of HIV-1 RT with catalytic residues; polymerase and RNase H... 24	
Figure 10 The processes of reverse transcription (32).....	25
Figure 11 The structure and function of HIV-1 PR.....	26
Figure 12 Morphology of mushroom.....	30
Figure 13 Structures of compounds found in <i>A. hygrometricus</i>	38
Figure 14 HIV-1 protease inhibitor screening kit (Fluorometric).....	40
Figure 15 The theory of Reverse transcriptase assay, colourimetric kit.....	41
Figure 16 Typical morphology of HIV-induced syncytia.....	43
Figure 17 Experimental workflow.....	49
Figure 18 Schematic representation of the sequential mushroom extraction.....	52
Figure 19 Flow diagram for APH isolation.....	57

Figure 20 The percentage of relative inhibition on HIV-1 PR of DMSO (1%, v/v) and pepstatin (1 mM) as well as crude extracts (1 mg/ml).	65
Figure 21 The percentage of relative inhibition on HIV-1 RT of DMSO (1%, v/v) and NVP (200 μ M) as well as crude extracts (1 mg/ml).	66
Figure 22 The association graph between time and absorbance at 490 nm of different cell density.....	67
Figure 23 The cytotoxicity at various concentrations of DMSO on MOLT-4 cells after 24, 48 and 72 hours of treatments.	68
Figure 24 The cytotoxicity at various concentrations of AP crude extracts on MOLT-4 cells after 24, 48 and 72 hours of treatments.	69
Figure 25 The cytotoxicity at various concentrations of LR crude extract on MOLT-4 cells after 24, 48 and 72 hours of treatments.	70
Figure 26 The cytotoxicity at various concentrations of AH crude extracts on MOLT-4 cells after 24, 48 and 72 hours of treatments.	71
Figure 27 The cytotoxicity at various concentrations of DRV and NVP on MOLT-4 cells after 24, 48 and 72 hours of treatments.....	72
Figure 28 The standard curve of HIV-1 p24. A white circle represent the stock of virus at 1,000 dilution	73
Figure 29 The HIV-1 induced syncytial formation of MOLT-4 cells.	75
Figure 30 Inhibitory effect on p24 production in HIV-1 infected MOLT-4 cells of LR and AP crude extracts.	77
Figure 31 Real-time PCR analysis of HIV-1 DNAs expression.	78
Figure 32 Schematic representation of APH isolation	79
Figure 33 Gas Chromatogram of crude APH.....	81
Figure 34 Standard curve of ergosterol by GC-MS analysis	82

Figure 35 Gas chromatogram of commercial ergosterol at 10 mg/ml.	83
Figure 36 ¹ H NMR spectrum of F1 showing the elucidated core structure and protons responsible for the chemical shifts observed	85
Figure 37 Hydrolysis reaction of F1.	87
Figure 38 ¹ H NMR spectrum of hydrolysed products from F1, showing a signal of protons responding to methyl ester at the chemical shift of 3.666 ppm	88
Figure 39 The validation methods for molecular docking study of HIV-1 PR.....	93
Figure 40 The interaction of candidate ligand and control at active site of HIV-1 PR.	95
Figure 41 The validation methods for molecular docking study of HIV-1 RT at DNA polymerase domain.....	97
Figure 42 The interaction of candidate ligand and control at DNA polymerase active site of HIV-1 RT.	99
Figure 43 The validation methods for molecular docking study of HIV-1 RT at RNase H domain.....	100
Figure 44 The interaction of candidate ligand and control at RNase H active site of HIV-1 RT.....	102
Figure 45 The cytotoxicity at various concentrations of ergosterol, palmitic acid, linoleic acid, oleic acid and stearic acid on MOLT-4 cells after 24, 48 and 72 hours of treatments.....	104
Figure 46 Inhibitory effect on p24 production in HIV-1 infected MOLT-4 cells of APH isolated compounds.....	105
Figure 47 Real-time PCR analysis of HIV-1 DNAs expression.	106

CHAPTER I

INTRODUCTION

Acquire immunodeficiency syndrome (AIDS) is caused by the human immunodeficiency virus (HIV) which is classified into two types: HIV-1 and HIV-2. The HIV-1 is a major type of HIV which spreads worldwide. Moreover, there are more severity of infection and progression of disease in infected patients than HIV-2 (1, 2). According to HIV-1 life cycle, the virus needs three important enzymes: reverse transcriptase (HIV-1 RT), integrase (HIV-1 IN) and protease (HIV-1 PR) for its replication. HIV-1 PR is an enzyme for viral maturation. A responsibility of this enzyme is cleavage of Gag and Gag-Pol polyproteins to functional proteins: matrix, capsid (p24), nucleocapsid and viral enzymes. The other enzyme is HIV-1 RT, it has two enzymatic functions including DNA polymerase and ribonuclease H (RNase H) activities. The role of DNA polymerase is for generation of DNA from viral RNA template, while RNase H is for degradation of RNA template. The two enzymatic activities of HIV-1 RT cooperate to convert the viral RNA into cDNA in reverse transcription step of HIV-1 replication cycle (3). At present, most of available antiretroviral drugs are HIV-1 PR and RT inhibitors. However, they still have limitations such as drug resistant strains (4) and adverse effects of medication (5-9). A search for novel compounds from plant-based source is one of important studies to save patient life.

Mushrooms have been reported in medical benefits such as anti-microbial activity, anti-tumor activity as well as anti HIV-1 activity. *Auricularia polytricha* (AP) displayed anti-proliferative (10, 11), anti-oxidant (12-15), anti-chloresterolemic (16, 17) and hypoglycemic activities (18). *Lignosus rhinoceros* (LR) was reported as a medicinal mushroom with anti-inflammatory, anti-asthmatic (19), anti-proliferative (20, 21) and anti-oxidant activities (21). Moreover, it showed anti-viral activity on human papilloma virus (HPV) and dengue virus type-2 (22). The other interesting edible mushroom is *Astraeus spp.* (AH), it revealed anti-tumor (23), anti-oxidant (24) and immunomodulatory properties (25). However, these mushrooms have never been reported for anti-HIV-1 activity. From

medicinal properties of these mushrooms, we hypothesized that the mushrooms might be composed of compounds which can inhibit HIV-1 PR or HIV-1 RT activities. The research discovery would have an impact on antiretroviral drugs development and additive value of the mushrooms.

In this study, we screened inhibitory activities on HIV-1 PR and RT of mushroom crude extracts in *in vitro* non-cell based assays. The inhibition of p24 levels and viral DNAs: -sssDNA and fDNA synthesis in HIV-1 infected MOLT-4 cells were determined. The crude extract that provides the strong inhibition on both enzymes was studied further. Its chemical constituents were isolated using chromatography techniques. The chemical structures of isolated compounds were identified using spectroscopy methods. Then, *in silico* screening assay was performed to evaluate binding affinities of the identified compounds to binding pockets of HIV-1 PR and RT. Furthermore, the inhibitory effects of the identified compounds on both enzymes were examined in the infected cells.

1.1 Research objectives

1. To determine HIV-1 PR and HIV-1 RT inhibitory activity of mushroom extracts in *in vitro* non-cell based and cell based assays
2. To identify chemical compounds of mushroom extracts
3. To predict interaction between identified compounds from mushroom extracts with HIV-1 RT and HIV-1 PR by *in silico* computational studies

1.2 Research hypothesis

1. Mushroom extracts could inhibit HIV-1 infection by blocking HIV-1 PR and/or RT *in vitro* non-cell based and cell based assays
2. Identified compounds of mushroom extract could inhibit HIV-1 infection by blocking HIV-1 PR and/or RT *in vitro* non-cell based and cell based assays
3. Identified compounds of mushroom extract could bind to binding site of HIV-1 PR and/or RT in agreement with known drug inhibitors

1.3 Conceptual framework

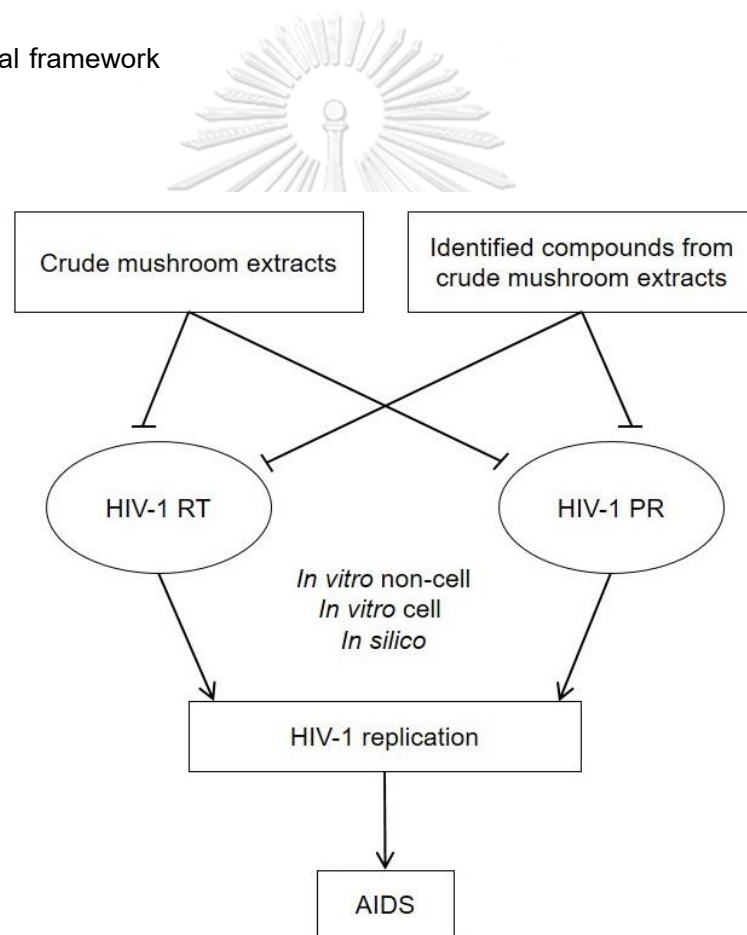


Figure 1 Conceptual framework

CHAPTER II

LITERATURE REVIEW

2.1 Human immunodeficiency virus (HIV)

Human immunodeficiency virus (HIV) is a virus in Retroviridae family. Based on the nucleotide sequence, HIV is classified into two types including HIV-1 and HIV-2. At present, HIV-1 is spreading worldwide while HIV-2 is found more frequently in West Africa (1, 2). The severity of infection and progression of disease in HIV-1 infected patients are higher than that of HIV-2 infected patients. A main target of HIV-1 infection is CD4⁺ T cell, an important immune cell. The viruses use the host cell machinery to replicate themselves and finally destroy the host cells. This process causes immunocompromised patients, called acquired immunodeficiency syndrome (AIDS). It leads to opportunistic infections and death.

HIV-1 replication cycle has several complicated steps. The understanding of viral growth is a key knowledge to develop new classes of antiretroviral drugs. The followings are essential steps of HIV-1 replication (26):

1. **Attachment.** The HIV-1 envelope comprises glycoprotein gp120 interact with the surface receptor CD4 of the T cells and co-receptor, either CC-chemokine receptor 5 (CCR5) or CXCR4. The selected co-receptor depends on viral strains, R5-tropic HIV-1 needs CCR5 while X4-tropic HIV-1 needs CXCR4.
2. **Fusion.** The attachment is leading to fusion of viral envelopes and host membranes and then HIV core enters the cell. The HIV core, which includes the replication enzymes: reverse transcriptase (RT) and integrase (IN) as well as viral genomic RNA, is encased by a cone-shaped shell. The shell is uncoated for reverse transcription
3. **Reverse Transcription.** The viral RNA is transcribed to complementary DNA (cDNA) by using its RT. The final product is a complex, called pre-integration complex (PIC), including viral cDNA and its nuclear-imported proteins: matrix (MA), IN and viral protein regulatory (Vpr).

4. **Integration.** The PIC is imported into the nucleus. Then the viral cDNA is integrated with host DNA by using IN.

5. **Gene expression.** The pro-viral transcription mediated by host RNA polymerase II (RNA Pol II), yields viral mRNAs. The viral mRNAs serve templates for protein production.

6. **Assembly.** The viral polyproteins: Gag and Gag-Pol and viral RNA are incorporated into viral particles.

7. **Budding.** The viral particles are released from the host cell.

8. **Maturation.** The PR cleaves polyproteins to viral proteins, including matrix (MA), capsid (CA, p24) and nucleocapsid as well as viral enzymes: RT, IN and PR. This step creates infectious viral particles.

In the HIV-1 replication cycle, the virus needs three important enzymes: RT, IN and PR to copy itself. Presently, these enzymes are important targets of antiretroviral drug development.

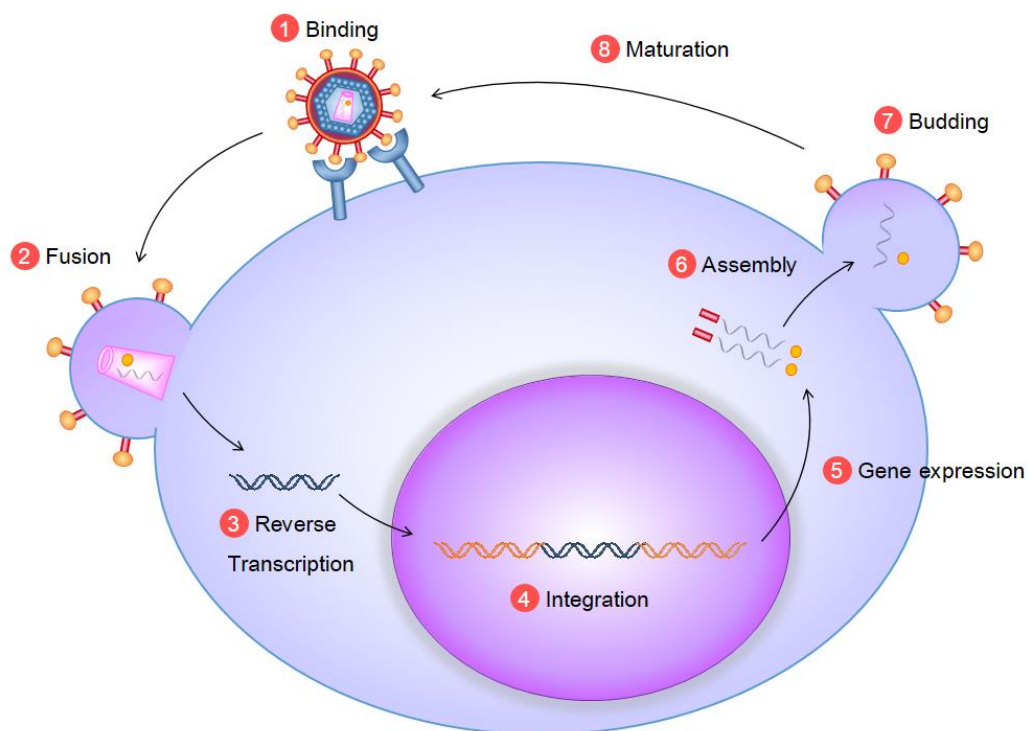


Figure 2 HIV-1 replication cycle

2.2 Antiretroviral Drugs and Drug Targets

2.2.1 Antiretroviral drugs

Currently, there are many antiretroviral drugs available for treating HIV-1 infection. They are classified into six classes by their molecular mechanisms of inhibition and targets. The following are a list of FDA-approved drugs (27, 28):

1. **Co-receptor antagonists:** maraviroc (CCR5 antagonist)
2. **Fusion inhibitors:** enfuvirtide
3. **Nucleoside-analogue reverse transcriptase inhibitors (NRTIs):** abacavir, didanosine, emtricitabine, lamivudine, stavudine, zalcitabine, zidovudine and tenofovir
4. **Nonnucleoside-analogue reverse transcriptase inhibitors (NNRTIs):** etravirine, delavirdine, efavirenz and nevirapine
5. **Integrase inhibitors:** raltegravir
6. **Protease inhibitors (PIs):** amprenavir, atazanavir, darunavir, fosamprenavir, indinavir, lopinavir, nelfinavir, ritonavir, saquinavir and tipranavir.

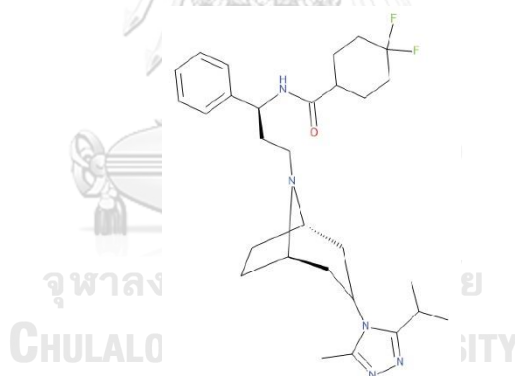


Figure 3 Structure of maraviroc, co-receptor antagonists

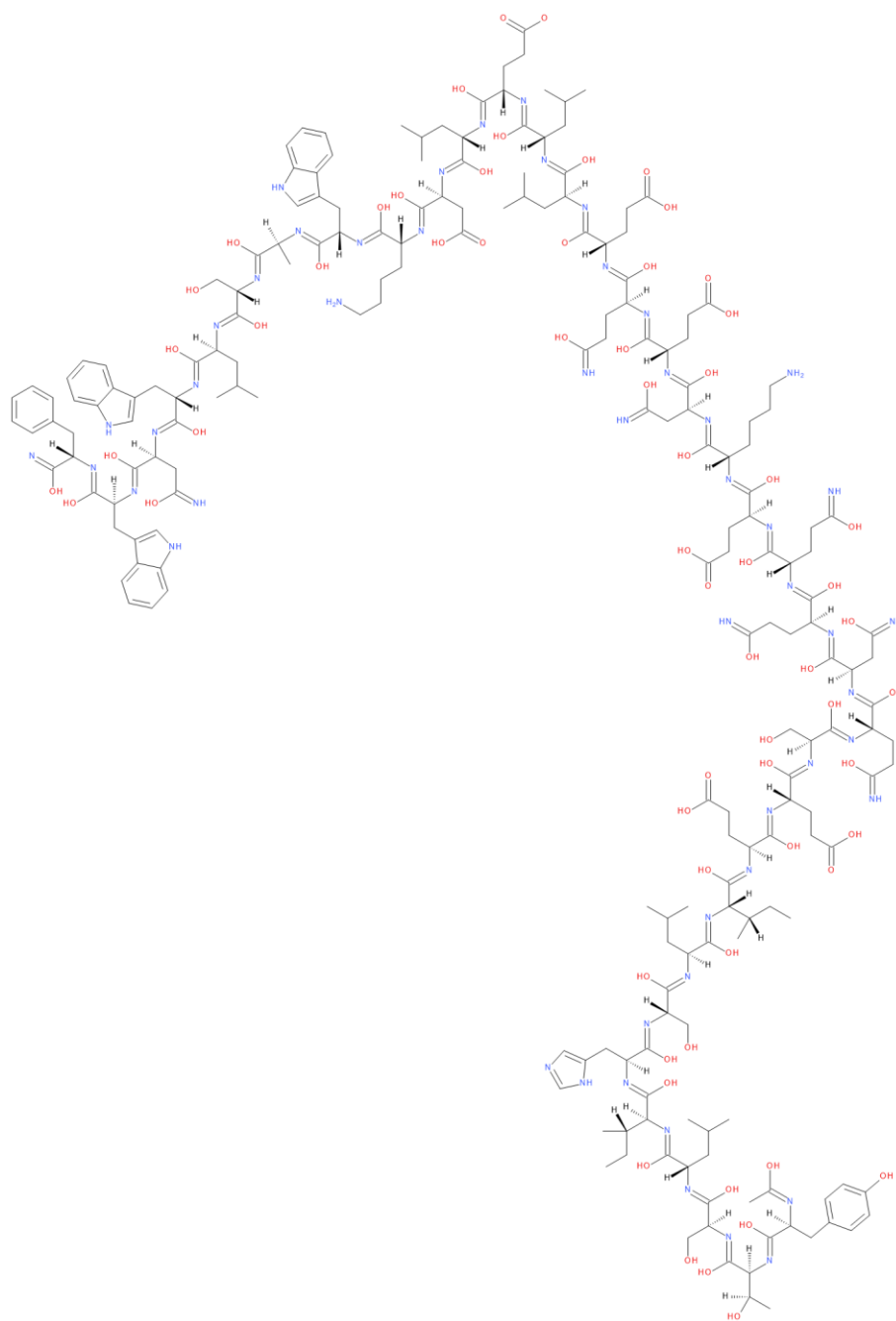


Figure 4 Structure of enfuvirtide, fusion inhibitor

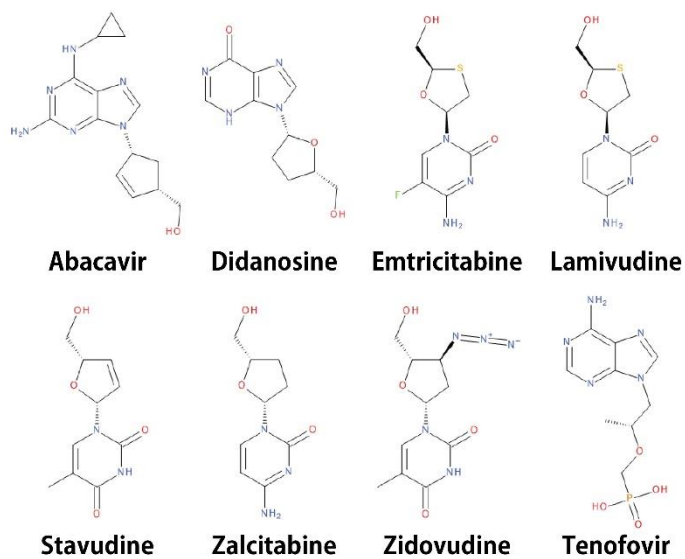


Figure 5 Structure of nucleoside-analogue reverse transcriptase inhibitors (NRTIs)



Figure 6 Structure of nonnucleoside-analogue reverse transcriptase inhibitors (NNRTIs)

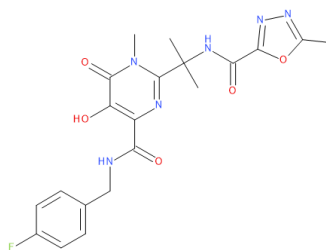


Figure 7 Structure of raltegravir, integrase inhibitor

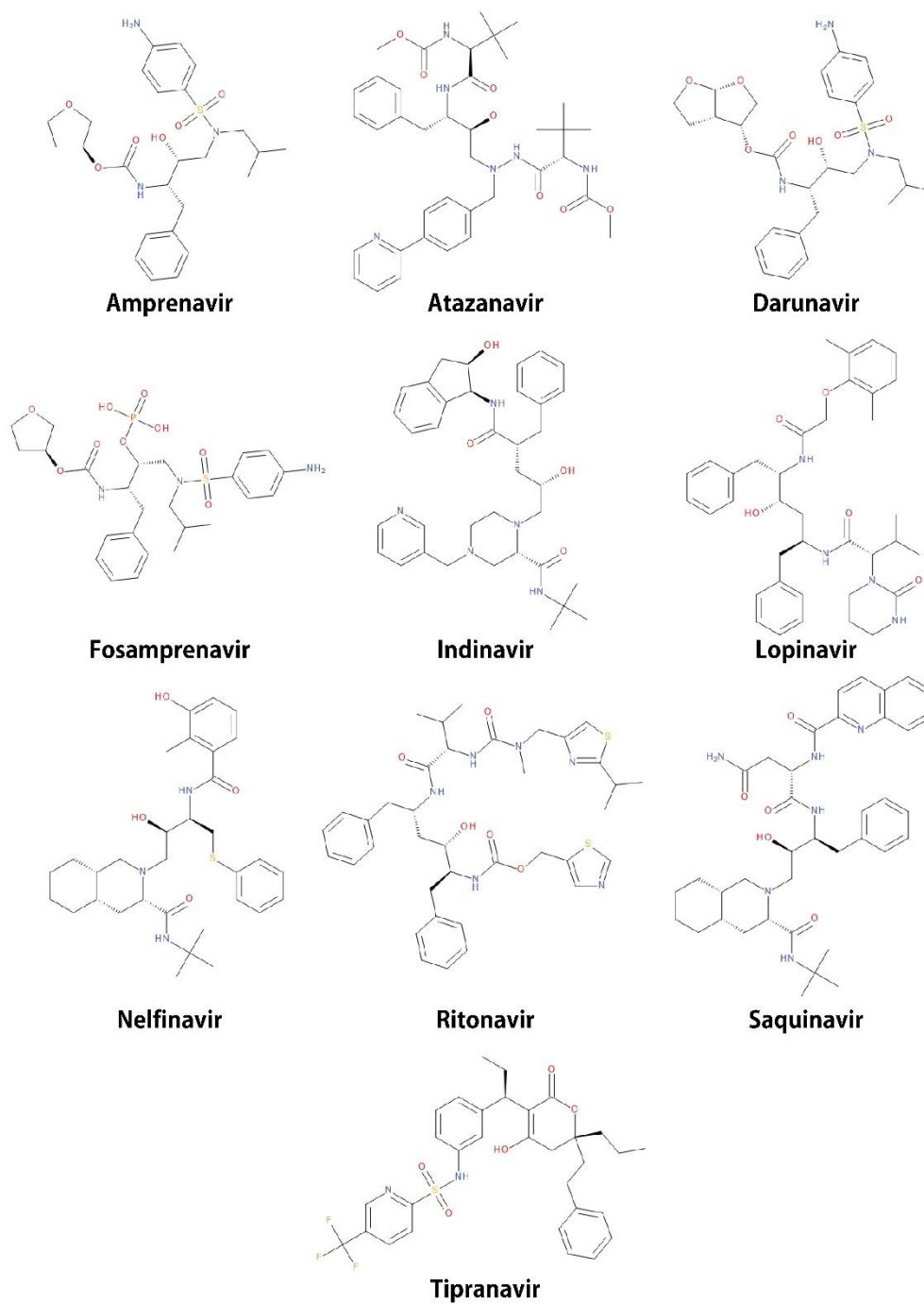


Figure 8 Structure of protease inhibitors (PIs)

According to the WHO guideline for antiretroviral drugs, the first-line antiretroviral therapy (ART) regimen should be a combination of three anti-retroviral drugs, called highly active antiretroviral therapy (HAART). It is composed of two NRTIs with one NNRTI or PI which is highly effective with low side effects. For HIV treatment, RT and PR are the main

enzymes generally and successfully targeted by the antiretroviral drugs (29). Therefore, we focus on those two enzymes as targets of drug development in this study.

2.2.2 Antiretroviral drugs targets

HIV-1 RT is an asymmetric heterodimer enzyme comprised of two different protein subunits: p66 and p51. These subunits are built from 560 and 440 amino acids in length, respectively. It has two enzymatic functions, DNA polymerase and RNase H activities. DNA polymerase generates cDNA from viral RNA template while RNase H degrades viral RNA. The two enzymatic activities of HIV-1 RT cooperate to convert the viral RNA into cDNA in reverse transcription step of the HIV-1 replication cycle. The p66 subunit contains both enzymatic activities while the p55 subunit plays an only structural role (3).

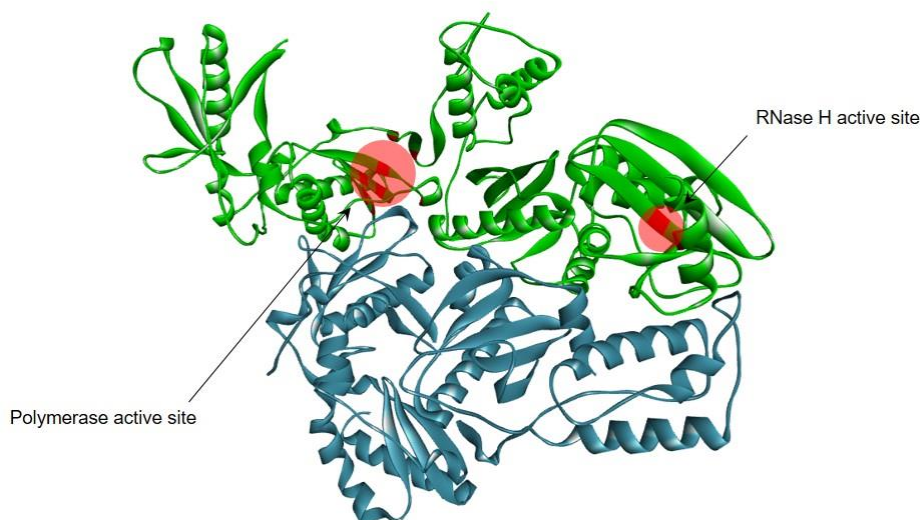


Figure 9 The structure of HIV-1 RT with catalytic residues; polymerase and RNase H. p66 and p51 subunits are represented in green and blue, respectively.

There are several steps of reverse transcription. Each step produces different DNA products which are indicated an end point of each step. DNA product which is produced from the first step of reverse transcription is minus strand strong stop DNA (-ssDNA). Besides, DNA which is generated from the last step of reverse transcription is

full-length DNA (fDNA) (30, 31). These DNA products are used to determine molecular mechanism of inhibition in HIV drug development research (Figure 10).

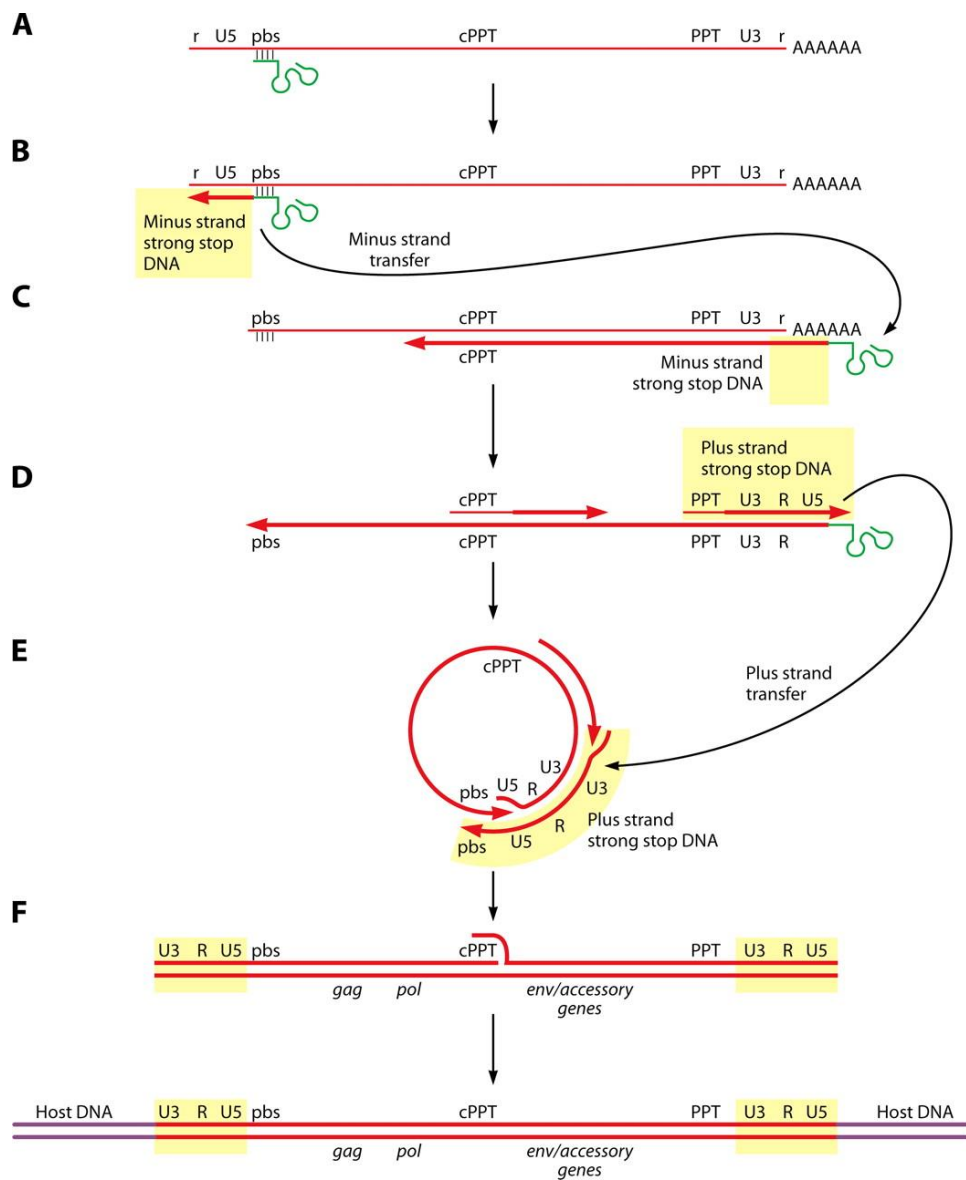


Figure 10 The processes of reverse transcription (32)

HIV-1 PR is homodimeric aspartyl enzyme comprised of two symmetric protein subunits; there are 99 amino acids in chains. The active site of this enzyme is in the centre of the molecule, as shown in **Figure 11A**. This enzyme plays an important role in maturation step, it cleaves polyproteins: Gag (p55) and Gag-Pol (p160) into functional proteins. For Gag polyprotein, it is turned to matrix MA (p17), CA (p24) and nucleocapsid (p7). While Gag-Pol polyprotein is cleaved into MA, CA, PR (p10), RT (p66/p51) and IN (p32) (29, 33) (**Figure 11B**). These protein products are necessary for HIV-1 replication. At present, p24 is a distinctive HIV antigen. It is a marker of HIV-1 disease used for HIV-1 detection in many types of research and clinical laboratories.

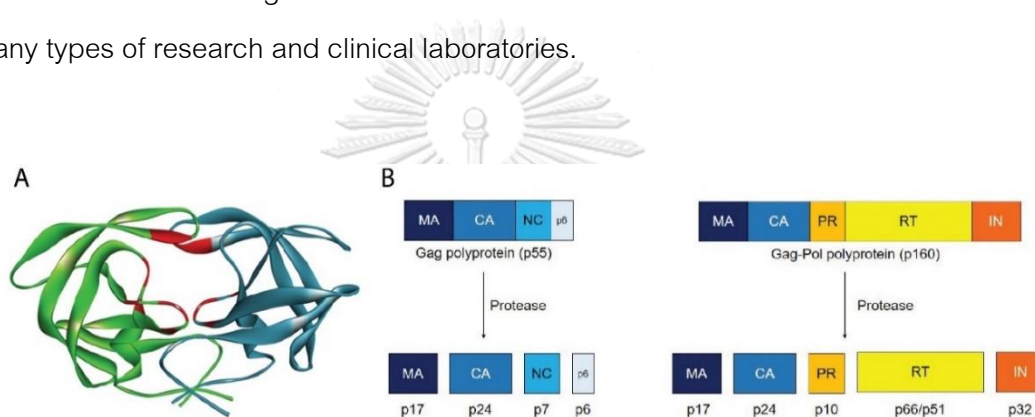


Figure 11 The structure and function of HIV-1 PR.

(A) The catalytic site (red) and (B) the cleavage of Gag and Gag-Pol polyproteins by HIV-1 PR

2.3 Natural products

Although the available antiretroviral drugs are highly effective, deaths due to AIDS still high in number. Moreover, long-term medication leads to many side effects such as mitochondrial toxicity (5), liver toxicity (6), hypersensitivity, abnormal fat distribution (7, 8) and drug resistance (4). Therefore, antiretroviral drugs development is a major issue for HIV-infected treatment. A discovery for novel compounds from mushroom sources may be a solution to save a patient life.

Mushrooms can be found throughout Thailand. They are a rich source of proteins, carbohydrates, fatty acid, vitamins, minerals and some of them possess medicinal properties. Previous studies found that Nebrodeolysin from *Pleurotus nebrodensis*

inhibited HIV-1 replication in CEM cell line, human T lymphoblast (34). In addition, Velleratretraol from *Lactarius vellereus* and melanin-glucan complex from *Fomes fomentarius* also inhibited HIV-1 infection compared to zidovudine, antiretroviral drug (35, 36).

Moreover, there are many reports about targets of HIV-1 inhibition by mushroom extracts. The important targets are HIV-1 RT and HIV-1 PR. The researchers found that several compounds could inhibit HIV-1 RT and HIV-1 PR, as tabulated in the Table 1 and 2, respectively.

Table 1 The list of compounds from mushroom extracts which possess HIV-1 RT inhibitory activity

Species	Active Compounds	References
<i>Agaricus bisporus</i>	Lectins	(37)
<i>Agaricus placomyces</i>	68-kDa laccase	(38)
<i>Agrocybe cylindracea</i>	58-kDa laccase and agrocybin	(39, 40)
<i>Amanita hemibapha</i>	45-kDa ribonuclease	(41)
<i>Boletus edulis</i>	D-Lactose, melibiose- and xylose-cospecific	(42)
<i>Boletus speciosus</i>	Hemagglutinin	(43)
<i>Cordyceps militaris</i>	Cordymin, Haemagglutinin	(44, 45)
<i>Cordyceps sobolifera</i>	Cordysobin	(46)
<i>Coriolus versicolor</i>	Polysaccharopeptide	(47)
<i>Flammulina velutipes</i>	13.8-kDa single-chained and ribosome inactivating protein (velutin)	(48)
<i>Ganoderma lucidum</i>	75-kDa laccase	(49)
<i>Hericium coralloides</i>	65-kDa laccase	(50)

Species	Active Compounds	References
<i>Hericium erinaceum</i>	51-kDa lectin (hericium erinaceum agglutinin,HEA) and 63-kDa laccase	(51, 52)
<i>Hohenbuehelia serotina</i>	27-kDa ribonuclease	(53)
<i>Hygrophorus russula</i>	28-kDa ribonuclease	(54)
<i>Hypsizigus marmoreus</i>	Marmorin and 20-kDa ribosome-inactivating protein (hypsin)	(55, 56)
<i>Inocybe umbrinella</i>	17-kDa lectin	(57)
<i>Lactarius flavidulus</i>	14.6-kDa ribonuclease and 29.8-kDa lectin	(58, 59)
<i>Lentinus edodes</i>	67-kDa laccase and lentin	(60, 61)
<i>Lentinus tigrinus</i>	59-kDa laccase	(62)
<i>Lepista nuda</i>	20.9-kDa metalloprotease and 56-kDa laccase	(63, 64)
<i>Lyophyllum shimeiji</i>	14.5-kDa ribonuclease, 20-kDa ribosome-inactivating protein (lyophyllin) and Lyophyllum antifungal protein (LAP)	(65, 66)
<i>Paxillus involutus</i>	28-kDa lectin (inulin and O-nitrophenyl- β -D-galactopyranoside)	(67)
<i>Pholiota adiposa</i>	methyl gallate, 16-kDa lectin and inulin	(42, 68, 69)
<i>Pleurotus abalonus</i>	polysaccharide-peptide complex and 120-kDa polysaccharide	(70)
<i>Pleurotus citrinopileatus</i>	32.4-kDa homodimeric lectin	(71)
<i>Pleurotus cornucopiae</i>	66-kDa laccase	(72)

Species	Active Compounds	References
<i>Pleurotus eryngii</i>	34-kDa laccase and pleureryn	(73, 74)
<i>Pleurotus ostreatus</i>	12.5-kDa glycoprotein and pleurotus ubiquitin-like protein (PULP)	(75)
<i>Russula delica</i>	60-kDa lectin	(76)
<i>Russula paludosa</i>	4.5-kDa peptide	(77)
<i>Schizophyllum commune</i>	20-kDa ribonuclease, 29-kDa monomeric hemolysin (schizolysin) and 64-kDa homodimeric lactose-binding lectin	(78-80)
<i>Stropharia rugosoannulata</i>	38-kDa lectin	(81)
<i>Thelephora ganbajun</i>	30-kDa ribonuclease	(82)
<i>Tricholoma giganteum</i>	Trichogin and 43-kDa laccase	(83, 84)
<i>Tricholoma mongolicum</i>	66-kDa laccase	(85)
<i>Xylaria hypoxylon</i>	43-kDa monomeric protein (aspartic protase)	(86)

Table 2 The list of compounds from mushroom extracts which possess HIV-1 PR inhibitory activity

Species	Active compounds	References
<i>Fuscoporia obliqua</i>	Water-soluble lignin derivative of high molecular weight	(87)
<i>Ganoderma colossum</i>	Farnesyl hydroquinone, Ganomycin I, Ganomycin B, Colossolactone V, Colossolactone VI,	(88, 89)

Species	Active compounds	References
	Colossolactone VII, Colossolactone VIII and Colossolactone E	
<i>Ganoderma lucidum</i>	Triterpenoid	(90)
<i>Pholiota adiposa</i>	Methyl gallate	(68)
<i>Pleurotus eryngii</i>	Pleureryn	(74)

In this study, we focus on three mushrooms including *Auricularia polytricha* (AP), *Lignosus rhinocerus* (LR) and *Astraeus spp.* (AH). All mushrooms display several medicinal properties and there is no report of anti-HIV-1 activity by these mushrooms.



Figure 12 Morphology of mushroom.

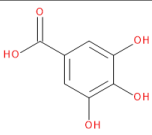
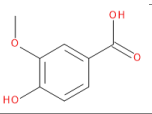
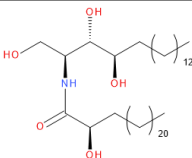
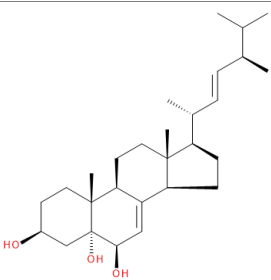
(A) *Auricularia polytricha*, (B) *Lignosus rhinocerus* and (C) *Astraeus spp.*

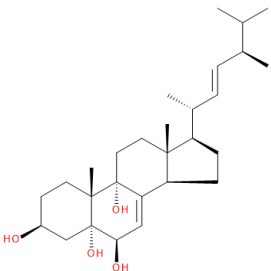
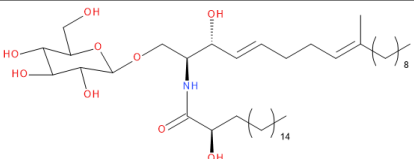
A. polytricha (AP), known as wood ear mushroom is an edible mushroom of the Auriculariaceae family, naturally used for traditional medicine (91). From previous studies, Chen Y, *et al.* reported that water-soluble polysaccharide from AP showed anti-oxidant activity (15). Yu J, *et al.* found that polysaccharides extracted from AP could inhibited proliferation and DNA synthesis of A549, human lung cancer cells (11). Besides, Song G, *et al.* showed that polysaccharide isolated from AP, exhibited anti-cancer activity against sarcoma-180 cells in mice (92). Moreover, salt-soluble polysaccharide from AP which is a 1,3- β -glucan, 1,6- α -glucan, 1,4- α -glucan and 1,3- α -glucan backbone with a single

1,6- α -D-glucopyranosyl side-branching unit on every nine residues has been reported as an anti-mutagenic agent by preventing *in vivo* DNA-damaging effect of mice (93). Furthermore, Arora S, *et al.* demonstrated that aqueous extract of AP provided less toxicity on normal kidney cells (NRK-52E cells) compared with 5-Fluorouracil (5-FU), known chemotherapeutic drug (94). In addition, AP extract exhibited hypolipidemic activity by reducing serum total cholesterol, triglyceride and LDL levels as well as increasing HDL level in rats (16, 17). Aqueous extract of AP also showed protective effect against paracetamol-induced hepatotoxicity, hepatic lipid accumulation and inflammatory activity in rats (12, 95).

AP chemical constituent analysis revealed that 95% ethanol extract comprised of phenolic compounds such as gallic acid and vanillic acid (96). Koyama, *et al.* found ceramide, cerevisterol and 9-hydroxycerevisterol from dichloromethane extract and cerebositide from methanol extract of AP fruiting bodies (97) (Table 3).

Table 3 Chemical constituents found in *A. polytricha* extracts

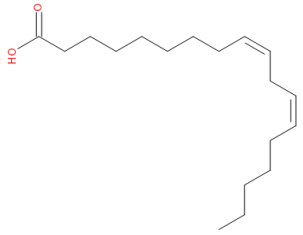
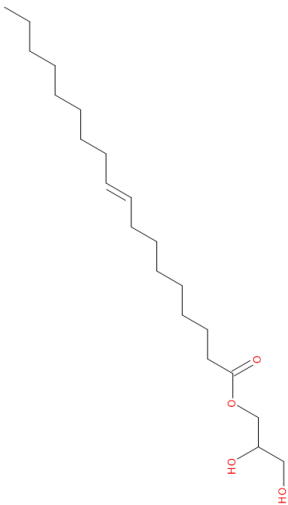
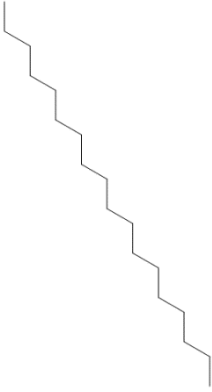
Compounds	Molecular formula	Structures
Gallic acid	$C_7H_6O_5$	
Vanillic acid	$C_8H_8O_4$	
Ceramide	$C_{42}H_{85}NO_5$	
Cerevisterol	$C_{28}H_{46}O_3$	

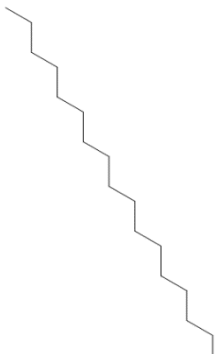
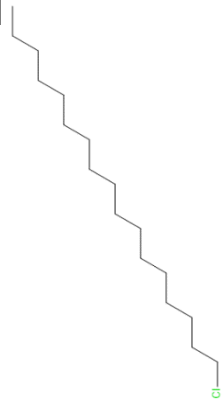
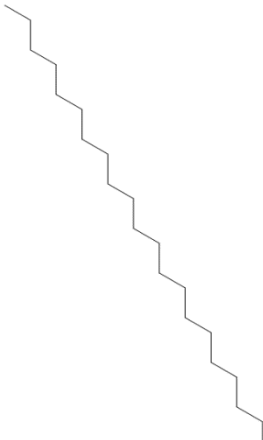
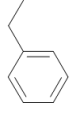
Compounds	Molecular formula	Structures
9-hydroxycervisterol	$C_{28}H_{46}O_4$	
Cerebroside	$C_{43}H_{81}NO_9$	

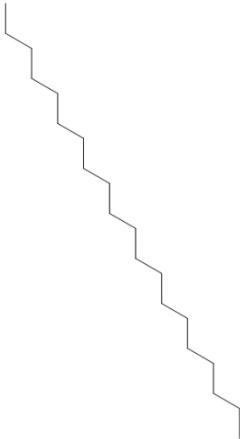
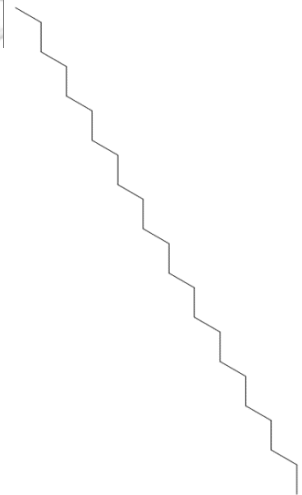
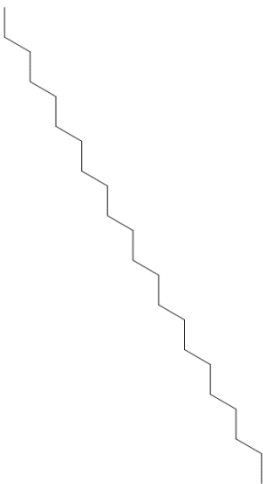
L. rhinocerus (LR) or tiger milk mushroom is naturally found in Southeast Asia countries, China, Australia and Malaysia. Sclerotium of this mushroom displayed several medicinal properties. According to previous report, researchers found that water extract of this mushroom could stimulate neurite outgrowth in the PC-12 cell line (98). Cold water extract showed antiproliferative activity on breast cancer (MCF-7) and lung cancer (A549) cell lines (20). Hot water extract displayed anti-inflammatory and anti-asthmatic activity by increasing the levels of immunoglobulin E (IgE) in serum and T-helper 2 cytokines: IL-4, IL-5 and IL-13 in bronchoalveolar lavage fluid (BALF), as well as decreasing eosinophil numbers in BALF (19). Also, hot water extract showed anti-viral activity on human papilloma virus (HPV) and dengue virus type-2 (22). Moreover, a toxicity study of LR extract exhibited that at 1,000 mg/kg of the extract which fed orally to rat did not cause any adverse effects (99).

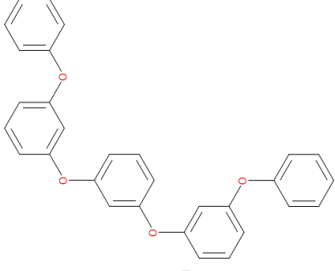
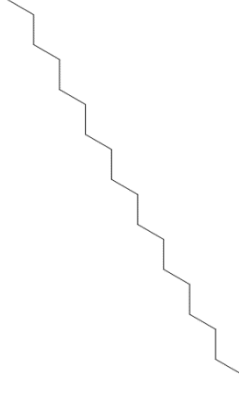
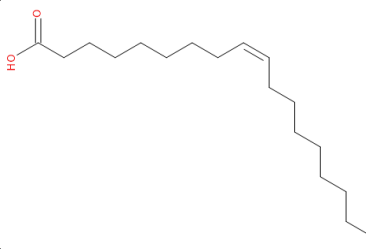
Phytochemical profile of LR was studied by sequential extracted using five solvents: petroleum ether, diethyl ether, hexane, ethyl acetate and methanol then completed with GC-MS analysis. The result presented 18 chemical constituents (Table 4) which were classified into five groups, including alkane, fatty acids, benzene, phenol and dicarboxylic acid. The major compounds of the extracts are linoleic acid, octadecane and 2,3-dihydroxypropyl elaidate (19).

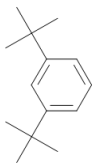

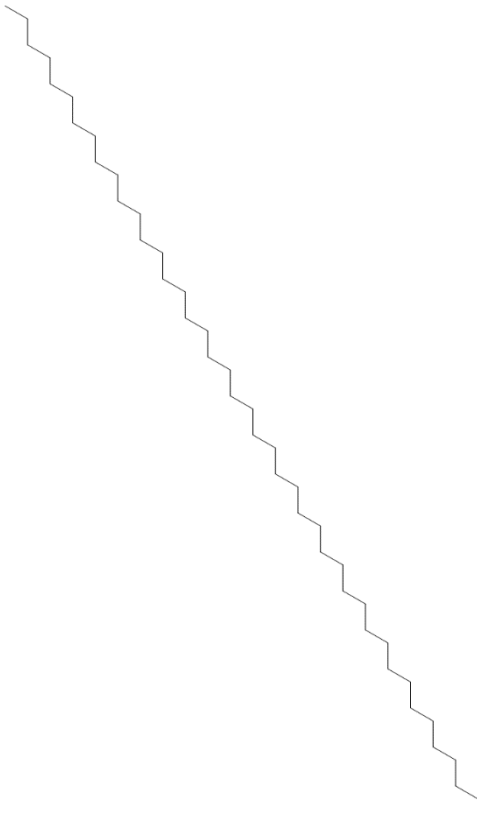
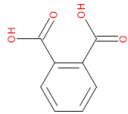
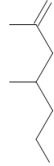
Table 4 Phytochemical profile of *L.rhinocerus*

Compounds	Molecular formula	Structures	% Relative
Linoleic acid	$C_{18}H_{32}O_2$		21.35
2,3-Dihydroxypropyl elaidate	$C_{21}H_{40}O_4$		11.82
Octadecane	$C_{18}H_{34}$		10.47

Compounds	Molecular formula	Structures	% Relative
Heptadecane	$C_{17}H_{36}$		9.29
1-Chlorooctadecane	$C_{18}H_{37}Cl$		6.69
Heneicosane	$C_{21}H_{44}$		6.22
Ethylbenzene	C_8H_{10}		4.87

Compounds	Molecular formula	Structures	% Relative
Eicosane	$C_{20}H_{42}$		4.77
Tricosane	$C_{23}H_{48}$		4.00
Docosane	$C_{22}H_{46}$		3.54

Compounds	Molecular formula	Structures	% Relative
Benzene, 1,3-bis (3-phenoxyphenoxy)	$C_{30}H_{22}O_4$		3.43
Nonadecane	$C_{19}H_{40}$		2.61
Oleic acid	$C_{18}H_{34}O_2$		2.55

Compounds	Molecular formula	Structures	% Relative
1,3-Di-tert-butylbenzene	$C_{14}H_{22}$		2.38
Phytane	$C_{20}H_{42}$		2.30
Tritetracontane	$C_{43}H_{88}$		2.25
Phthalic acid	$C_8H_6O_4$		1.10
2,4-Dimethyl-1-heptene	C_9H_{18}		0.36

Astraeus spp. (AH) or false earthstar mushroom is an edible mushroom. The phytochemical compounds extracted from AH fruit body display many benefits in medicinal uses. According to previous studies, researchers found that polysaccharide that was isolated by hot alkaline extraction from AH showed immunomodulatory activity in a murine model (25). Also, heteroglucans isolated from this mushroom show antitumor activity via the activation of immune system of Swiss albino mice model (23). Moreover, they found that triterpenoids: astrakurkurone and astrakurkuro (Figure 2.12) isolated from this mushroom show *in vitro* toxicities against *Candida albican* (100). Besides, astrakurkurone could inhibit the growth of *Leishmania donovani* promastigotes not only *in vitro* but also *in vivo* studies (24, 100, 101).

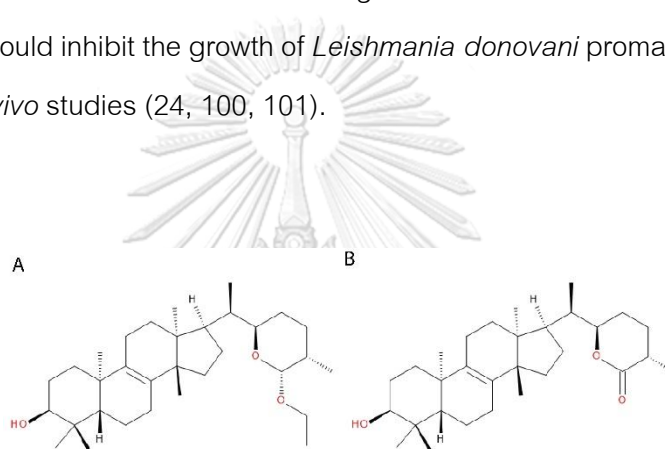


Figure 13 Structures of compounds found in *A. hygrometricus*.

(A) and (B) represent astrakurkuro and astrakurkurone, respectively.

2.4 Computer-Aided Molecular Modelling

At present, bioinformatics tools are used in many scientific studies such as molecular modelling and drug design. Molecular docking is one of essential tools for drug development study. It can assist in the understanding of the interaction between the macromolecule and a small molecule. The macromolecules can be any proteins, receptors or enzymes. Moreover, the small molecules can be inhibitor or substrates, which are called ligands.

Herein, Discovery studio 4.5 programs (102) would be performed to determine the interaction ligand-protein complex such as ligand-amino acid interaction, binding pocket, bond interaction and bond length. Also, it also performs molecular docking; it contains

two different docking methods including CDOCKER and Libdock. The CDOCKER generates random conformations by applying CHARMM forcefield (103), and receptor-ligand interaction are further optimized using CHARMM. During the refinement, the receptor is held rigid while the ligands are allowed to be flexible to search for best binding conformation and interactions. The CDOCKER interaction energy from CDOCKER analysis is considered to evaluating the ability of compounds to bind the target protein. The lower energy represented, the better binding affinity. The other docking program, LibDock will be performed in this study. The LibDock analysis is high-throughput docking algorithm to predict a binding ability between interested ligands and receptor, based on polar interaction sites. The outcome of this calculation was a LibDock score. The complex conformation with the higher score represented, the stronger binding affinity.

However, the molecular docking programs are only the tools to predict the possible interactions between protein and ligand; these results might not occur in reality. Therefore, the inhibitory effects should be validated by performing *in vitro* and *in vivo* experiments.

2.5 *In vitro* HIV-1 PR and RT inhibitor Screening Kits

Now, *in vitro* commercial kits for screening HIV-1 PR and RT inhibitor are available. They are used to determine the ability of a tested compound to inhibit HIV-1 PR and RT. These kits are developed from many methods of detection such as radioactive and non-radioactive assays. In this study, the non-radioactive assay kits would be used. For HIV-1 PR inhibitor screening, we use HIV-1 protease inhibitor screening kit (Fluorometric) from BioVision, USA. It works on the conjugated-peptide substrate and HIV-1 PR by using fluorescence resonance energy transfer (FRET) assay. If the tested compound can inhibit the enzyme activity, the peptide will not be cleaved and the fluorescence will be decreased or cannot be detected in the reaction. On the other hand, if it absents of inhibitor in the assay, the enzyme will cleave the peptides, and the fluorescence can be detected at excitation/emission wavelength of 330/450 nm.

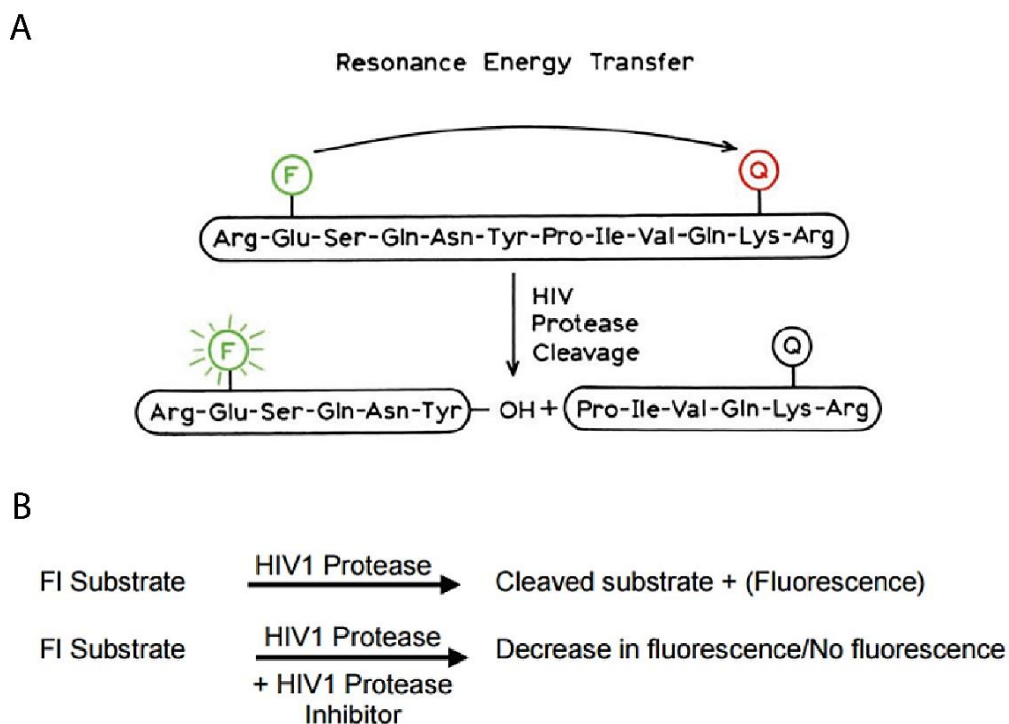


Figure 14 HIV-1 protease inhibitor screening kit (Fluorometric).

The schematic (A) theory of fluorescence resonance energy transfer and (B) the equation of the reaction

For HIV-1 RT inhibitory activity determination, Reverse transcriptase assay, colourimetric kit (Roche, Germany) will be used in this study. This kit detects the ability of reverse transcriptase to synthesize DNA from poly A template by using digoxigenin (DIG)- and biotin-labelled nucleotides. The synthesized DNA will be detected by following a sandwich ELISA protocol. The biotin-labelled DNA bind to streptavidin that has been pre-coated at the bottom of the microplate. Then peroxidase conjugated anti-DIG (anti-DIG-POD) bind to the DIG-labelled DNA. In the last step, the peroxidase substrate ABTS is added. The peroxidase catalyzes the substrate and produces a coloured reaction product. The absorbance of the product can be measured using microplate reader at a wavelength of 405 nm and referent wavelength of 490 nm. The absorbance level is directly correlated to the level of RT activity in the sample.

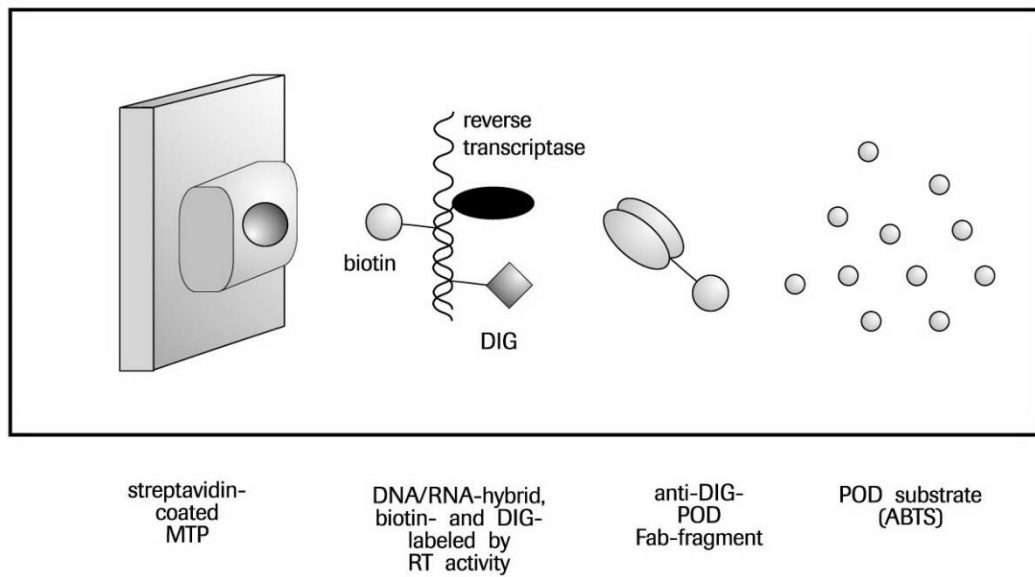


Figure 15 The theory of Reverse transcriptase assay, colourimetric kit

2.6 Cell Models

Form literature search, several cell lines are used for *in vitro* HIV-1 infection and expression studies. The cell lines that are susceptible to *in vitro* HIV-1 infection must present of CD4 and either CXCR4 or CCR5 on their surface. The CD4⁺ cell line that commonly used for HIV-1 research are tabulated in **Table 5** (104).

Table 5 CD4⁺ T lymphocytic cell lines used for HIV-1 infection and expression

Lineage	Entry co-receptor expression	The efficiency of HIV-1 replication ^a	Notes
Jurkat-E6	CXCR4	High	-
CEM, A3.01	CXCR4	High	-
Sup-T1	CXCR4	High	CD4 and CD8 expression, highly fusogenic
MOLT-4	CXCR4	High	Highly fusogenic
HUT-78/H-9	CXCR4	High	Highly fusogenic
PM-1	CCR5 and CXCR4	High	Susceptible to both CCR5 and CXCR4 HIV strain
MT-2	CXCR4	Very High	Highly fusogenic and cytophatic infection
MT-4	CXCR4	Very High	Highly fusogenic and cytophatic infection
ACH-2	CXCR4	NA	HIV-1 expression by PMA, TNF- α , CD30L, and interferons

^aNA indicates not applicable

In this study, we use MOLT-4 and ACH-2 for target cell model and HIV-1 expression, respectively. The MOL-4 cell is human T lymphoblast, acute lymphoblastic leukaemia cell line. It mainly displays CD4 and CXCR4 on its surface, these receptor and co-receptor are necessary for HIV-1 infection. It is generally used for HIV-1 research such as cytotoxicity assay as well as a target for HIV-1 infection (105). The ACH-2 is also human T lymphoblast, acute lymphoblastic leukaemia cell line. The distinctive characteristic of this cell is it can generate infectious HIV-1 by induction of PMA, TNF- α , CD30L, or interferons. Therefore, this cell is used for HIV-1 expression and the infectious HIV-1 will be used for infection of target cell furthermore (106).

Cytopathic effect (CPE) is a common characteristic for determining *in vitro* HIV-1 infection. Here, we will observe a syncytial formation of HIV-1 induced cytopathic effect. It is a cell fusion, which is caused by the formation of multinucleated giant cells as shown in **Figure 16**. This morphology can be observed with an inverted microscope (107).

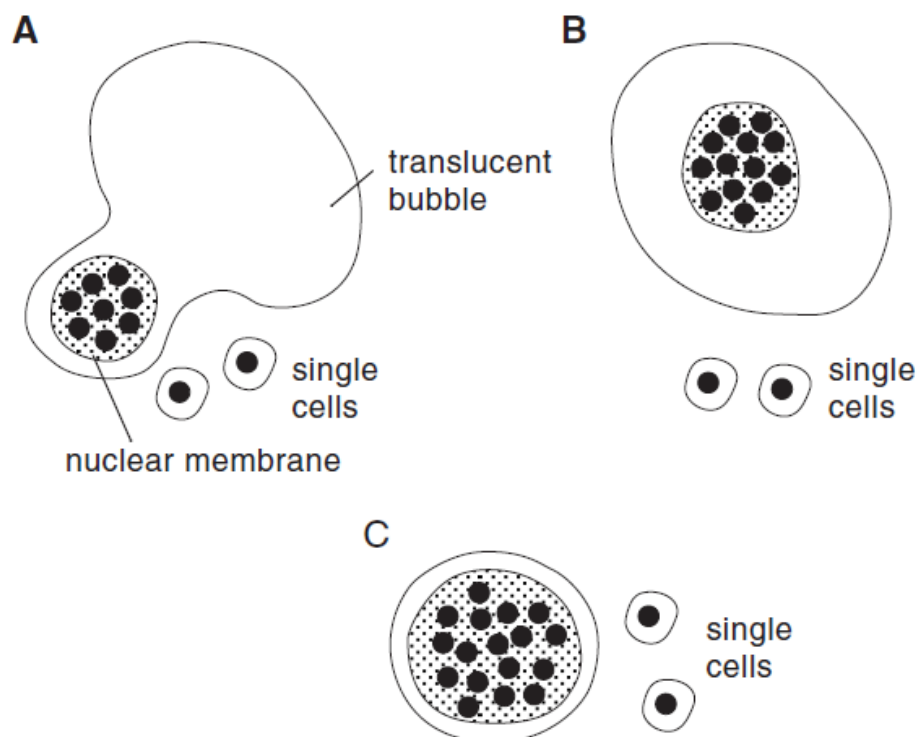


Figure 16 Typical morphology of HIV-induced syncytia.

(A) moreover, (B) are commonly found in HIV-1 infection cell line after 48 or 72 hours of infection. (C) are an old syncytia which are found after several days of infection (107)

CHAPTER III

MATERIALS AND METHODS

3.1 Laboratory Instruments and Equipment

-20°C freezer	Panasonic, Japan
-80°C deep freezer	Eppendorf, Germany
4°C refrigerator	Sanyo, Japan
48-well cell culture plate	SPL, Korea
96-well cell culture plate	SPL, Korea
Analytical balance	Mettler Toledo, Switzerland
Autoclave	Hirayama, Japan
Autopipette 0.2-2 µl	Gilson, France
Autopipette 1-10 µl	Gilson, France
Autopipette 2-20 µl	Gilson, France
Autopipette 10-100 µl	Gilson, France
Autopipette 20-200 µl	Gilson, France
Autopipette 100-1000 µl	Gilson, France
Beaker (50, 100, 250, 500 and 1000 ml)	Schott Duran, Germany
Cell culture flask (25 cm ³)	SPL, Korea

Cell culture flask (75 cm ³)	SPL, Korea
Centrifuge	Hitachi, Japan
Centrifuge tube (15 and 50 ml)	Nest, China
CO ₂ incubator	Thermo Scientific, USA
Chromatography glass column	Pyrex, UK
Cryovial tube 2 ml	Corning, USA
Disposable serological pipette (5, 10 ml)	Corning, USA
ELISA plate reader	PerkinElmer, USA
Erlenmeyer flask (, 250, 500 and 1000 ml)	Schott Duran, Germany
Exicycler™ 96 real-time PCR	Bioneer, Korea
Filter tip 10 µl	Corning, USA
Filter tip 200 µl	Corning, USA
Filter tip 10000 µl	Corning, USA
Fourier-transform infrared spectroscopy	Thermo Scientific, USA
Freeze dryer	Thermo Electron, USA
Gas chromatography-Mass spectrometry	Agilent, USA
Glass bottle (250, 500 and 1000 ml)	Schott Duran, Germany
Hemocytometer	Hausser Scientific, USA
High-resolution mass spectroscopy	Agilent, USA

Hot air oven	Memmert, Germany
Incubator shaker	INFORS HT, Switzerland
Inverted light microscope	Olympus, Japan
Laminar flow	Labconco, USA
Light microscope	Olympus, Japan
Microcentrifuge	Eppendorf, Germany
Microcentrifuge tube 1.7 ml	Sorenson, USA
Multichannel pipette	Gilson, France
Nanodrop 1000 spectrophotometer	Thermo Scientific, USA
Nuclear magnetic resonance spectroscopy	Agilent, USA
Plate shaker	Biosan, Latvia
Preparative Liquid chromatography	Buchi, Switzerland
Rotary evaporator	Heidolph Instruments, Germany
Sterile syringe filter 0.2 μm	Corning, USA
TLC plate silica gel	Merck, Germany
Tip 10 μl	Nest, China
Tip 200 μl	Nest, China
Tip 1000 μl	Nest, China
Ultrapure Lab Water System	Merck, Germany

Vortex mixer FINEPCR, Korea

Water bath Memmert, Germany

3.2 Chemicals and Reagents

3-(4, 5 dimethylthiazol-2-yl)-5- Promega, USA

(3-carboxymethoxyphenyl)-2-(4-sulfophenyl)-
2H-tetrazolium (MTS)

4-(2-hydroxyethyl)-1- Thermo Scientific HyClone, USA
piperazineethanesulfonic acid (HEPES)

AccuPower® 2X GreenStar™ Bioneer, Korea
qPCR Master Mix

AccuPrep® Genomic DNA Extraction kit Bioneer, Korea

Darunavir NIH-AIDS Reagent and Reference
Program, USA

Dimethyl sulfoxide RCI Labscan, Thailand

Ergosterol Sigma Aldrich, USA

Ethanol Merck, Germany

Ethyl acetate Merck, Germany

Fetal bovine serum Thermo Scientific HyClone, USA

Hexane Merck, Germany

HIV-1 p24 SimpleStep ELISA kit	Abcam, UK
HIV-1 Protease Inhibitor Screening kit	Biovision Incorporated, USA
HIV-1 Reverse Transcriptase Assay kit	Roche Diagnostics, Germany
Linoleic acid	Sigma Aldrich, USA
Nevirapine	NIH-AIDS Reagent and Reference Program, USA
Oleic acid	Sigma Aldrich, USA
Palmitic acid	Sigma Aldrich, USA
Phorbol myristate acetate	Sigma Aldrich, USA
Phosphate buffered saline	Thermo Scientific HyClone, USA
Roswell Park Memorial Institute-1640 medium	Thermo Scientific HyClone, USA
Stearic acid	Sigma Aldrich, USA

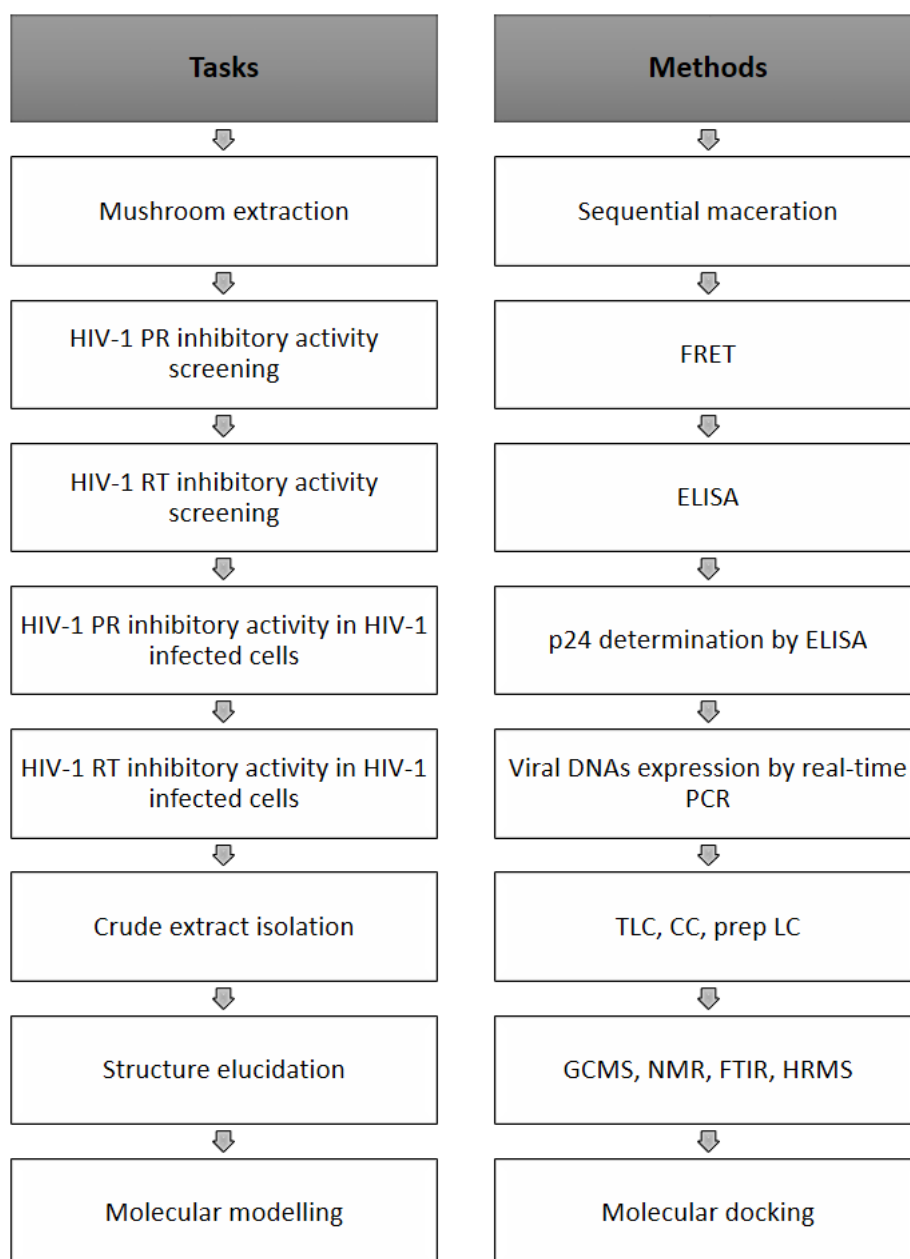


Figure 17 Experimental workflow

3.3 Mushroom Materials

A.polytricha fruiting bodies were collected from a Chang Daeng mushroom farm in Prapradaeng, Samutprakarn, Thailand. *Astraeus spp.* were collected from Kanchanaburi, Thailand. The fruiting bodies were cleaned with water and dried under sunlight then put

in an oven at a temperature of 60°C for overnight. The dried mushrooms were grounded into powder by a blender. In addition, sclerotia powder of *L. rhinocerus* was obtained from LiGNO Biotech Sdn Bhd, Selangor, Malaysia.

3.4 Mushroom species identification

Dried mushrooms were cleaned with 70% ethanol then grounded into powder. Total genomic DNA (gDNA) was extracted by CTAB (hexadecyltrimethylammonium bromide) method. Briefly, the mushroom powder and CTAB were mixed and incubated at 65°C for an hour. Chloroform/isoamyl alcohol (24:1) was added into the incubated mixture then spin down at 15,000 rpm, 18°C for 8 minutes. The clear upper part was collected. DNA was precipitated by adding isopropanol and incubated at -20°C for 30 minutes. After that, the sample was centrifuged at 8,000 rpm, 4°C for 5 minutes for DNA pellet collection. Ethanol (70%, v/v) was added into the pellet for washing. Finally, the DNA pellet was dissolved in TE buffer.

The DNA was submitted to Bioneer sequencing service (Bioneer Corporation, Korea) for polymerase chain reaction (PCR) amplification of the internal transcribed spacer (ITS) region using primer pair ITS1/ITS4, then the DNA sequence was analysed. The mushroom species were identified by comparing nucleotide sequences database on GenBank.

3.5 Extraction

Mushroom samples were extracted by sequential maceration method, followed Figure 3.2. *A. polytricha* (AP) powder (1 kg) was macerated twice with hexane (10 L) in an incubator shaker at 225 rpm, room temperature for 72 hours. The combined extracts were filtrated through a filter paper (Whatman® No.2) then the hexane was evaporated under reduced pressure to give a crude hexane extract (APH) as a thick yellow paste (3.90 g). After hexane extraction, the residue was dried in fume hood then the dried residue was extracted twice with ethanol (10 L) at room temperature for 72 hours in the

incubator shaker. The pooled extracts were filtered and evaporated under reduced pressure to give a crude ethanol extract (APE) as a dark purple thick paste (4.74 g). Next, the residue from ethanol extraction was dried and extracted with water (10 L) in 4°C refrigerator for 72 hours with a magnetic stirrer. The combined extracts were filtrated and removed water by freeze-dry lyophilizer to give crude water extract (APW) as a thick brown paste (19.88 g).

For *Astraeus spp.* (AH) extraction, the mushroom material (100 g) was sequentially extracted with hexane (1 L), ethanol (1 L) and water (1 L) by following the protocol of *A. polytricha* extraction. This extraction obtained three crude extracts, including crude hexane extract (AHH), crude ethanol extract (AHE) and crude water extract (AHW) as a yellow wax (0.91 g), a brown powder (2.99 g) and a black paste (5.35 g), respectively.

L. rhinoceros (LR) powder (100 g) was extracted with hexane (1 L), ethanol (1 L) and water (1 L), respectively by following the previous protocol. It gave three crude extracts: crude hexane extract (LRH), crude ethanol extract (LRE) and crude water extract (LRW). The morphology of these extracts was a thick yellow paste (0.28 g), a thick brown paste (0.62 g) and a brown powder (12.18 g), respectively. Percentage of yield from mushroom extractions were calculated by the following equation.

$$\% \text{ Yield} = \left(\frac{\text{Weight of crude extract}}{\text{Dry weight}} \right) \times 100$$

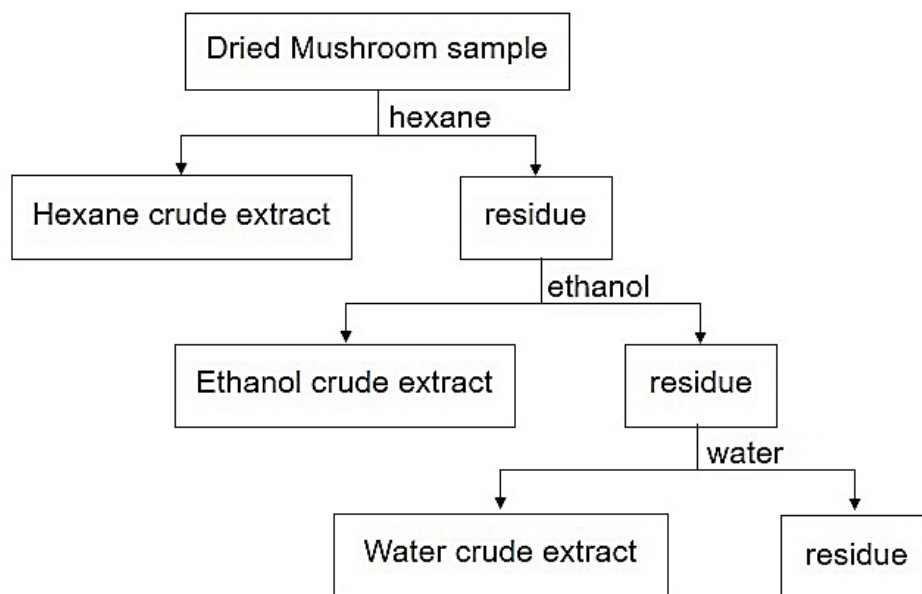


Figure 18 Schematic representation of the sequential mushroom extraction

3.6 *In Vitro* Non-Cell Based Assays for Anti-HIV-1 Activity

3.6.1 HIV-1 Protease Inhibition

HIV-1 Protease Inhibitor Screening Kit (Fluorometric) from Biovision Incorporated (Milpitas, CA, USA) was used to measure the inhibitory effect of samples on HIV-1 protease activity. Pepstatin (1 mM) was used as a positive control, and DMSO (1%, v/v) was used as a solvent control. The assay was performed according to the manufacturer's instruction. Briefly, sample (1 mg/ml) was incubated with HIV-1 protease enzyme at room temperature for 15 minutes. Then the HIV-1 protease fluorescent substrate was added and measured fluorescence (Excitation/Emission = 330/450 nm) in a kinetic mode for 90 minutes at 37°C using PerkinElmer EnSpire plate reader. Percentage of relative inhibition of HIV-1 PR activity was calculated by the following equation.

$$\% \text{ Relative inhibition of HIV-1 PR activity} = \left(\frac{\text{Slope of enzymatic control} - \text{Slope of sample}}{\text{Slope of enzymatic control}} \right) \times 100$$

3.6.2 HIV-1 Reverse Transcriptase Inhibition

HIV-1 Reverse Transcriptase Assay, colourimetric kit from Roche, Germany was performed to screen HIV-1 RT inhibitory activity of the extracts. Nevirapine (200 μ M), known non-nucleotide reverse transcriptase inhibitor and DMSO (1%, v/v) were used as positive and vehicle control, respectively. The samples (1 mg/ml) were tested by following the manufacturer's instruction. Each sample was incubated with HIV-1 RT and reaction mixture, including poly A template, biotin-conjugated dUTP and DIG-conjugated dUTP for an hour at 37 °C. After that, the incubated mixtures were transferred to the pre-coated streptavidin microplate module then incubated at 37 °C for an hour. Then the reaction wells were washed with washing buffer for remove unbound products. Next, POD-conjugated anti-DIG were added into the reaction wells and incubated for an hour at 37 °C. The reaction well were wash with washing buffer again then added ABTS substrate and incubated at room temperature for 15 minutes on incubator shaker at 250 rpm. The final products were measure absorbance at 405 nm with reference wavelength at 490 nm. Percentage of relative inhibition of HIV-1 RT activity was computed by compared to a buffer control, followed the next equation.

$$\% \text{ Relative inhibition of HIV-1 RT activity} = 100 - \left(\frac{\text{Absorbance of sample}}{\text{Absorbance of buffer control}} \right) \times 100$$

3.7 *In Vitro* Cell-Based Assays for Anti-HIV-1 Activity

3.7.1 Cell culture

T lymphoblasts, MOLT-4 cells were cultured in RPMI-1640 supplemented with 10% (v/v) of FBS at 37 °C in a humidified incubator with 5% of CO₂. ACH-2 cells, HIV-1 latent T cells were maintained in RPMI-1640 supplemented with 10 mM HEPES and 10% (v/v) FBS at the same condition as the MOLT-4 cells.

3.7.2 Cytotoxicity Assay

Mushroom extracts and their phytochemical compounds have tested cytotoxicity on MOLT-4 cell line, human T lymphoblast by MTS assay. The extracts and pure compounds were dissolved in 0.1% (v/v) of dimethyl sulfoxide (DMSO) at varying concentrations. The

crude extracts were prepared to final concentrations of 1.00, 0.50, 0.25, 0.13, 0.06 and 0.03 mg/ml, while the pure compounds were prepared to final concentrations of 2.00, 1.00, 0.50, 0.25 and 0.13 μM . The MOLT-4 cells (1×10^4 cells, 100 μl) were seeded in each wells of 96-well plate. Then the cells were treated with the compounds (100 μl) for 24, 48 and 72 hours. The DMSO at 0.1% (v/v) was used as vehicle control and the untreated cell condition was used as a normal control. At the end of each incubation periods, MTS reagent (20 μl) was added in each wells of treatments. After four hours of incubation, absorbance was observed at wavelength of 490 nm. The percentages of cell viability were determined by comparing to untreated cell control, as the following equation.

$$\% \text{ Cell viability} = \frac{\text{Absorbance of treatment}}{\text{The absorbance of untreated cell control}} \times 100$$

The results were reported in CC_{50} values, calculated by standard curve analysis of four parameters logistic in Sigma plot 12.0 software.

3.7.3 Virus expression

ACH-2 cell line (1×10^6 cells/ml), an HIV-1 latent T cell clone with one integrated proviral copy of Lymphadenopathy-associated virus (LAV) was cultured in culture medium with 100 nM of phorbol myristate acetate (PMA) for induced virus expression. After three days of incubation, all culture medium was collected and centrifuged at 300 x g for 10 minutes. The cell culture supernatant was filtered pass through 0.45 μm filter for gave a virus stock. The virus stock was determined a quantitative of p24 by using HIV-1 p24 ELISA kit (Abcam, UK). The stock was either used immediately or kept at $-80\text{ }^{\circ}\text{C}$ for further usage (106).

3.7.4 Infectivity Assay

MOLT-4 cells (2×10^5 cells) were cultured with vary concentrations of HIV-1 viruses; there are including 2×10^3 , 2×10^4 and 2×10^5 pg of HIV-1 p24. Then the cells and viruses were incubated at $37\text{ }^{\circ}\text{C}$ and 5% of CO_2 for two hours. The uninfected viruses were removed by washing three times with phosphate buffer saline (PBS). The infected cells

were re-suspended with culture medium then cultured on 48-well plate. After 72 hours of incubation, cytopathic effect (CPE), HIV-1 induced syncytial formation was observed by an inverted light microscope.

3.7.5 Viral p24 determination

MOLT-4 cells (2×10^5 cells) were infected with HIV-1 viruses (2×10^4 pg of HIV-1 p24) for two hours at 37 °C and 5% of CO₂. Then the cells were washed three times with PBS to eliminate unbounded viruses. The infected cells were re-suspended in complete culture media (200 µl) and treated with compounds (200 µl) to make final concentrations at CC₅₀ of each compound. The treated cells were cultured on 48-well plate for 72 hours. Then the culture media were collected in 1.5 ml microcentrifuge tube and centrifuged at 2,000g for 10 minutes. The clear supernatants were determined HIV-1 p24 levels by using HIV-1 p24 ELISA kit (Abcam, UK). The assay was performed according to the manufacturer's instruction. Briefly, the samples (50 µl) were added to anti-tag antibody-coated wells, followed by the antibody cocktail, which is included capture and reporter antibody (50 µl). After one hour of incubation, the wells were washed to remove unbound complex. TMB substrate was added to catalyse HRP, the colour of reactions was turned to blue. Then stop solution was added to stop the reaction and changed the colour to yellow. The final colour of the reactions was measured absorbance at 450 nm. The quantitative of HIV1 p24 was calculated by comparing to the standard curve. Uninfected (no virus) and untreated cells (no treatment) were used as negative and positive controls, respectively. The percentage of relative inhibition of p24 level was calculated and reported by the below equation.

$$\% \text{ Relative inhibition of p24 level} = 100 - \left(\frac{\text{p24 level of treatment}}{\text{p24 level of untreated cell}} \right) \times 100$$

3.7.6 Viral DNA extraction and Real-Time PCR

MOLT-4 cells (5×10^5 cells/ well) were infected with HIV-1 viruses (1×10^5 pg of HIV-1 p24). After 2 hours, the cells were washed with PBS for three times. The infected cells

were cultured with treatments for 24 hours. Uninfected cells and untreated cell were utilised as negative and positive controls, respectively. NVP (2 μ M) was used as drug inhibitor control in this experiment. Extraction of DNA using AccuPrep[®] Genomic DNA Extraction kit (Bioneer) was performed following the manufacturer's instructions. Real-time PCR assays were performed using AccuPower[®] 2X GreenStar[™] qPCR Master Mix (Bioneer) by an Exicycler[™] 96 (Bioneer). The β -actin, β 2-microglobulin and GAPDH were amplified with primer pairs U5-R forward/ U5-R reverse, U5-gag forward/ U5-gag reverse and GAPDH forward/ GAPDH reverse, respectively (Table 6). Quantified amplification products were calculated using the delta-delta Ct method.

Table 6 Primer pairs for viral DNA amplification (108)

Primer	Sequence
U5-R forward	5'-TTAGACCAGATCTGAGCCTGGGAG-3'
U5-R reverse	5'-GGGTCTGAGGGATCTCAGTTACC-3'
U5-gag forward	5'-TGTGTGCCCGTCTGTTGTGTGA-3'
U5-gag reverse	5'-GAGTCCTGCGTCGAGAGAGCT-3'
GAPDH forward	5'-ATCATCCCTGCCTCTACTGG-3'
GAPDH reverse	5'-GTCAGGTCCACCACTGACAC-3'

3.8 Isolation and Purification

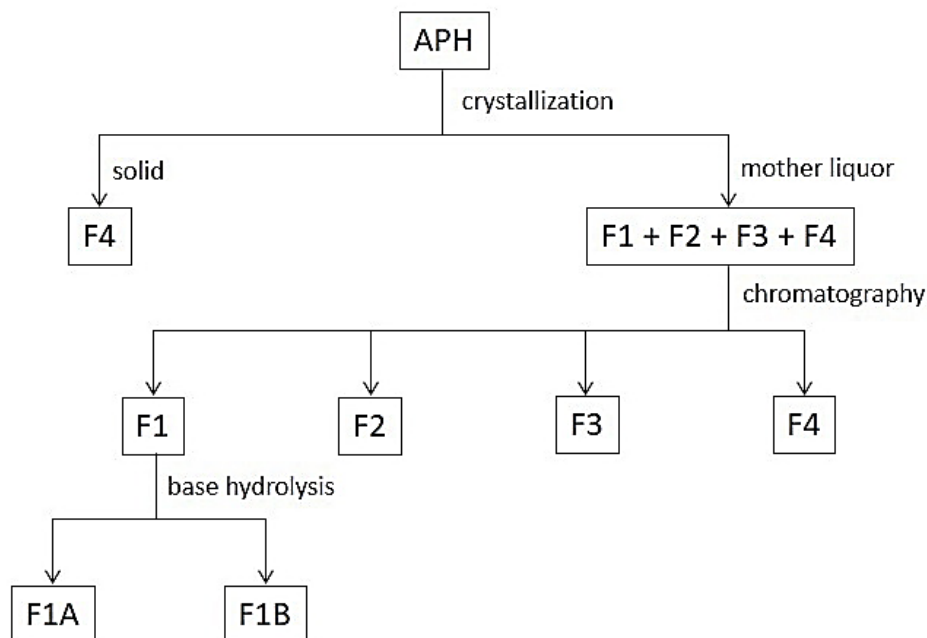


Figure 19 Flow diagram for APH isolation

3.8.1 Thin Layer Chromatography (TLC)

The APH mixture was analysed using the TLC plate silica gel 60 F254, aluminium sheet (Merck). The plate was developed hexane/ethyl acetate (100:10, 90:10, 80:20, 70:30, 60:40 and 50:50; v/v) as mobile phases. The results were observed under UV light at a wavelength of 254 and 365 nm. The mobile phase (80:20, v/v) provided the best separation of four fractions which were named fraction 1 (F1), fraction 2 (F2), fraction 3 (F3) and fraction 4 (F4). This solvent system was further used for APH isolation. A retention factor (R_f) of each fraction was calculated by the following equation.

$$R_f = \frac{\text{Distance travelled by the compound}}{\text{Distance travelled by the solvent front}}$$

3.8.2 Crystallization of fraction 4 (F4)

The APH crude extract (650.2 mg) was dissolved in ethyl acetate to induce the crystallization of F4 from the mixture. The crystals were filtrated through a filter paper. The crystals (15.7 mg) were further dried under a stream of nitrogen gas. The mother liquor was collected, and the solvent was removed to give the thick oil (634.5 mg) which was used in the next purifying process.

3.8.3 Column Chromatography

The APH crude mixture after crystallisation of F4 (634.5 mg) was separated by flash silica gel 60 (0.04 – 0.06 mm) column chromatography (hexane/ethyl acetate, 80:20, v/v) to give three fractions. Each fraction was evaporated under reduced pressure to give F1+F2 (392.0 mg), F3 (118.0 mg) and F4 (116.0 mg).

3.8.4 Preparative Liquid Chromatography (prep LC)

The pre-crystallisation APH crude mixture (450.0 mg) was purified by Reveleris[®] prep purification system with Reveleris[®] C18 reversed-phase flash cartridge (24 g) in flash liquid mode using hexane/ethyl acetate (80:20, v/v) as a mobile phase at 32 ml/min of flow rate. Signals of each fraction were detected by UV detector at wavelength 254 and 365 nm with UV threshold of 0.05 AU to give four fractions. Each fraction was evaporated under reduced pressure to give F1+F2 (168.2 mg), F1+F2+F3 (142.3 mg), F3 (52.7 mg) and F4 (75.4 mg).

The mixture of F1+F2 (168.2 mg) was purified by Reveleris[®] prep purification system using hexane/ethyl acetate (95:5, v/v) as a mobile phase. The other conditions were set as the parameters that were mentioned above. The solvents were removed under reduced pressure to give F1 (149.9 mg) and F2 (2.2 mg).

The mixture of F1+F2+F3 (20 mg) was purified by TLC plate silica gel 60 F254, aluminium sheet (Chem-supply) and performed by using hexane/ethyl acetate (80:20, v/v) as a mobile phase. The band of F2 was scrapped by spatula and stirred in ethyl acetate (20 mL) for 20. The silica was filtered, and ethyl acetate was removed under reduced pressure to give F2 (1.2 mg).

3.9 Compound Identification

3.9.1 Fourier-Transform Infrared Spectroscopy (FTIR)

The FTIR analyses were performed using Nicolet 6700 FTIR spectrometer (Thermo scientific). The spectra were recorded by OMNIC software.

3.9.2 Nuclear Magnetic Resonance Spectroscopy (NMR)

The ^1H (500 MHz), ^{13}C (125 MHz) and 2D NMR: COSY and DEPT NMR analyses were performed using 500MHz Agilent spectrometer. The dried samples were dissolved in 0.5 ml of deuterated chloroform (CDCl_3). A tetramethylsilane (TMS) was used as a reference.

3.9.3 High-Resolution Mass Spectrometry (HRMS)

High-resolution ESI-MS was performed on an Agilent Technologies 6510 Q-TOF LC/MS. Conditions applied were as follows: positive ion mode, 4,000 V of capillary voltage, drying gas at 7 L/min@300 °C, sheath gas at 11 L/min@350 °C, nebulizer at 35 psi, fragmentor at 170 V and MS scan between 100 to 150 m/z.

3.9.4 Gas Chromatography-Mass Spectrometry (GC-MS)

The GC-MS analyses were performed using Agilent 6870/5973 system. The column used was Zebron ZB-5MS (30 m \times 0.25 mm \times 0.25 μm). The samples were analysed using an injector temperature of 240 °C, split ratio 15:1, 1.5 ml/min of He flow rate with an oven temperature of 50 °C to 220 °C (2 min) at 7 °C/min, then 270 °C (5 min) at 7 °C/min, followed by 310 °C at 5 °C/min.

3.9.5 Base hydrolysis of fraction 1 (F1)

0.5 M of methanolic sodium hydroxide (5 mL) was added to F1 (110 mg). The mixture was heated with stirring at 90 °C for 10 minutes. The reaction was cooled in an ice bath, then 5 ml of methanol was added and heated at 90 °C for another 10 minutes.

Upon cooling, pH of the reaction mixture was adjusted to zero by adding 1 M of HCl (10 mL). Then the acidic solution was extracted with dichloromethane (3 × 15 mL). The combined extracts were dried over anhydrous sodium sulfate and filtered. The solvent was removed under reduced pressure to give a crude product (107 mg).

3.9.6 Structural elucidation

Fraction 1 (F1): R_f value (TLC): 0.88 (ethyl acetate/hexane, 20:80). HRMS (ESI): m/z 884.5865 $[M]^+$ (calculated for $C_{57}H_{104}O_6 = 884.7827$). FTIR spectra (cm^{-1}): 2921.41, 2852.12 (C-H) and 1742.29 (C=O). 1H NMR spectra ($CDCl_3$, 500 MHz) δ_H (ppm): 5.349 (m, CH=CH), 5.264 (m, CH), 4.286 (dd, CH_2), 4.151 (dd, CH_2), 2.770 (t, =CH- CH_2 -CH=), 2.315 (t, CH_2CO_2), 2.042 (m, $CH_2CH=CH$), 1.607 (m, $CH_2CH_2CO_2$), 1.254 (m, CH_2) and 0.881 (t, CH_3). ^{13}C NMR spectra ($CDCl_3$, 125 MHz) δ_C (ppm): 173.306, 173.261, 172.859 (C), 130.240, 130.039, 130.023, 129.697, 128.077, 127.910 (CH), 68.891 (CH), 62.106, 62.104 (CH_2), 34.212, 34.068, 34.038, 31.940, 31.917, 31.537, 29.781, 29.720, 29.716, 29.675, 29.641, 29.625, 29.622, 29.542, 29.496, 29.375, 29.360, 29.345, 29.330, 29.288, 29.212, 29.193, 29.147, 29.136, 29.098, 29.064, 27.239, 27.213, 27.211, 27.190, 25.642, 24.898, 24.879, 24.849, 22.702, 22.694, 22.584 (CH_2), 14.128, 14.082 (CH_3).

Fraction 2 (F2): R_f value (TLC): 0.61 (ethyl acetate/hexane, 20:80). HRMS (ESI): m/z 862.6072 $[M]^+$ (calculated for $C_{55}H_{106}O_6 = 862.7984$). FTIR spectra (cm^{-1}): 2960.97, 2913.33, 2849.18 (C-H) and 1735.55 (C=O). 1H NMR spectra ($CDCl_3$, 500 MHz) δ_H (ppm): 5.349 (m, CH=CH), 5.264 (m, CH), 4.282 (dd, CH_2), 4.148 (dd, CH_2), 2.769 (t, =CH- CH_2 -CH=), 2.323 (t, CH_2CO_2), 2.040 (m, $CH_2CH=CH$), 1.598 (m, $CH_2CH_2CO_2$), 1.253 (m, CH_2) and 0.880 (t, CH_3).

Fraction 3 (F3): R_f value (TLC): 0.44 (ethyl acetate/hexane, 20:80). HRMS (ESI): m/z 281.2468 $[M+H]^+$ (calculated for $C_{18}H_{33}O_2 = 281.2475$). FTIR spectra (cm^{-1}): 2955.28, 2914.71, 2847.62 (C-H), 1699.69 (C=O), 1471.38, 1462.96 and 1429.69 (C=C). 1H NMR spectra ($CDCl_3$, 500 MHz) δ_H (ppm) 5.344 (m, CH=CH), 2.771 (t, =CH- CH_2 -CH=), 2.345 (t, CH_2CO_2), 2.042 (m, $CH_2CH=CH$), 1.631 (m, $CH_2CH_2CO_2$), 1.255 (m, CH_2) and 0.880 (t, CH_3).

Fraction 4 (F4): R_f value (TLC): 0.27 (ethyl acetate/hexane, 20:80). HRMS (ESI): m/z 395.3303 $[M-H]^+$ (calculated for $C_{28}H_{43}O = 395.3304$). GCMS (EI) m/z 396 $[M]^+$. FTIR spectra (cm^{-1}) 3414.02 (O-H); 2952.17, 2928.38 and 2868.82 (C-H) and 1655.20 (C=C). 1H NMR spectra ($CDCl_3$, 500 MHz) δ_H (ppm): 5.575 (dd, 1H), 5.385 (m, 1H), 5.205 (m, 1H), 3.639 (m, 2H), 2.459 (ddd, 2H), 2.284 (t, 2H); the position of this signal varied from 1.250–2.080 ppm in the other saturated methylene and methine protons (total 18H); 1.044 (d, 3H), 0.948 (s, 3H), 0.925 (d, 3H), 0.833 (t, 6H) and 0.632 (s, 3H). ^{13}C NMR spectra ($CDCl_3$, 125 MHz) δ_C (ppm): 141.351, 139.769 (C), 135.551, 131.962, 119.573, 116.273, 70.457, 55.728, 54.555, 46.244 (CH), 42.830 (C), 42.815 (CH), 40.797 (CH_2), 40.418 (CH), 39.082, 38.373 (CH_2), 37.026 (C), 33.085 (CH), 31.997, 28.283, 22.991, 21.110 (CH_2), 21.098, 19.949, 19.642, 17.601, 16.281 and 12.047 (CH_3).

3.10 Molecular Modelling

All computational studies were carried out using Discovery Studio 4.5 (BIOVIA). The X-ray crystal structure of HIV-1 protease (HIV-1 PR) in complex with amprenavir (APV) with the resolution 1.8 Å (PDB ID: 5KR0) (109) and HIV-1 reverse transcriptase (HIV-1 RT) in complex with RNase H inhibitor and nevirapine (NVP) (resolution 2.09 Å, PDB ID: 3QIP) (110) were retrieved from RCSB Protein Data Bank.

3.10.1 Protein Preparation

The target proteins were prepared for docking studies; first by removing ligands and water molecules and adding missing hydrogens. The binding site was assigned from the original binding sites of the original ligands. For instance, the X-ray structure of HIV-1 PR co-crystallised with amprenavir ligand was first removed. All crystallographic water molecules in each protein were removed, and the missing hydrogen atoms were added using the CHARMM forcefield (103) in the “Prepare Protein” module. The resulting target protein structures were subsequently utilised to define the docking site using the “Define Binding Site” tool.

3.10.2 Ligand Preparation

The ligand structures were drawn and minimised using the smart minimiser algorithm of 2,000 step with 0.01 minimizing the root mean squared (RMS) gradient and CHARMM forcefield parameter. The ligands were prepared using prepare ligands tool in DS 4.5; the parameters were set as default.

3.10.3 Molecular Docking

Two different docking methods: CDOCKER and LibDock docking protocols available in DS 4.5 were used to perform molecular docking studies. Scoring for the LibDock method was performed with a set of scoring functions employed in the LibDock module, including LibDock Score and RMS Gradient. For the conformer generation of the different ligands in the library, a maximum of 200 conformations was permitted and the “BEST Conformer Method” algorithm was used. The CDOCKER method uses the CHARMM forcefield and the parameters were set as default, allowing for 10 Top Hits and 10 Random Conformations to occur. The CDOCKER method scored the ligands using the CDOCKER Energy and CDOCKER Interaction Energy functions in the CDOCKER module. These functions calculate the energy values using the Gibb's Free Energy (ΔG) (111) of the interaction between the ligand and the receptor with the highest score determined as the best possible ligand.

Once docking was performed, the binding energies were calculated using the “Calculate Binding Energies” protocol in DS4.5. The “Ligand Conformational Entropy” function was set to true, the conformation method was set to use the BEST algorithm and up to 1000 conformations were permitted.

The results of HIV-1 PR docking were compared to amprenavir, the original ligand of this protein complex. The results of HIV-1 RT docking at polymerase and RNase H active sites were compared to nevirapine and 5-hydroxy-4-oxo-2-[(2-phenyl-1H-indol-3-yl)methyl]-1H-pyrimidine-6-carboxylic acid (P4Y), the original ligands, respectively.

3.11 Statistical Analysis

All experiments were triplicated analyses. The results were present as the mean of three independent experiments \pm SEM. Statistic significant was analysed by one-way ANOVA using SPSS 16.0 software. Comparisons with P values less than 0.05 were considered as statistically significant.



CHAPTER IV

RESULTS

4.1 Extraction

A.polytricha (AP), *L. rhinocerusl* (LR) and *Astraeus spp.* (AH) were individually sequential extracted with hexane, ethanol and cold water, respectively. Percentages of yield compared to the dry weight of nine crude extracts are tabulated in **Table 7**

Table 7 Solvent extractive values of crude extracts

Crude extract	% Yield
APH	0.39
APE	0.47
APW	1.99
LRH	0.28
LRE	0.62
LRW	12.18
AHH	0.91
AHE	2.99
AHW	5.35

4.2 HIV-1 PR Inhibitor Screening

Crude extracts at 1 mg/ml were screened for their inhibitory activity on HIV-1 PR. DMSO (1%, v/v) and pepstatin (1 mM) showed the percentage of inhibition at 8.07 ± 0.13 and 81.48 ± 0.76 , respectively. All crude extracts significantly inhibited HIV-1 PR activity, except APW. Interestingly, three crude hexane extracts inhibited HIV-1 PR greater than 50%. LRH displayed the highest inhibition effect at $88.97 \pm 1.57\%$ followed by AHH ($75.53 \pm 0.41\%$) and APH ($71.07 \pm 2.17\%$), respectively. Surprisingly, LRH displayed the percentage of inhibition greater than pepstatin, which is a known protease inhibitor.

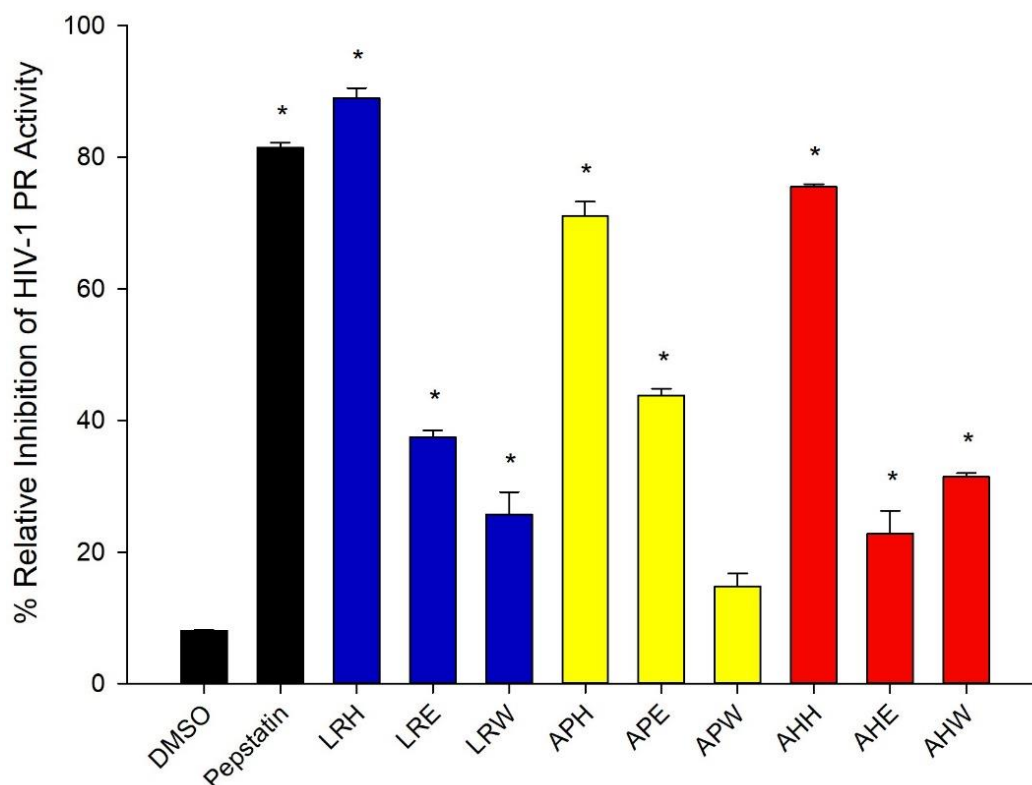


Figure 20 The percentage of relative inhibition on HIV-1 PR of DMSO (1%, v/v) and pepstatin (1 mM) as well as crude extracts (1 mg/ml).

Blue, yellow and red bar represent LR, AP and AH crude extracts, respectively. All data are shown as the mean \pm SEM of triplicate values. Statistical significance was analyzed by one-way ANOVA, Dunnett's test. * indicates $P < 0.05$, versus the vehicle control.

4.3 HIV-1 RT Inhibitor Screening

The extracts (1 mg/ml) were tested for their anti-HIV-1 RT activity using HIV-1 RT colourimetric assay kit. DMSO (1%, v/v) and NVP (200 μ M) exhibited percentage of inhibition at 2.34 and 99.04, respectively. Only LRH showed insignificant inhibition at $9.94 \pm 3.12\%$. All others significantly inhibited HIV-1 RT activity ranges from 37 to 48%. Moreover, two extracts displayed strong inhibition greater than 50%, including LRW ($55.56 \pm 3.51\%$) and LRE ($53.03 \pm 3.32\%$).

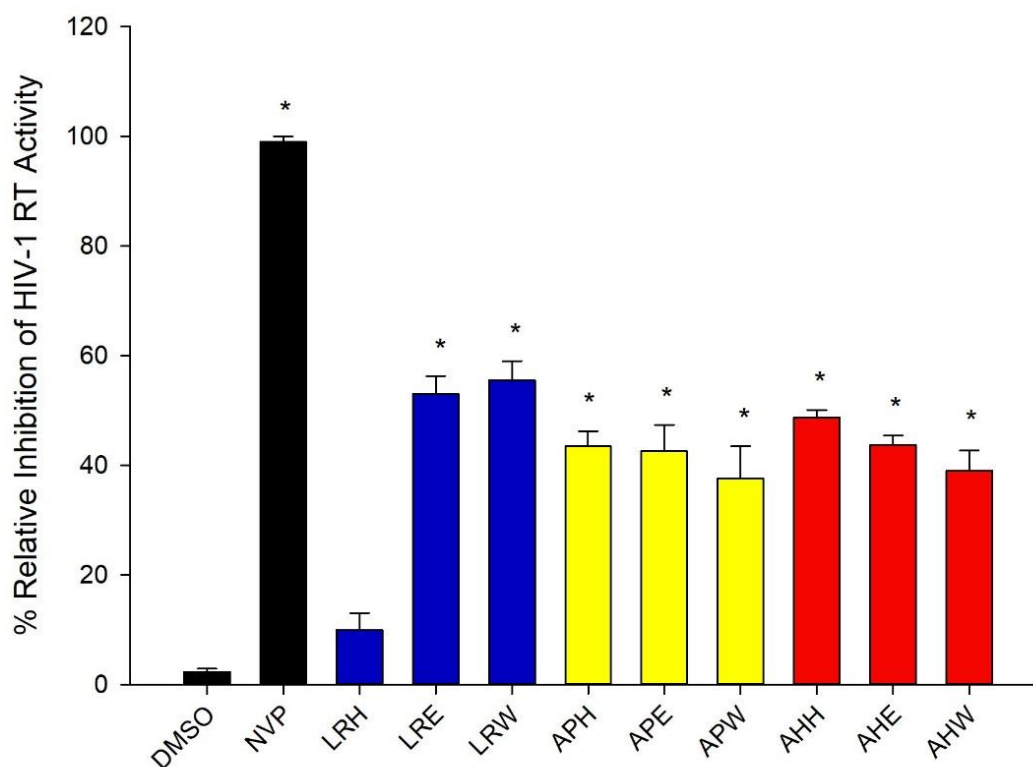


Figure 21 The percentage of relative inhibition on HIV-1 RT of DMSO (1%, v/v) and NVP (200 μ M) as well as crude extracts (1 mg/ml).

Blue, yellow and red bar represent LR, AP and AH crude extracts, respectively. All data are shown as the mean \pm SEM of triplicate values. Statistical significance was analyzed by one-way ANOVA, Dunnett's test. * indicates $P < 0.05$, versus the vehicle control.

4.4 Cytotoxicity of Crude Extracts

Toxicities of crude extracts against MOLT-4 cells were determined by MTS method. Firstly, an appropriate number of cells was evaluated by varying cell densities 5×10^3 , 1×10^4 , 1.5×10^4 , 2×10^4 , 2.5×10^4 , 3×10^4 cells. A graph between the time of incubation and absorbance was shown in the following figure.

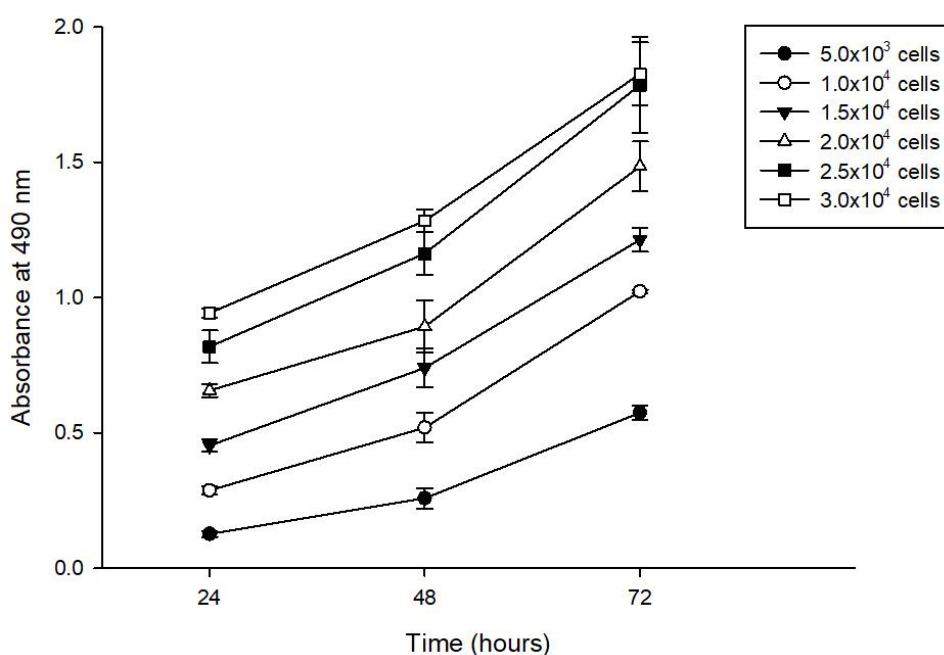


Figure 22 The association graph between time and absorbance at 490 nm of different cell density.

The densities of cells at 5×10^3 and 1×10^4 cells showed an acceptable range of absorbance which was between 0.1 and 1.0 (Figure 22 and Table A5). To determine a correlation between time and absorbance, linear regression of each cell densities were tested (Table A6). R-square (R^2) value of 1×10^4 cells density ($R^2 = 0.9565$) was higher than 5×10^3 cells density ($R^2 = 0.9468$). These results indicate that the 1×10^4 cells density could give a better association between time and absorbance than the 5×10^3 cells density. Therefore, the cell number at 1×10^4 cells was selected for further MTS assay.

In this study, DMSO was used as a solvent to dissolve the crude extracts. However, at high concentration of DMSO can cause toxicity to mammalian cells. To determine a proper concentration of DMSO, the toxicity of DMSO on MOLT-4 cells at various concentrations: 0.10, 0.25, 0.50, 0.75 and 1.00% (v/v) was examined at 24, 48 and 72 hours post-treatment. The results showed that at a concentration higher than or equal to 0.25% (v/v) of DMSO significantly decrease the MOLT-4 cell viability compared to untreated cell control (Figure 23). Therefore, an optimal concentration of DMSO which is

non-toxic to the MOLT-4 cell is 0.10% (v/v), this concentration was used for each compounds preparation in the next assays.

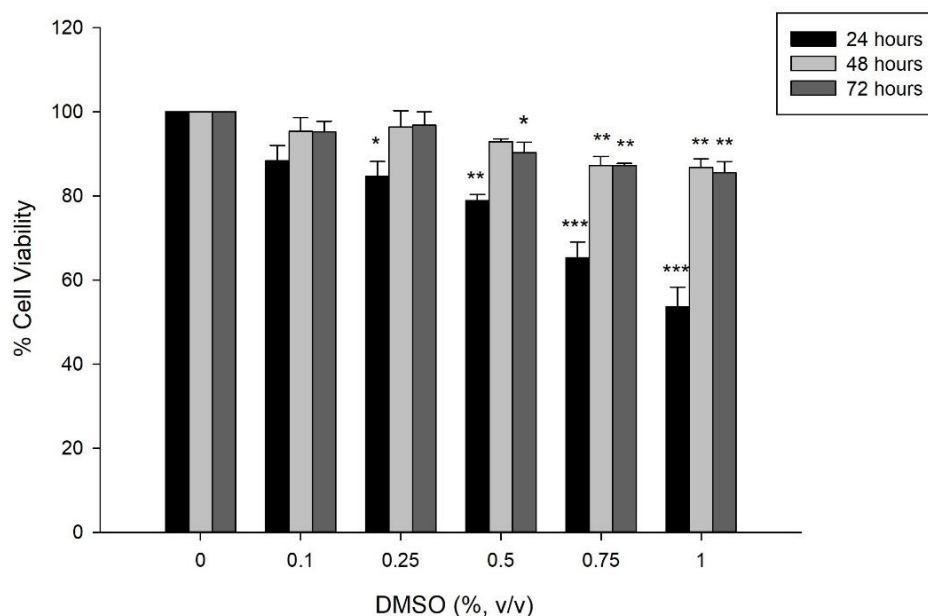


Figure 23 The cytotoxicity at various concentrations of DMSO on MOLT-4 cells after 24, 48 and 72 hours of treatments.

All data are shown as the mean \pm SEM of triplicate values. Statistical significance was analyzed by one-way ANOVA, Dunnett's test. * $P < 0.05$, ** $P < 0.01$ and *** $P < 0.001$ versus the vehicle control.

วิทยาลัย
CHULALONGKORN UNIVERSITY

The cytotoxicity of crude extracts on MOLT-4 cell line were presented in CC_{50} (Table 8). All AP extracts showed time and dose-dependent manners (Figure 24A to 24C). The CC_{50} of APH were range from 0.05 to 0.50 mg/ml. Meanwhile, APW showed the CC_{50} range from 0.06 to 0.09 mg/ml. Moreover, APE showed constant CC_{50} of 0.32 mg/ml at three-time points.

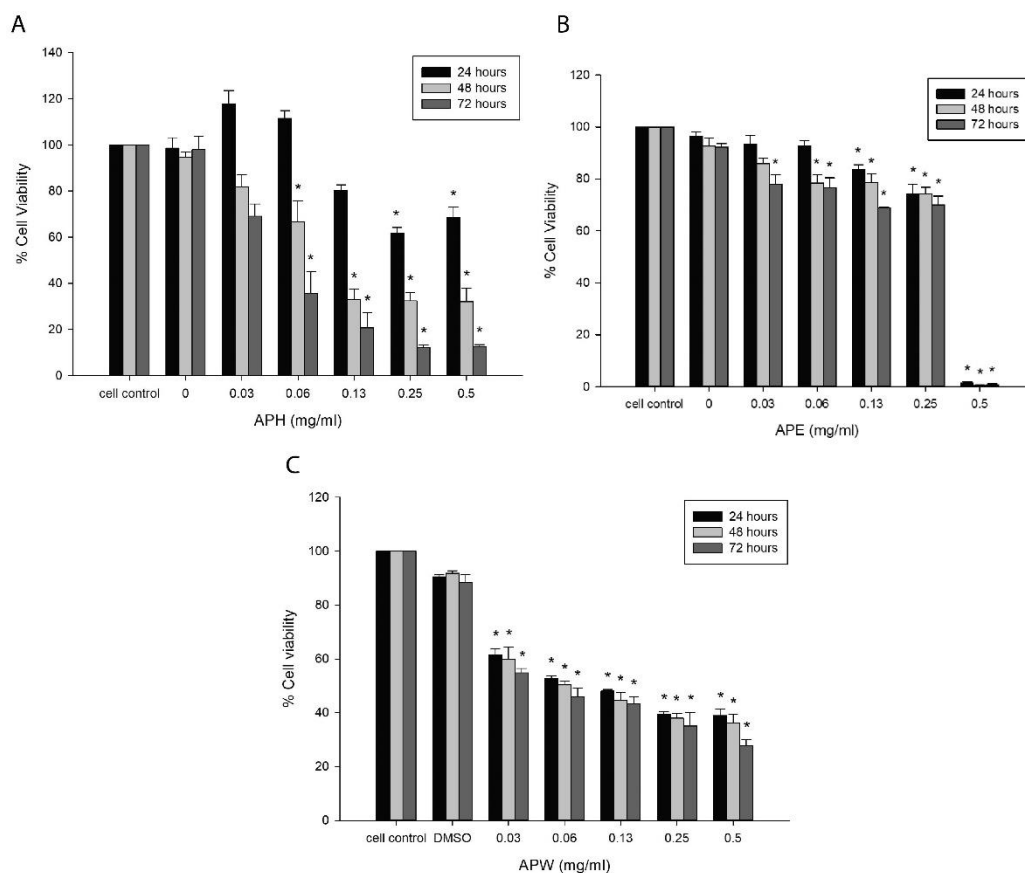


Figure 24 The cytotoxicity at various concentrations of AP crude extracts on MOLT-4 cells after 24, 48 and 72 hours of treatments.

All data are shown as the mean \pm SEM of triplicate values. Statistical significance was analyzed by one-way ANOVA, Dunnett's test. * indicates $P < 0.05$, versus the vehicle control.

In addition, LRH and LRE extracts displayed the reduction of percentage cell viabilities in both time and dose-dependent manners (Figure 25A to 25C). LRH and LRE exhibited the CC_{50} range from 0.08 to 0.14 mg/ml. On the contrary, LRW had no toxicity effect greater than 50% on MOLT-4 cells when tested with high concentration, 0.5 mg/ml.

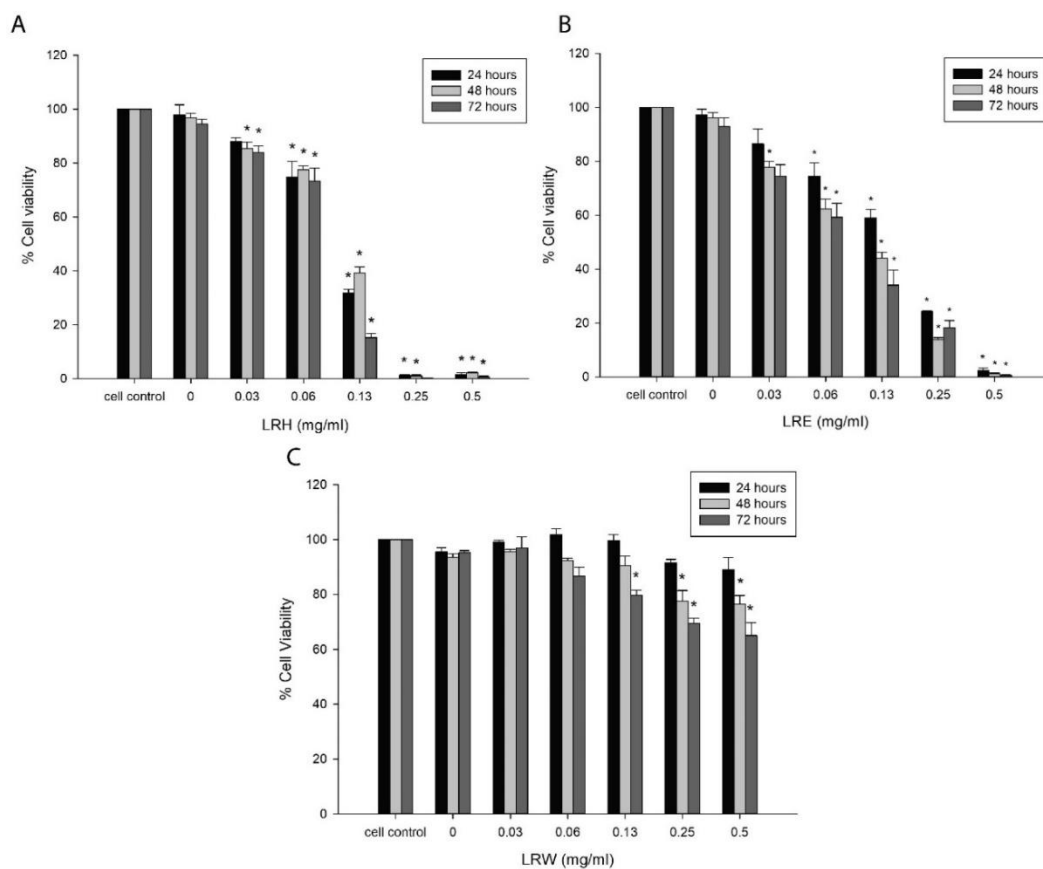


Figure 25 The cytotoxicity at various concentrations of LR crude extract on MOLT-4 cells after 24, 48 and 72 hours of treatments.

All data are shown as the mean \pm SEM of triplicate values. Statistical significance was analyzed by one-way ANOVA, Dunnett's test. * indicates $P < 0.05$, versus the vehicle control.

For AH extracts, AHH and AHE showed strong toxicities on MOLT-4 cells even when evaluated at low concentration, 0.03 mg/ml (Figure 26A and 26B). In contrast, AHW displayed more than 50% of cell death when treated with 0.5 mg/ml for 24 and 48 hours (Figure 26C). Due to the toxicity of AH extracts on cell model, the extracts of AP and LR at selected concentrations will be further studied on anti-HIV-1 in infected cells.

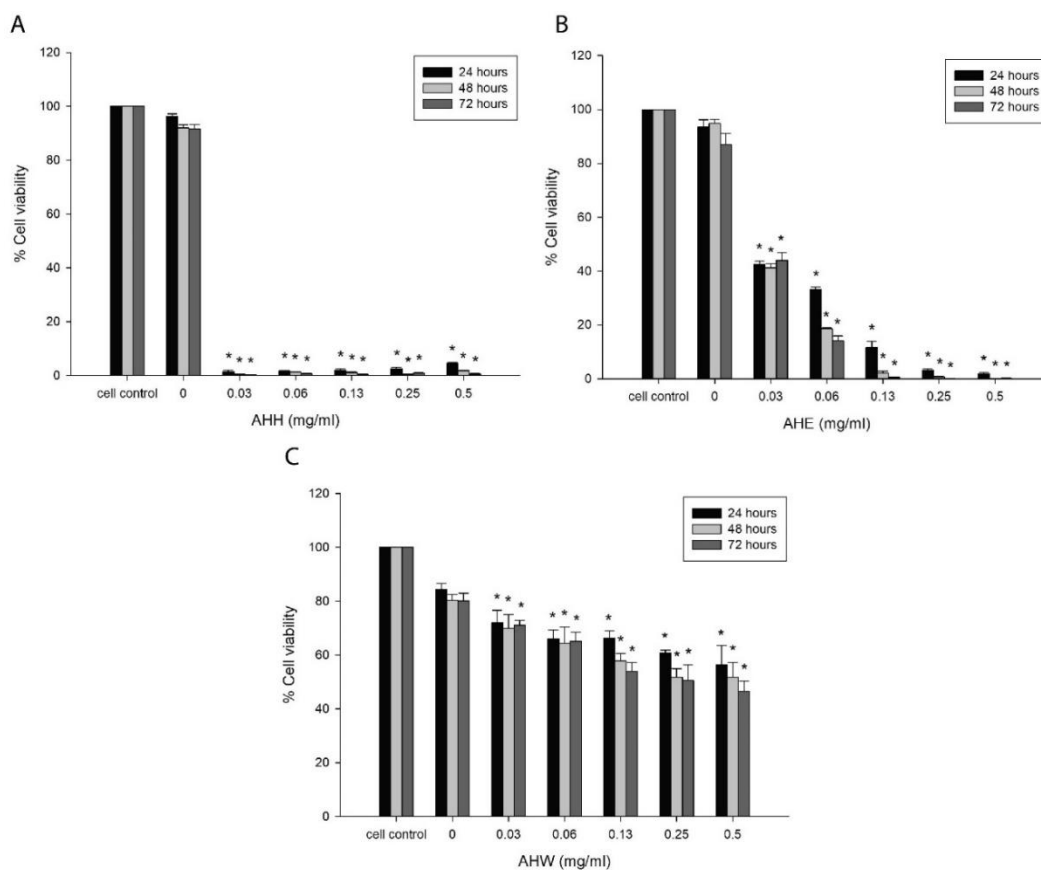


Figure 26 The cytotoxicity at various concentrations of AH crude extracts on MOLT-4 cells after 24, 48 and 72 hours of treatments.

All data are shown as the mean \pm SEM of triplicate values. Statistical significance was analyzed by one-way ANOVA, Dunnett's test. * indicates $P < 0.05$, versus the vehicle control.

Besides, the toxicities of DRV and NVP which were used as drug inhibitor controls were also determined. The results showed that both DRV and NVP at 2.00 μ M did not harm the cells higher than 50% (Figure 27A and 27B).

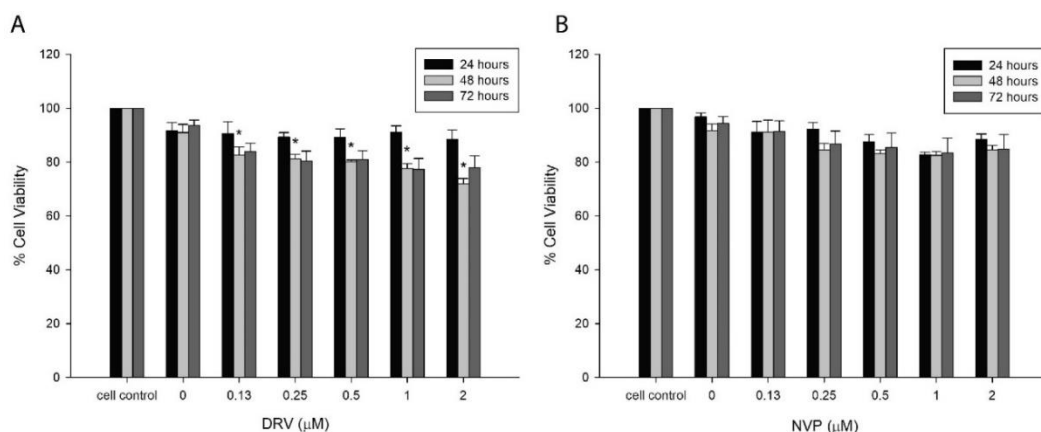


Figure 27 The cytotoxicity at various concentrations of DRV and NVP on MOLT-4 cells after 24, 48 and 72 hours of treatments.

All data are shown as the mean \pm SEM of triplicate values. Statistical significance was analyzed by one-way ANOVA, Dunnett's test. * indicates $P < 0.05$, versus the vehicle control.

Table 8 The fifty percent cytotoxic concentration (CC_{50}) of crude extracts at 24, 48 and 72 hours after treatment

Crude extract/ Compound	CC_{50}		
	24 hours	48 hours	72 hours
APH	0.50 ± 0.08^a	0.11 ± 0.02^a	0.05 ± 0.01^a
APE	0.32 ± 0.02^a	0.32 ± 0.01^a	0.32 ± 0.02^a
APW	0.09 ± 0.00^a	0.08 ± 0.01^a	0.06 ± 0.02^a
LRH	0.09 ± 0.01^a	0.11 ± 0.01^a	0.08 ± 0.00^a
LRE	0.14 ± 0.01^a	0.10 ± 0.01^a	0.08 ± 0.01^a
LRW	$> 0.50^a$	$> 0.50^a$	$> 0.50^a$
AHH	$< 0.03^a$	$< 0.03^a$	$< 0.03^a$
AHE	$< 0.03^a$	$< 0.03^a$	$< 0.03^a$
AHW	$> 0.50^a$	$> 0.50^a$	0.25 ± 0.07^a
Nevirapine	$> 2.00^b$	$> 2.00^b$	$> 2.00^b$
Darunavir	$> 2.00^b$	$> 2.00^b$	$> 2.00^b$

^a CC_{50} were presented in mg/ml. ^b CC_{50} were presented in μ M.

4.5 Virus expression

ACH-2 cell line was used for virus expression in these experiments. The cells (6×10^3 cells) were stimulated with 0.1 mM PMA to produce HIV-1 proviral particles. After 72 hours of incubation, a HIV-1 p24 level was determined by HIV-1 p24 ELISA kit. The results showed that the ACH-2 cells generated viral particle around 85,000 pg/ml, which was calculated from a standard curve of HIV-1 p24 (Figure 28). This stock of virus was used in the further experiments for infection.

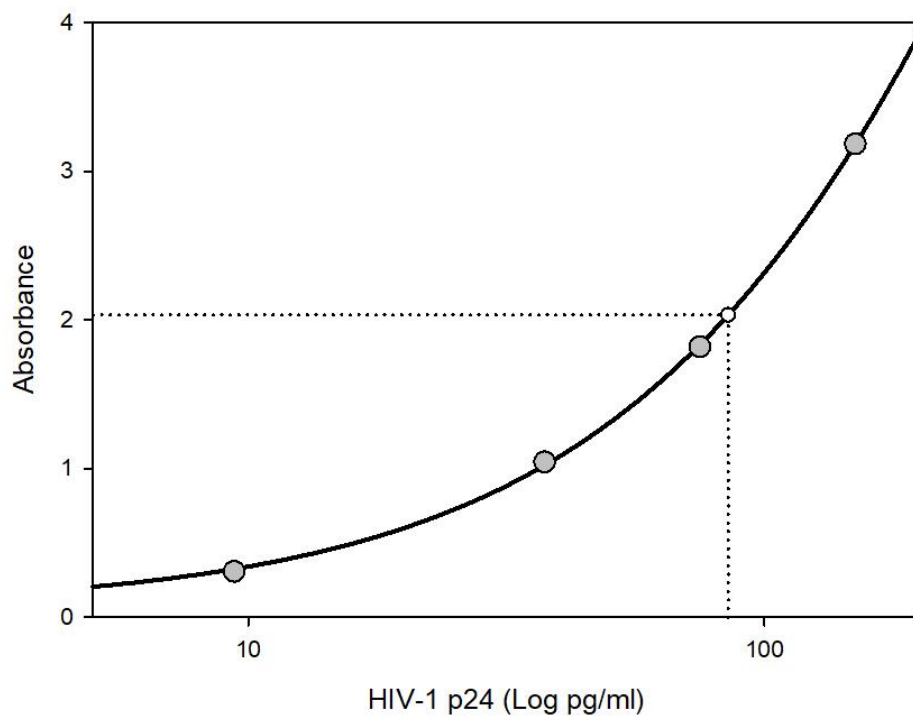


Figure 28 The standard curve of HIV-1 p24. A white circle represent the stock of virus at 1,000 dilution

4.5 Infectivity Assay

The infectivity assay was determined to ensure that the stock virus was still active and can be used to infect the targeted cell model. MOLT-4 cells were infected with the viruses at different concentrations of HIV-1 p24: 2×10^3 , 2×10^4 and 2×10^5 pg. Next, HIV-induced cytopathic effect (CPE), a formation of multinucleated giant cells (syncytia) was observed by phase-contrast microscope after 72 hours of infection. The results demonstrated that the infected cells presented HIV-1 induced CPE. In contrast, the uninfected cell did not show the syncytial formation (Figure 29A). Moreover, the cells were infected with the viruses at 2×10^3 , 2×10^4 and 2×10^5 pg of HIV-1 p24 exhibited average numbers of syncytial cells at 2.1, 2.5 and 2.7 cells per high power field (HPF), respectively (Figure 29B to 29D). These results displayed the effect of virus on CPE formation in a dose-dependent manner (Figure 29E).

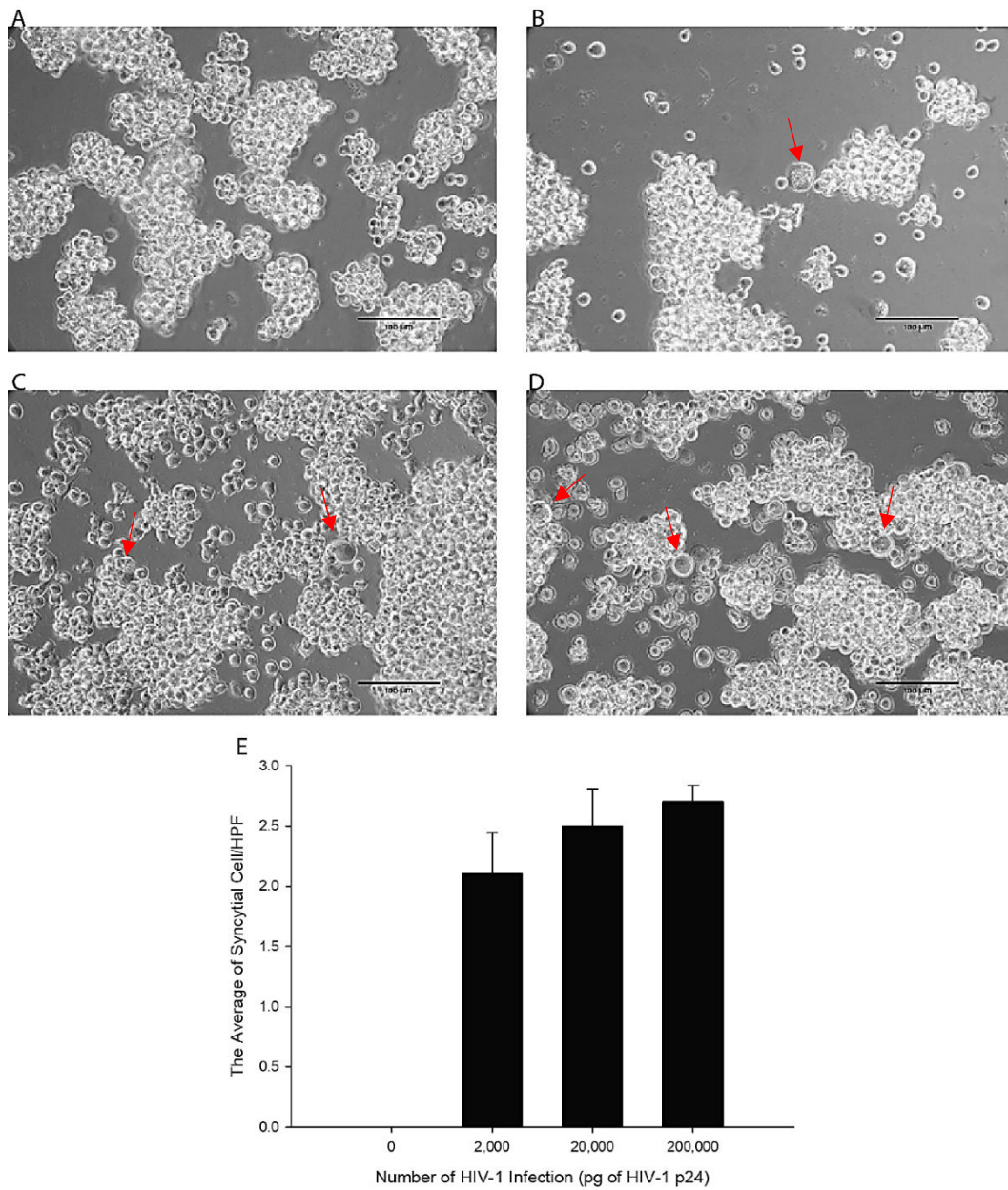


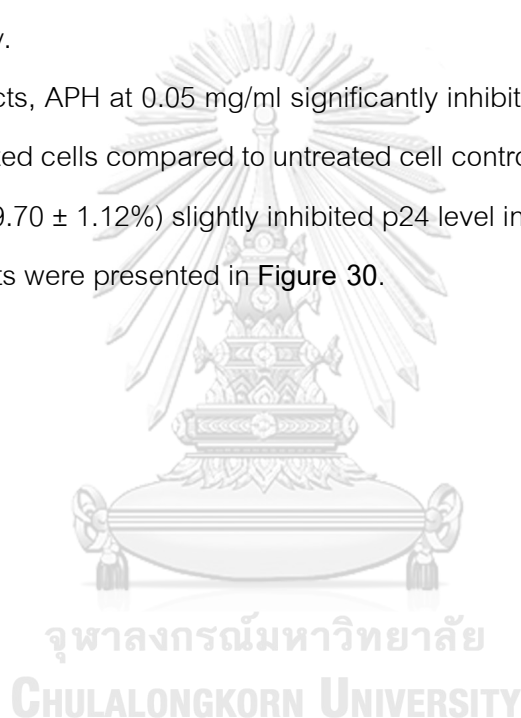
Figure 29 The HIV-1 induced syncytial formation of MOLT-4 cells.

The uninfected (A), 2×10^3 (B), 2×10^4 (C) and 2×10^5 (D) of HIV-1 p24 infected MOLT-4 cells were observed by a phase-contrast microscope at 40X magnification. Association between the number of HIV-1 infection and the average of the syncytial cell (E). All data are shown as the mean \pm SEM of triplicate values.

4.6 Anti-HIV-1 PR Activity of Crude Extracts in HIV-1 Infected MOLT-4 Cells

The p24 or capsid protein is a cleavage product of Gag and Gag-Pol polyproteins from HIV-1 PR activity. Inhibition of HIV-1 PR induced the decrease of p24 production in HIV-1 infected cells. To study the anti-HIV-1 PR effect on infected MOLT-4 cells of the extracts, p24 levels were measured using HIV-1 p24 ELISA kit. Our data showed that 0.08 mg/ml LRH and LRE as well as 0.50 mg/ml LRW significantly inhibited the production of p24 in agreement with 2 μ M of DRV ($55.89 \pm 0.15\%$). Also, LRH, LRE and LRW displayed the percentages of relative inhibition of p24 level at 50.42 ± 1.59 , 49.25 ± 0.69 and 28.07 ± 3.68 , respectively.

For AP extracts, APH at 0.05 mg/ml significantly inhibited p24 production ($17.81 \pm 0.29\%$) of the infected cells compared to untreated cell controls. Conversely, APE ($4.59 \pm 4.23\%$) and APW ($9.70 \pm 1.12\%$) slightly inhibited p24 level in line with 0.1% DMSO ($7.33 \pm 0.71\%$), the results were presented in **Figure 30**.



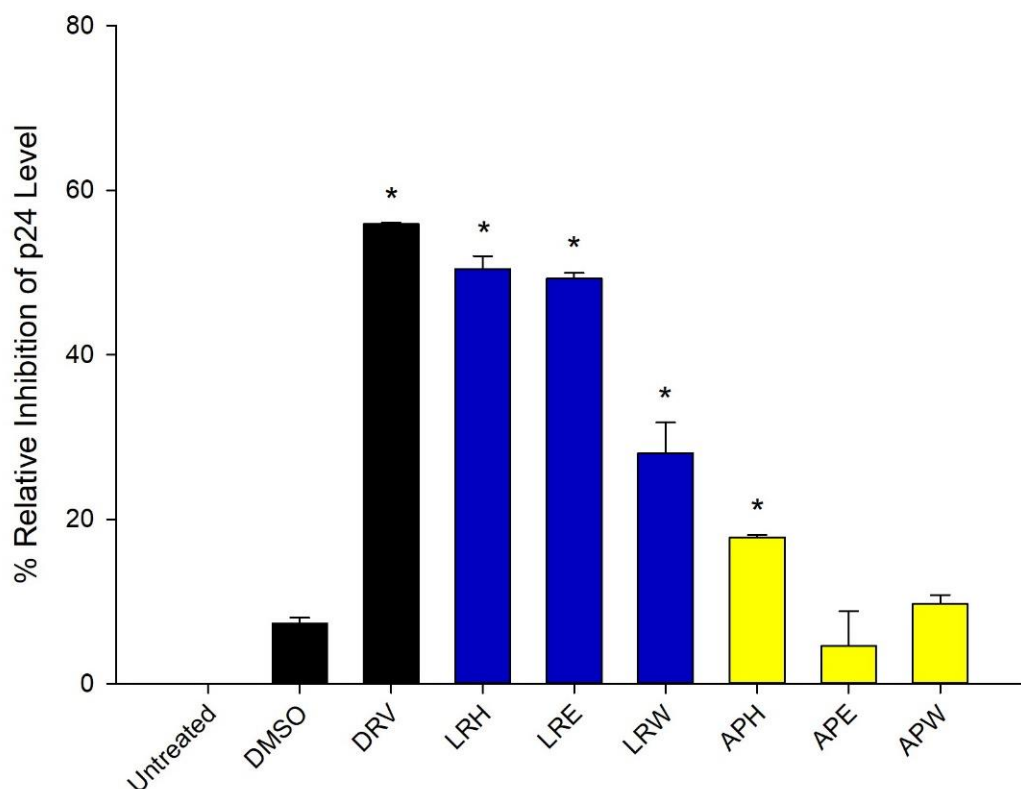


Figure 30 Inhibitory effect on p24 production in HIV-1 infected MOLT-4 cells of LR and AP crude extracts.

Blue and yellow bar represent LR and AP crude extracts. All data are shown as the mean \pm SEM of triplicate values. Statistical significance was analyzed by one-way ANOVA, Dunnett's test. * indicates $P < 0.05$, versus the vehicle control.

CHULALONGKORN UNIVERSITY

4.7 Anti-HIV-1 RT Activity of Crude Extracts in HIV-1 Infected MOLT-4 Cells

HIV-1 RT inhibitory activity of the crude extracts was examined by measuring the viral DNAs expression: -sssDNA and fIDNA. In the reverse transcription process, -sssDNA and fIDNA were synthesised in an early and late states of reverse transcription, respectively. The results showed that all LR extracts and DMSO showed an insignificant effect on the -sssDNA level (**Figure 31A**). Interestingly, only LRH significantly decreased the levels of fIDNA. On the contrary, LRE and LRW showed a slight reduction of the fIDNA levels in infected cells (**Figure 31B**).

Moreover, all AP extracts insignificantly decreased the –sssDNA levels (Figure 31A). In addition, APE and APH significantly inhibited fIDNA synthesis, in agreement with the effect of NVP. Conversely, APW weakly inhibited the fIDNA level (Figure 31B).

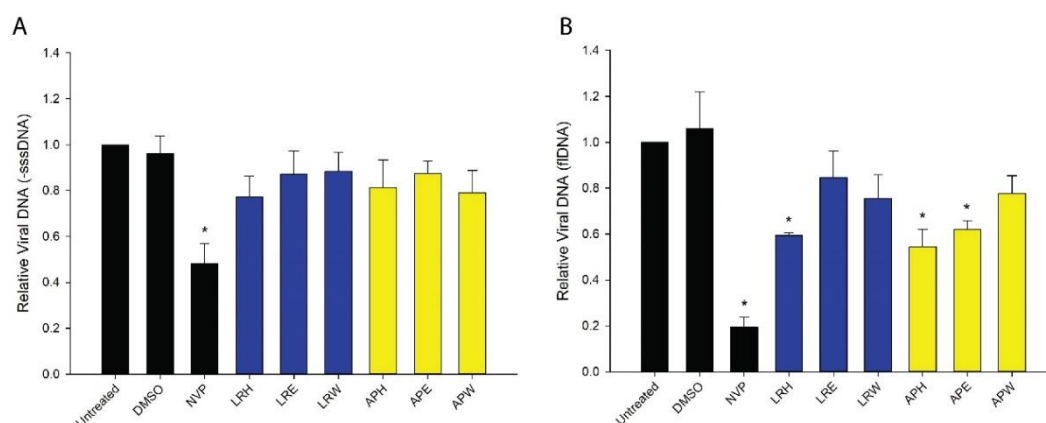


Figure 31 Real-time PCR analysis of HIV-1 DNAs expression.

(A) –sssDNA and (B) fIDNA expression in LR (blue) and AP (yellow) crude extracts treated HIV-1 infected MOL-4 cell line. All data are shown as the mean \pm SEM of triplicate values. Statistical significance was analyzed by one-way ANOVA, Dunnett's test.

* indicates $P < 0.05$, versus the vehicle control.

According to the *in vitro* non-cell based and cell-based assays, APH and LRH exhibited significant inhibition on both HIV-1 PR and RT. Since AP is a common edible mushroom, compounds presented within the crude extract, therefore are non-toxic. The phytochemicals that are responsible for the observed inhibitory activity would be valuable compounds for HIV-1 drug discovery. To our knowledge, the chemical constituents in AP have not been reported in the literature. The lacking of this important information, warrant investigation and identification of the phytochemicals in the APH crude extract as out next stage of research.

4.8 Isolation and Purification

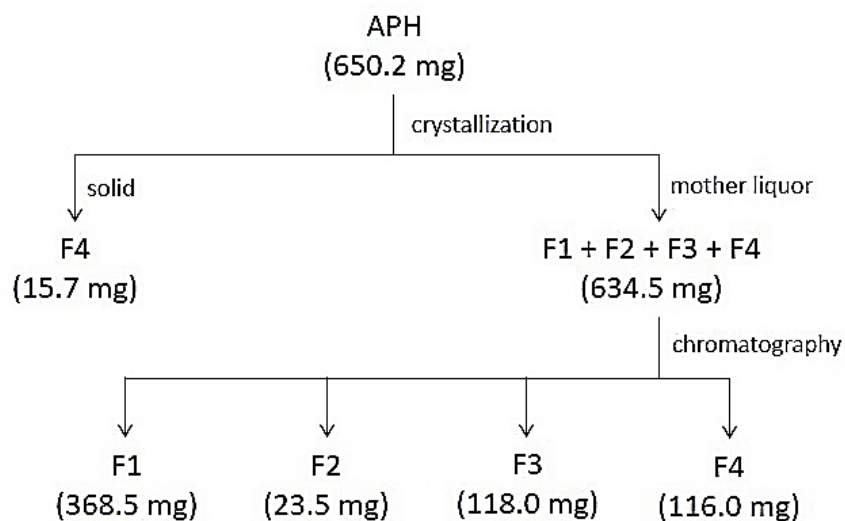


Figure 32 Schematic representation of APH isolation

Isolation and purification of APH were carried as summarised in Figure 4.13. The APH was analysed by TLC at varying proportion of hexane and ethyl acetate to develop an appropriate mobile phase system. The mobile phase system that provided a good separation was 80:20, v/v of hexane and ethyl acetate as showed in Table A1. Four fractions were isolated from this separation including F1, F2, F3 and F4. The F1, F2 and F4 were observed under UV light at a short wavelength (254 nm) while the F3 was detected at a long wavelength of UV (365 nm). F1, F2, F3 and F4 gave a retention factor (R_f) of 0.88, 0.61, 0.44 and 0.27, respectively.

The crude APH (650.2 mg) was dissolved in ethyl acetate to recrystallisation as white needles form. The crystallised compound was analysed by TLC compared to APH; it showed a band at the same retention time of F4. The crude mixture recovered from the mother liquor was separated using silica gel chromatography on [hexane/ethyl acetate (80:20, v/v)]. Unfortunately, based on TLC analysis some collected fractions showed impurity. Therefore, the Reveleris[®] prep purification system was used for purification of the mixture. By TLC analysis, these fractions were pooled to give four fractions: F1, F2, F3

and F4. The quantities are F1 (368.5 mg), F2 (23.5 mg), F3 (118.0 mg) and F4 (131.7 mg), as shown in **Table 9**.

Table 9 Chromatograph yield of crude APH

Fraction	Quantity (mg)	Percentage of total (%)
F1	368.5	56.67
F2	23.5	3.62
F3	118.0	18.15
F4	131.7	20.26

4.9 Identification

4.9.1 GC-MS analysis of pre-crystallisation of APH crude extract

The APH crude extract was analysed a chemical profile using GC-MS. Gas chromatogram showed five major compounds at a retention time of 22.434, 24.795, 24.873, 25.185 and 40.771 minutes (**Figure 33**). In addition to mass spectrometry (EI-MS) analysis [M^+] found m/z of 256.3, 280.3, 282.3, 284.3 and 396.4. The mass spectral library identified these m/z to be palmitic acid (12.02%), linoleic acid (23.75%), oleic acid (23.23%), stearic acid (12.20%) and ergosterol (25.75%), respectively. Moreover, a group of small peaks was found at retention time varies from 36.00 to 37.00 min with m/z of 376.3, there represented anthraergostapentene (3.05%) (**Table 10**).

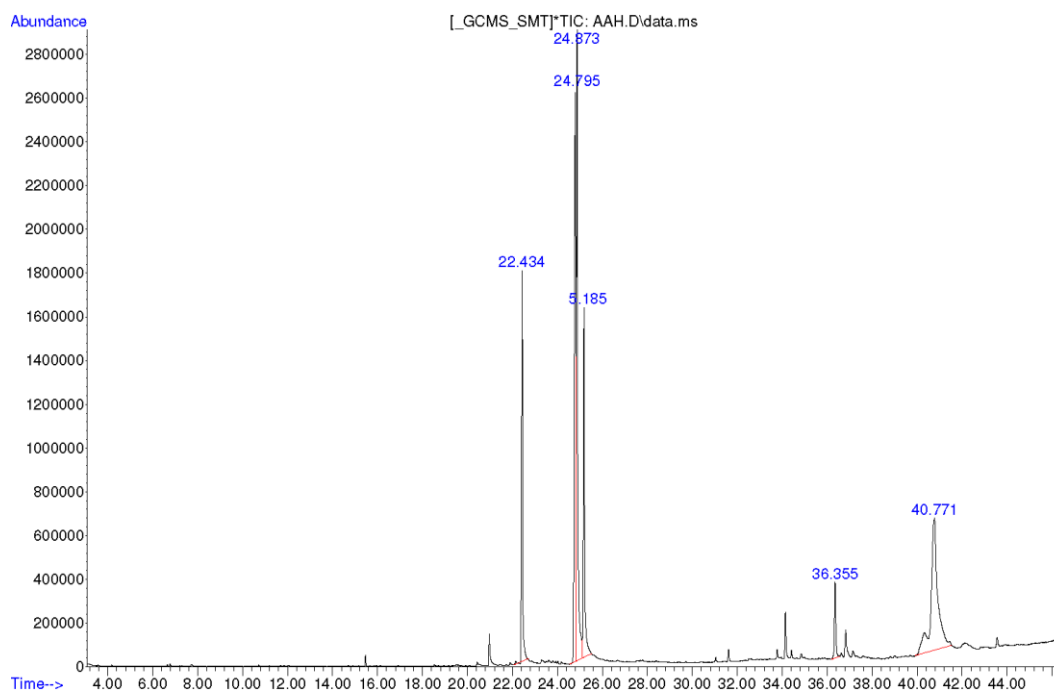


Figure 33 Gas Chromatogram of crude APH

Table 10 Chemical profile of APH from GC-MS analysis

RT (min)	Identified compounds	m/z	% Area of total
22.434	Palmitic acid	256.3	12.02
24.795	Linoleic acid	280.3	23.75
24.873	Oleic acid	282.3	23.23
25.185	Stearic acid	284.3	12.20
36.355	Anthraergostapentene	376.3	3.05
40.771	Ergosterol	396.4	25.75

The quantitative analysis of chemical constituents was determined by comparing with a standard curve of ergosterol. The commercial ergosterol was analysed by GC-MS with same method of the APH crude extract at vary concentrations: 0.5, 1.0, 2.0, 4.0, 6.0, 8.0 and 10.0 mg/ml. The abundance of peak area at each concentration was plotted to create the standard curve. The parameters of linear regression were calculated by

GraphPad Prism 7.03 software. The R square value (R^2) was 0.9983, the equation of slope was $Y = 184717209 \cdot X - 7406651$ (Figure 34).

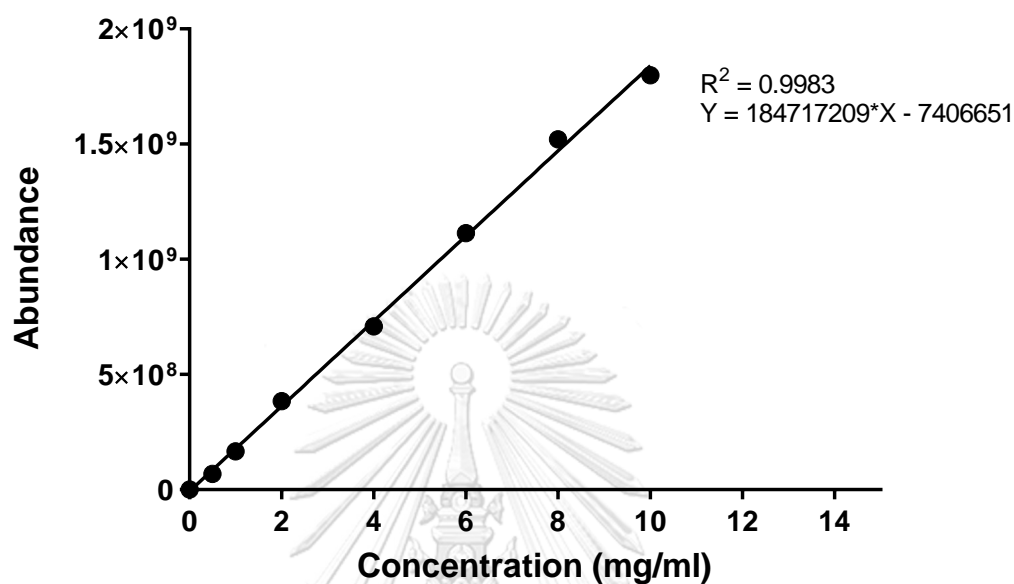


Figure 34 Standard curve of ergosterol by GC-MS analysis

From the GC-MS spectra, all concentrations of the pure ergosterol showed a group of minor peaks at retention time between 36.00 and 37.00 min with m/z of 376.4, there represent of anthraergostapentene (Figure 35). Moreover, the abundance of the peak areas was increased when increasing the concentration of the standard ergosterol. Therefore, the anthraergostapentene was more likely derived from the ergosterol. These data correlated with the APH crude extract chemical analysis, which also found the anthraergostapentene.

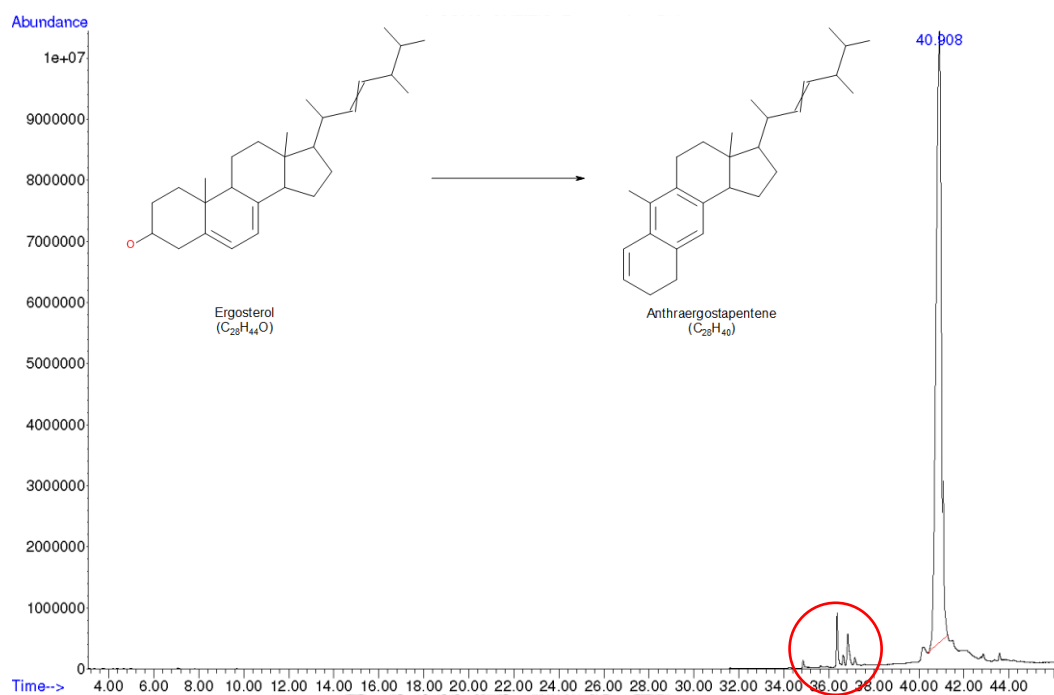


Figure 35 Gas chromatogram of commercial ergosterol at 10 mg/ml.

There showed the group of minor peaks in the red circle and structures of ergosterol and anthraergostapentene.

The quantity of APH (10 mg/ml) was analysed by GC-MS comparing with a standard curve of ergosterol. The results showed that at 10 mg/ml of APH was composed of palmitic acid, linoleic acid, oleic acid, stearic acid and ergosterol at concentrations of 0.733, 0.364, 0.679, 0.665 and 0.368 mg/ml, respectively (Table 11).

Table 11 Quantitative of APH analysis by GC-MS

Compound	Quantity (mg/10mg of APH)
Palmitic acid	0.364
Linoleic acid	0.679
Oleic acid	0.665
Steric acid	0.368
Anthraergostapentene	0.122
Ergosterol	0.733

From the quantitative profile analysis, 10 mg of APH crude extract yielded only 2.931 mg of total interested compounds or 29.31% of starting material. This value indicated a low productivity of GC-MS analysis. Some compounds were lost during the analysis. However, these results correlated with the calculation of the percentage of compounds. There showed a ratio of palmitic acid: linoleic acid: oleic acid: stearic acid: ergosterol is 1: 2: 2: 1: 2 in both of percentage and quantitative values.

4.9.2 The structure elucidation of fraction 1 (F1)

The F1 was obtained as pale yellow wax. The structure of F1 could be identified to triacylglycerol or fatty ester by its ^1H NMR signal pattern (**Figure 36**). The FTIR spectrum showed absorption bands at (cm^{-1}) 2921.41 and 2852.12 (C-H) and 1742.29 (C=O).

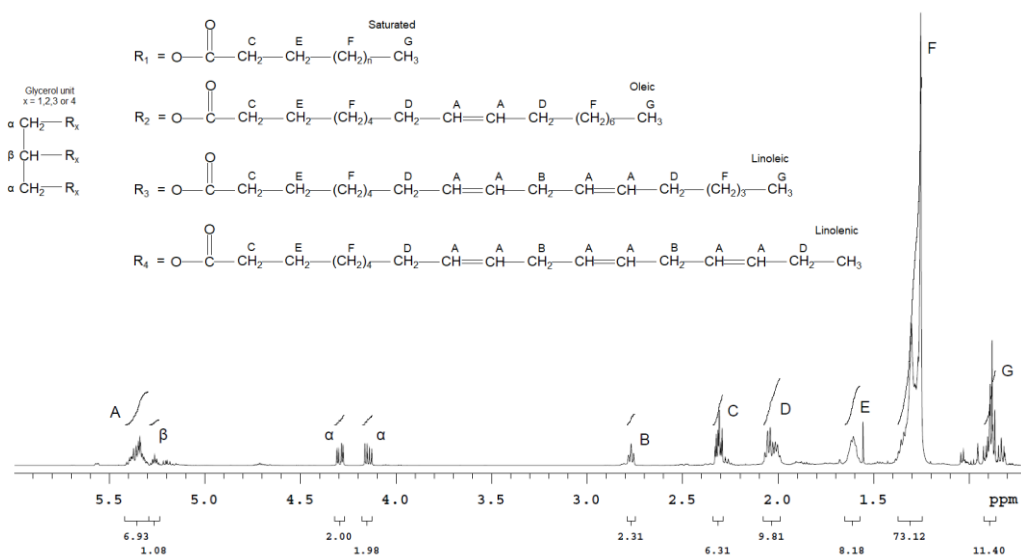


Figure 36 ^1H NMR spectrum of F1 showing the elucidated core structure and protons responsible for the chemical shifts observed

According to Chira N. *et al.* report, they suggested an evaluation of the computational methods for determining vegetable oils composition using ^1H NMR spectroscopy. Based on ^1H NMR spectra data, it was developed a system of chemometric equations leading to the determination of oils composition on four classes of fatty acids: linolenic acid, linoleic acid, mono-unsaturated fatty acids (oleic acid) and saturated fatty acids (palmitic acid, stearic acid) (112).

The following notations were adopted for following chemometric equations:

- X: molar ratio of linolenic acid
- Y: molar ratio of linoleic acid
- Z: molar ratio of mono-unsaturated fatty acid (oleic acid)
- T: molar ration of saturated fatty acid (palmitic acid, stearic acid)
- I_α , I_β , I_A , I_B , I_C , I_D , I_E , I_F , I_G : integral values of the corresponding signals
- k: spectrometer constant

$$k = \frac{\frac{I_E}{2} + \frac{I_C}{2} + \frac{I_{\omega-3} + I_G}{3}}{3} = \frac{\frac{8.18}{2} + \frac{6.31}{2} + \frac{0 + 11.40}{3}}{3} = 3.68$$

$$x = \frac{\frac{I_{\omega-3}}{3}}{3k} = \frac{\frac{0}{3}}{3 \cdot 3.68} = 0$$

$$y = \frac{\frac{I_B}{2} - 4kx}{2k} = \frac{2.31 - (4 \cdot 3.68 \cdot 0)}{2 \cdot 3.68} = 0.31$$

$$z = \frac{\frac{I_D}{4} - x - y}{4k} = \frac{\frac{9.81}{4} - 0 - 0.31}{4 \cdot 3.68} = 0.36$$

$$t = 1 - x - y - z = 1 - 0 - 0.31 - 0.36 = 0.33$$

$$\therefore x : y : z : t = 0 : 0.31 : 0.36 : 0.33 \approx 0 : 1 : 1 : 1$$

In conclusion, the chemometric calculation showed that triacylglycerol of F1 comprised linoleic acid, mono-unsaturated fatty acids and saturated fatty acids in the same proportion.

Hydrolysis of fraction (F1)

To confirm the fatty acids composition, the F1 was hydrolysed to form glycerol and three fatty acids (Figure 37). Then hydrolysed crude product was subjected to GC-MS analysis. Gas chromatogram showed four major peaks which are due to including palmitic acid, methyl ester (11.19%); linoleic acid, methyl ester (25.27%); oleic acid, methyl ester (20.99%) and stearic acid, methyl ester (12.20%) at retention time of 21.944, 24.259, 24.338 and 24.677, respectively. Moreover, the palmitic acid (3.56%), the incomplete esterification of fatty acid was found in this analysis, as shown in Table 12.

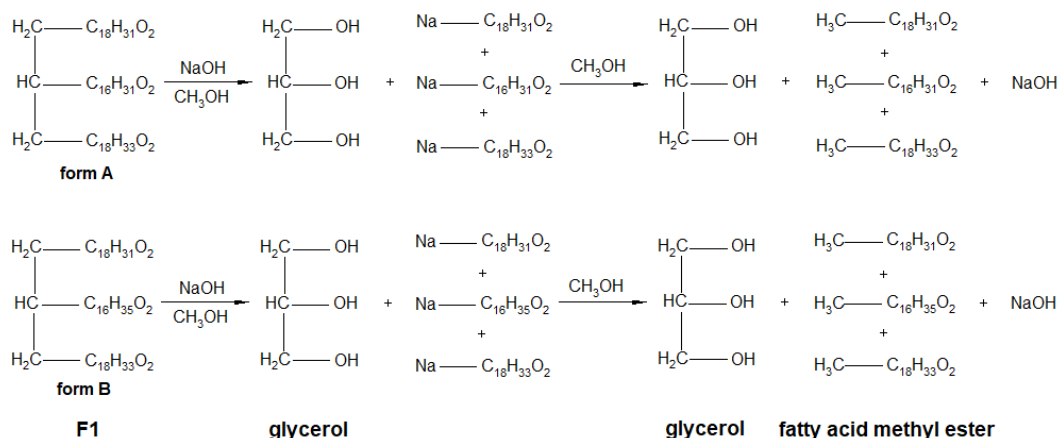


Figure 37 Hydrolysis reaction of F1.

$\text{CH}_3\text{C}_{16}\text{H}_{31}\text{O}_2$: palmitic acid, methyl ester; $\text{CH}_3\text{C}_{18}\text{H}_{31}\text{O}_2$: linoleic acid, methyl ester;
 $\text{CH}_3\text{C}_{18}\text{H}_{33}\text{O}_2$: oleic acid, methyl ester and $\text{CH}_3\text{C}_{18}\text{H}_{35}\text{O}_2$: stearic acid, methyl ester

These data indicated that the F1 contains two possible forms of triacylglycerols; form A and B. Form A of triacylglycerols should comprise a palmitic acid, linoleic acid and oleic acid. While form B of triacylglycerol comprises a stearic acid, linoleic acid and oleic acid. Two possible combinations were derived from the observed proportion of four fatty acids: palmitic acid, linoleic acid, oleic acid and stearic acid in the GC-MS analysis of hydrolysed F1. The ratio of the four acids was found to be 1 : 2 : 2 : 1, (Table 12). Due to oleic acid was classified as mono-unsaturated fatty acid, palmitic acid and stearic acid were classified as saturated fatty acids, the ratio of linoleic acid : mono-unsaturated fatty acid : saturated fatty acids is 1 : 1 : 1. These results correlated with the results from the chemometric calculation based on ^1H NMR analysis which was mentioned above.

Table 12 List of hydrolysed products and their corresponding fatty acids of F1 hydrolysis from GC-MS analysis

RT (min)	Hit name	m/z	% Area of total
21.944	Palmitic acid, methyl ester	270.3	11.188
22.435	Palmitic acid	256.3	3.561
24.259	Linoleic acid, methyl ester	294.3	25.269
24.338	Oleic acid, methyl ester	296.3	20.994
24.677	Stearic acid, methyl ester	298.3	12.199

Furthermore, the hydrolysed F1 was analysed by ^1H NMR spectroscopy; the ^1H NMR spectrum showed a signal of protons responding to methyl ester at a chemical shift of 3.666 ppm (Figure 4.20). These confirmed that fatty acid methyl esters were produced from the hydrolysis reaction and it related to the results of the GC-MS analysis.

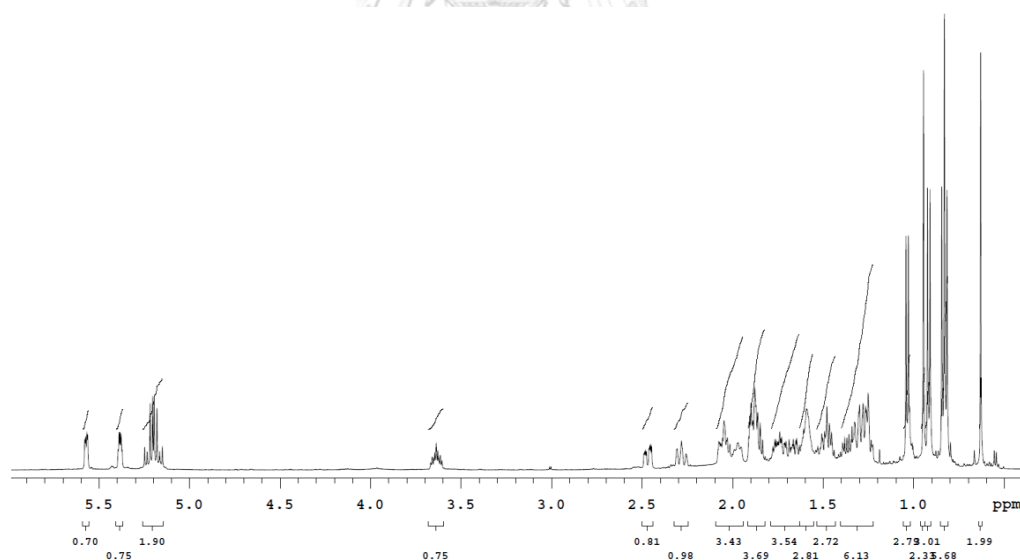


Figure 38 ^1H NMR spectrum of hydrolysed products from F1, showing a signal of protons responding to methyl ester at the chemical shift of 3.666 ppm

4.9.3 The structure elucidation of fraction (F2)

The F2 was obtained as yellow oil. The structure of F2 could be identified as triacylglycerol by its ^1H NMR signal pattern, and protons are responding to glycerol backbone at δ_{H} (ppm) 5.264 (1H at β -carbon), 4.282 (2H at α -carbon) and 4.148 (2H at α -carbon). Mass spectrum analysis indicated that the F2 has the molecular formula of $\text{C}_{55}\text{H}_{106}\text{O}_6$, which is supported by HRMS (ESI) $[\text{M}]^+ m/z$ 862.6072 (calculated for 862.7989). According to the molecular formula, the F2, triacylglycerol could be composed of two stearic acids and a palmitic acid in the molecule. Unfortunately, the ^1H and ^{13}C NMR spectra showed the sp^2 protons and sp^2 carbons. There should not be detected in the F2 because the stearic acid and palmitic acid are saturated fatty acids, they do not have sp^2 protons and sp^2 carbons in their molecules. These results indicated the impurity of F2; it contaminated with unsaturated fatty acids from the mixture.

Therefore, the preparative TLC was used to separate F2 from other compounds. The results showed good separation on the TLC plate when observed under UV light. Nevertheless, the ^1H NMR spectrum indicated the contaminated F2.

Even though the F2 could not be purified from the mixture, the F2 was identified as a triacylglycerol, which was composed of two stearic acid and palmitic acid from the spectroscopy data.

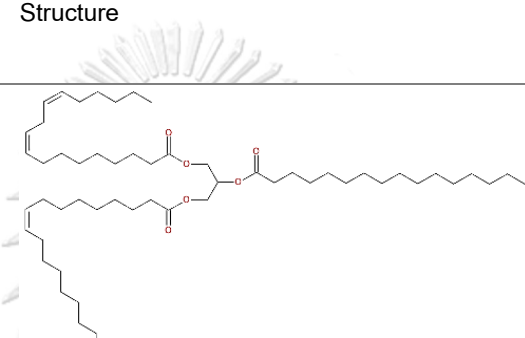
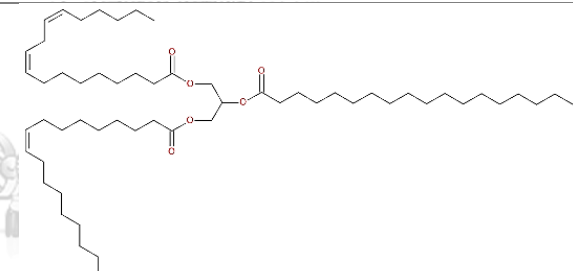
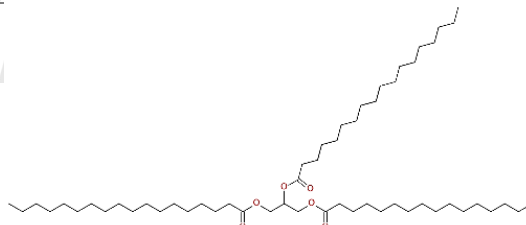
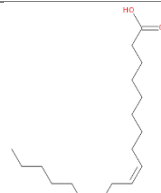
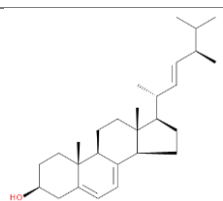
4.9.4 The structure elucidation of fraction (F3)

The F3 was obtained as a pale yellow oil. The structure of F3 could be identified as unsaturated fatty acid by its ^1H NMR signal pattern. The ^1H NMR showed peaks responding to alkene and allylic protons at δ_{H} (ppm) 5.344 ($\text{CH}=\text{CH}$) and 2.771 ($=\text{CH}-\text{CH}_2-\text{CH}=\text{}$), respectively. The FTIR spectrum showed absorption bands at (cm^{-1}) 2955.28, 2914.71 and 2847.62 (C-H); 1699.69 (C=O) and 1471.38, 1462.96 and 1429.69 (C=C). The mass spectroscopy data indicated that the F3 has the molecular formula of $\text{C}_{18}\text{H}_{32}\text{O}_2$, which is further supported by HRMS (ESI) $[\text{M} + \text{H}]^+ m/z$ 281.2468 (calculated for 281.2481). All spectroscopy data indicated that the F3 could be identified as linoleic acid (Table 13). F3, therefore, is one of the hydrolysed products from F1.

4.9.5 The structure elucidation of fraction (F4)

The F4 was obtained as white powder. Spectroscopy data indicated that the F4 has a molecular formula of $C_{28}H_{44}O$, it is supported by HRMS (ESI) $[M-H]^+$ found m/z 395.3303 (calculated for 395.3314). Moreover, the 1H and ^{13}C NMR data of F4 are in agreement with that reported in the literature for ergosterol (113) (Table 13).

Table 13 name, structure and molecular formula of constituent compounds of APH crude extract

Fraction	Name	Structure	Molecular formula
F1	Linoleoyl, oleoyl, palmitoylglycerol		$C_{55}H_{100}O_6$
	Linoleoyl, oleoyl, stearoylglycerol		$C_{57}H_{104}O_6$
F2	Distearoyl, palmitoylglycerol		$C_{55}H_{106}O_6$
F3	Linoleic acid		$C_{18}H_{32}O_2$
F4	Ergosterol		$C_{28}H_{44}O$

According to GC-MS analysis, there found five major compounds comprised four fatty acids and ergosterol. The structure elucidation of four fractions from chromatographed was identified that: F1 and F2 were triacylglycerols, F3 was linoleic acid and F4 was ergosterol. The results from GC-MS and spectroscopies of F3 and F4 were correlative, but F1 and F2 were not. This may occur due to the high temperature of GC-MS analysis induced a fragmentation of triacylglycerols to free fatty acids. Therefore the free fatty acids from triacylglycerols of F1 and F2 were found in the GC-MS analysis.

4.10 Molecular Modelling

All identified compounds and corresponding fatty acids were individually docked with HIV-1 PR and HIV-1 RT at the active site by using two different methods: CDOCKER and LibDock. The CDOCKER (114) generates random conformations by applying CHARMM forcefield and receptor-ligand interactions were further optimised using CHARMM. During the refinement, the receptor was held rigid while the ligands are allowed to be flexible. The CDOCKER interaction energy from CDOCKER analysis was considered to evaluating the ability of compounds to bind target protein. The lower energy represented, the better binding affinity. The other docking program, LibDock was performed in this study. The LibDock analysis is high-throughput docking algorithm to predict a binding ability between interested ligands and receptor, based on polar interaction sites. The outcome of this calculation was a LibDock score. The complex conformation with the higher score represented, the stronger binding affinity.

For molecular docking studies of HIV-1 PR, the X-ray crystal structure of HIV-1 PR in complex with amprenavir (APV) (PDB ID: 5KR0) was retrieved from RCSB Protein Data Bank. The inhibitor and water molecules were removed from the complex structure, then the protein structure was minimised to the stable conformation. To validate the CDOCKER protocol for HIV-1 PR docking, the APV was built and minimised energy conformation. Next, the inhibitor was re-docked into the same binding site of protein. The result from re-docking was compared to the original crystallographic conformation and position by overlapping the ligands from both methods. The 3D diagram of **Figure 39A** showed that

both ligands from extracted (green) and docked (purple) structures located at the same location. Moreover, the hydrogen bond interactions of APV with active site residues A: ASN25, A: GLY27, A: GLY47, B: GLY27, B: ASP30 and B: GLY49 also appeared in the docked pose of APV. The observed interactions validation indicated that this docking protocol was reasonable to determine the binding conformation accurately. In the meantime, LibDock protocol was validated by using the same method as CDOCKER. The **Figure 39B** displayed that docked APV (brown) was placed into the binding site of HIV-1 PR at the same pocket with the x-ray crystal structure. Moreover, they shared the hydrogen bond interactions at the active site only residue B: ASP30.



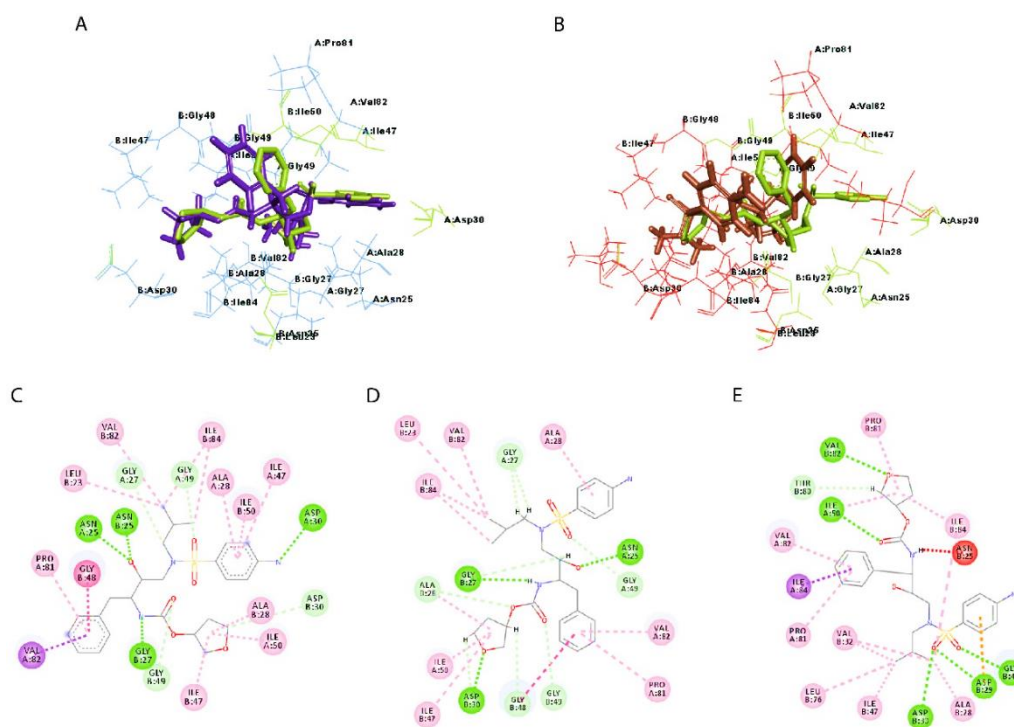


Figure 39 The validation methods for molecular docking study of HIV-1 PR.

The 3D diagrams of interaction between APV and HIV-1 PR at the active site (A) demonstrated overlapping between APV ligand from crystal (green) and CDOCKER (purple) and (B) demonstrated overlapping between APV from crystal (green) and LibDock (brown). The 2D ligands-receptor interactions of APV from (C) crystal, (D) CDOCKER and (E) LibDock structures with HIV-1 PR at the active site. Green and pink dashes represent hydrogen bond and hydrophobic bond, respectively.

The docking results showed that both CDOCKER and LibDock methods could be used to determine the binding interaction of a ligand at this binding site. However, the 3D diagrams showed that CDOCKER provided a better result compared to LibDock. Moreover, the ligand, when docked, was able to fit into the pocket in almost the same position and orientation as that of the reference inhibitor adopted in the crystal structure, using the CDOCKER method. While the ligand, from the LibDock experiment, was shown to be much more different, in both position and orientation. Also, CDOCKER showed a comparable number of hydrogen bond interactions as that observed between APV and the receptor.

site. While these interactions were found to be fewer when using LibDock. Therefore, CDOCKER could be a more suitable method than LibDock to be used in this study. As it can generate the structure almost same as reality. It was selected to determine the binding interactions of candidate ligands at the binding site of HIV-1 PR.

All candidate ligands were well docked into the HIV-1 PR active site except all triacylglycerols (F1 and F2). The bulkiness and large sizes of these molecules preventing them from binding into the receptor pockets. The ergosterol showed the lowest CDOCKER interaction energy (-55.6977 kcal/mol) among candidate ligands, followed by stearic acid (-47.7180 kcal/mol), oleic acid (-43.8028 kcal/mol), linoleic acid (-43.1114 kcal/mol) and palmitic acid (-40.6840 kcal/mol), respectively. Ergosterol has the closest binding score to reference inhibitor, APV (-64.8363 kcal/mol) which is approximately 10 kcal/mol higher. These results indicated that ergosterol is good candidate compound from CDOCKER analysis can bind the HIV-1 PR at the active site relatively very similar to the reference inhibitor.

Table 14 CDOCKER results at the active site of HIV-1 PR

Ligand	CDOCKER interaction energy (kcal/mol)
Ergosterol	-55.6977
Palmitic acid	-40.6840
Linoleic acid	-43.1114
Oleic acid	-43.8028
Stearic acid	-47.7180
APV	-64.8363

Although the CDOCKER interaction energies of the candidate compounds could not show the better energies than the reference inhibitor, they exhibited interesting results of the ligand-receptor interactions. The ligand-receptor interactions of these compounds displayed some sharing amino acid interactions with APV (Table A7). Notably, the

ergosterol shared amino acid interactions with the reference compound at active site residues A: ALA28, B: ALA28, B: ILE47 and B: ILE84, all of them interacted with hydrophobic bonds, as shown in the Figure 40.

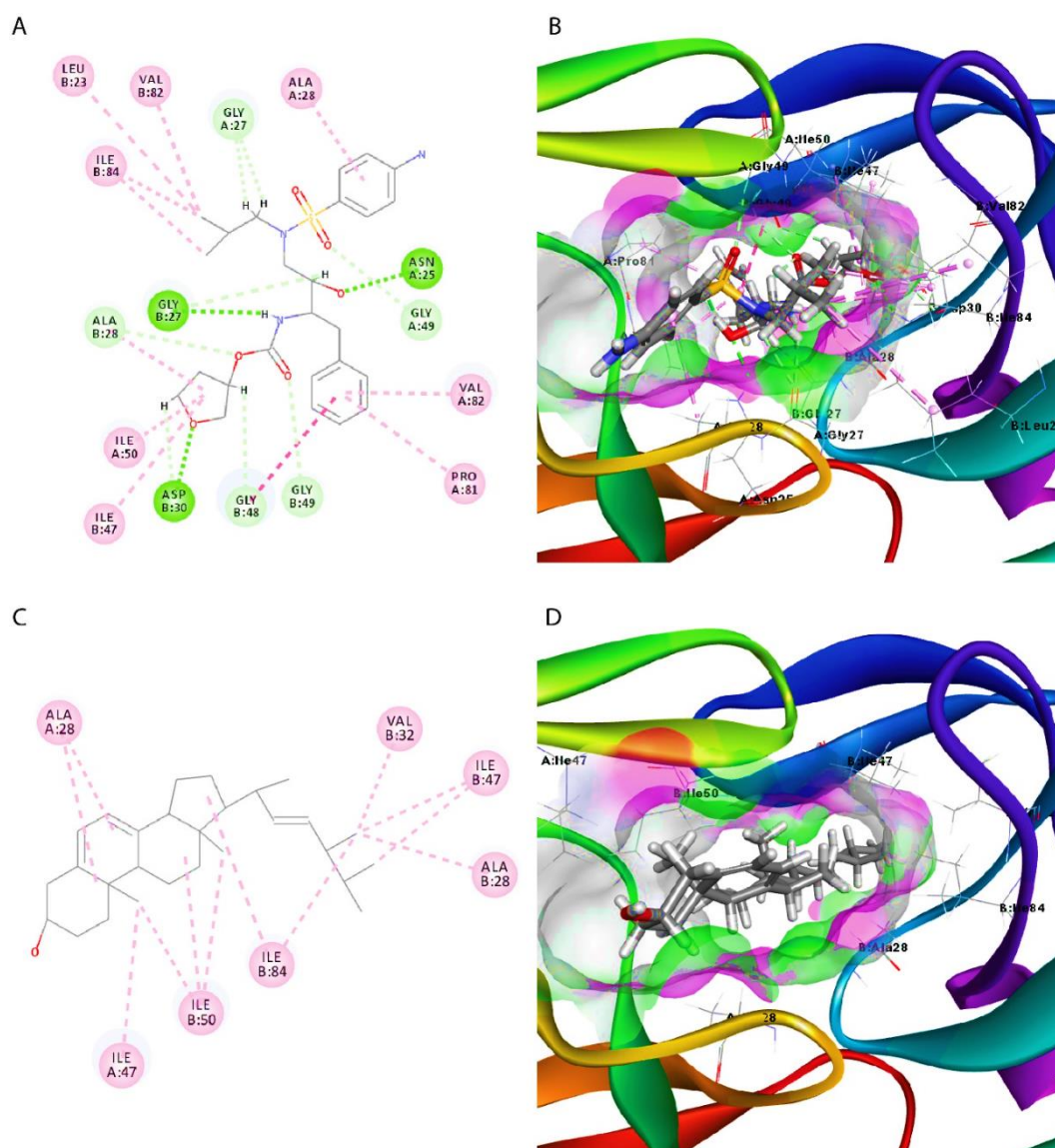


Figure 40 The interaction of candidate ligand and control at active site of HIV-1 PR.

The 2D and 3D interactions of (A and B) APV and (C and D) ergosterol at the active site of HIV-1 PR obtained from CDOCKER

Another interesting enzyme target to inhibit HIV-1 life cycle is HIV-1 RT. The HIV-1 RT is a multifunctional enzyme, including DNA polymerase and RNase H. In this study, we focused on both active sites of HIV-1 RT. At the DNA polymerase domain, the crystal structure of HIV-1 RT co-crystallised with nevirapine (NVP), the inhibitor of this active site (PDB ID: 3QIP) was used to perform molecular docking. To validate the protocol of CDOCKER, NVP was removed from the protein. The protein structure was minimised in DS 4.5 using the default setting. NVP was built and minimised separately to the lowest energy conformation in DS 4.5 using default parameters. NVP was re-docked into the same receptor pocket. The results of the re-docked structure was compared to x-ray crystal structure. The overlapping 3D diagrams of ligand from crystal (green) and docked (purple) structures showed that both of ligand located at the same location. Moreover, the all hydrogen bond interactions of NVP with active site residues A: LYS101 and A: TYR188 also found in the docked conformation of NVP (**Figure 41A**). For LibDock, the protocol was validated like previously described. The results show that NVP from LibDock was docked in the same pocket as NVP from the crystal structure. Both ligands from docked and crystal structure showed hydrogen bond interaction with A: LYS101 (**Figure 41B**). This validation indicated that CDOCKER provides more accurate determination of ligand binding conformation than that obtained using LibDock. The 3D diagram showed that CDOCKER almost perfectly overlapped with the extracted structure, while LibDock was a few differences. Therefore, to determine the binding affinity at DNA polymerase domain of HIV-1 RT, the CDOCKER was selected to perform docking experiment and bonding analysis.

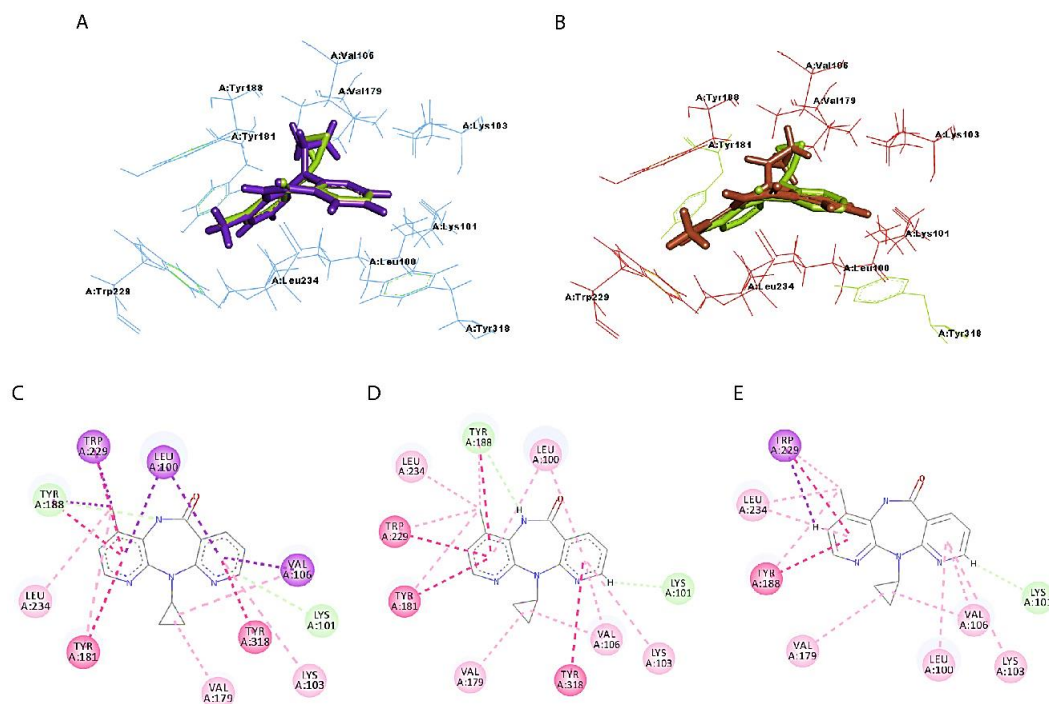


Figure 41 The validation methods for molecular docking study of HIV-1 RT at DNA polymerase domain.

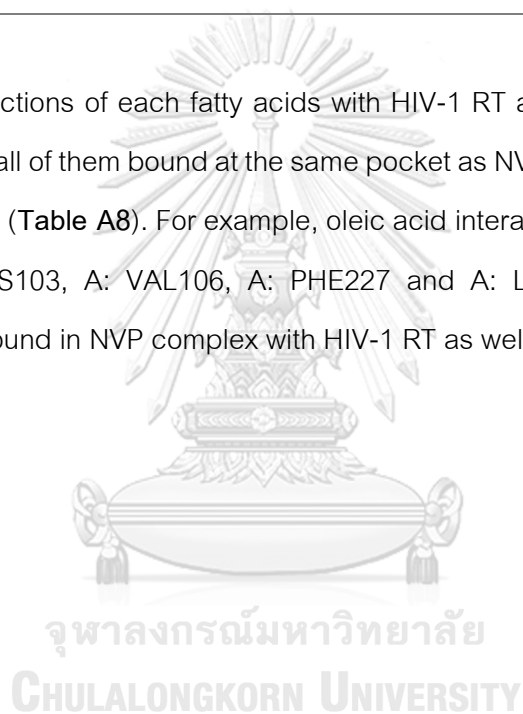
The 3D diagrams of interaction between NVP and HIV-1 RT at DNA polymerase active site. (A) demonstrated overlapping between NVP ligand from crystal (green) and CDOCKER (purple). (B) Demonstrated overlapping between NVP from crystal (green) and LibDock (orange). The ligand-receptor interactions of NVP from (C) crystal, (D) CDOCKER and (E) LibDock structures with HIV-1 RT at DNA polymerase domain.

The CDOCKER results between each all candidate compounds and HIV-1 RT at polymerase domain showed that all fatty acids could dock well in the pocket while ergosterol could not fit into this pocket. As this algorithm could not find the suitable poses for this ligand. Therefore, the CDOCKER program could not provide the CDOCKER interaction energy between ergosterol and HIV-1 RT at the DNA polymerase domain. All candidate fatty acids showed the lower CDOCKER interaction energies than NVP (-46.7181 kcal/mol), was used as a benchmark, except linoleic acid (-45.5989 kcal/mol). Oleic acid showed the lowest energy at -52.2567 kcal/mol, followed by stearic acid (-51.4032 kcal/mol) and palmitic acid (-50.2776 kcal/mol), respectively (Table 15).

Table 15 CDOCKER results at DNA polymerase domain of HIV-1 RT

Ligand	CDOCKER interaction energy (kcal/mol)
Ergosterol	No refine poses found for ligand
Palmitic acid	-50.2776
Linoleic acid	-45.5989
Oleic acid	-52.2567
Stearic acid	-51.4032
NVP	-46.7181

The interactions of each fatty acids with HIV-1 RT at DNA polymerase domain demonstrated that all of them bound at the same pocket as NVP and interacted with some similar amino acids (Table A8). For example, oleic acid interacts with active site residues A: LYS101, A: LYS103, A: VAL106, A: PHE227 and A: LEU234, these amino acid interactions were found in NVP complex with HIV-1 RT as well.



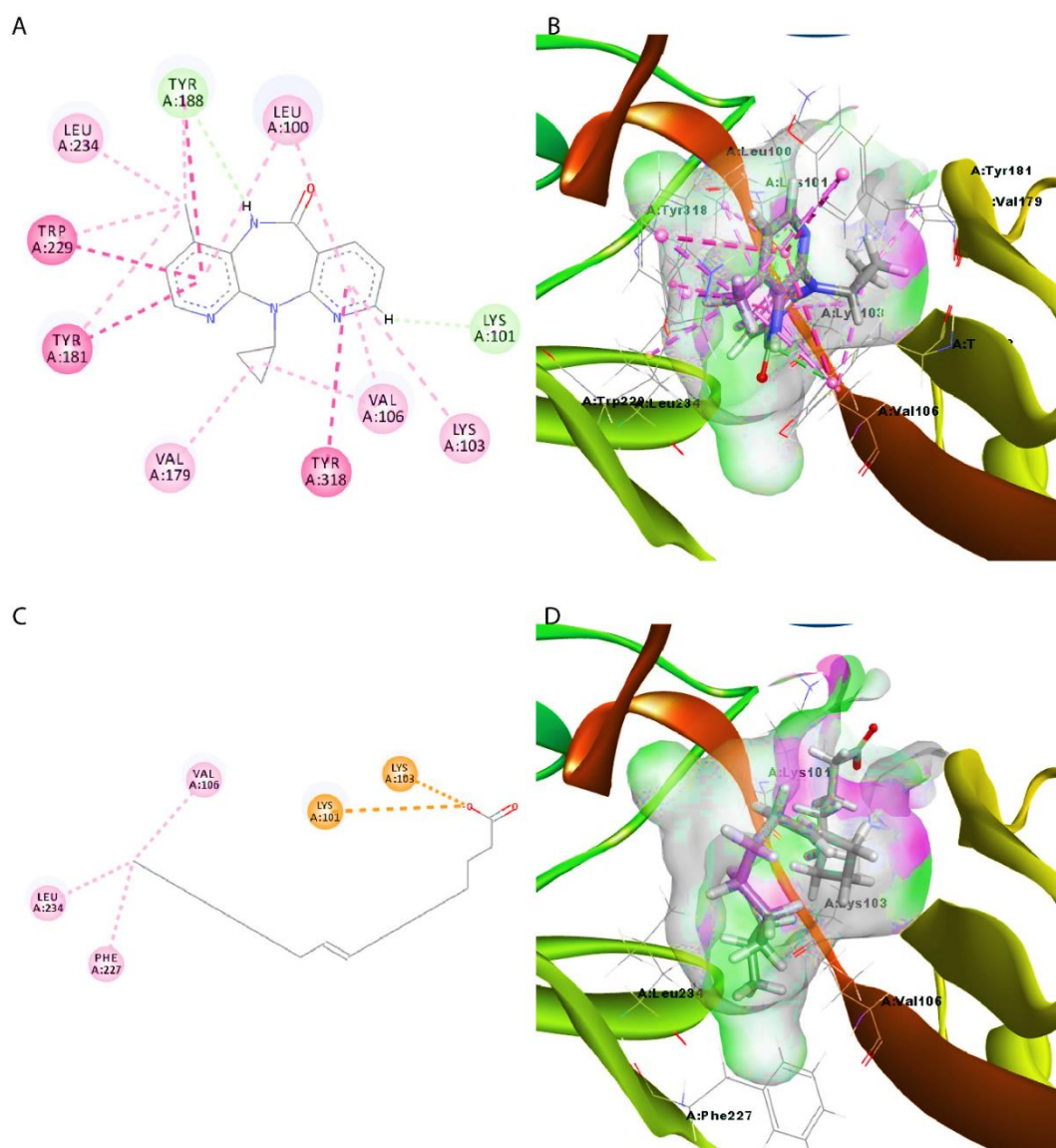


Figure 42 The interaction of candidate ligand and control at DNA polymerase active site of HIV-1 RT.

The 2D and 3D interactions of (A and B) NVP and (C and D) oleic acid at DNA polymerase domain of HIV-1 RT obtained from CDOCKER

For RNase H domain of HIV-1 RT, P4Y was docked into the binding site, which was defined by the original binding site of original RNase H inhibitor of HIV-1 RT (PDB ID: 3QIP). The CDOCKER analysis demonstrated the accuracy of this method, due to the P4Y placed on the same location as the structure from x-ray crystallisation. In addition, both ligands from crystal and docked structures shared some amino acid interactions: A:

ASP498 and A: ALA538 (Figure 43). The LibDock program also performed to determine the binding scores of the ligands. Unfortunately, all of the ligands included P4Y could not dock into RNase H active site. As the LibDock algorithm could not find the suitable binding site for the ligands. Therefore, the CDOCKER was used to perform molecular docking for HIV-1 RT at RNase H domain.

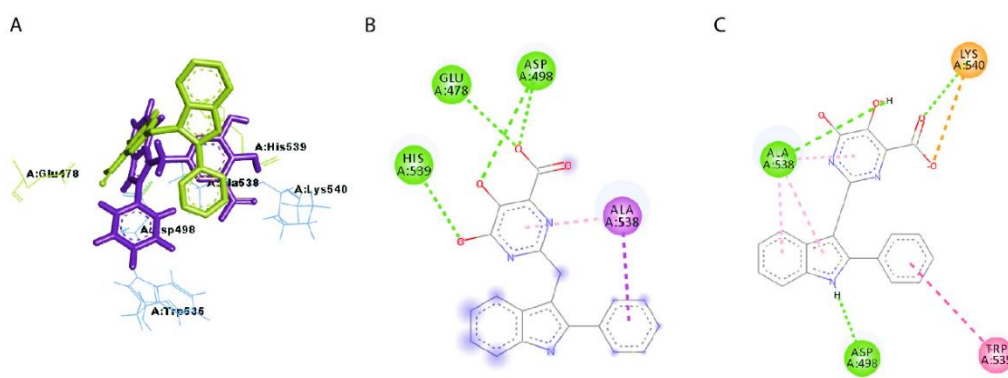


Figure 43 The validation methods for molecular docking study of HIV-1 RT at RNase H domain.

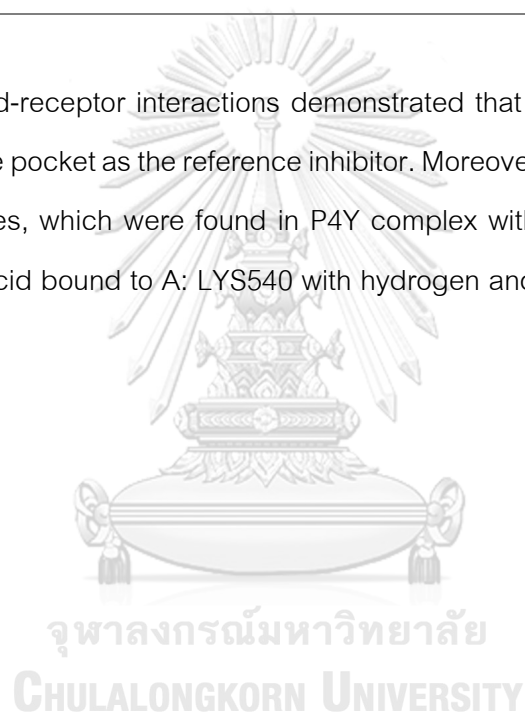
(A) The 3D diagrams of overlapping between P4Y ligand from crystal (green) and CDOCKER (purple) at RNase H active site of HIV-1 RT. The ligand-receptor interactions of P4Y from (B) crystal and (C) CDOCKER structures with HIV-1 RT at RNase H domain.

Surprisingly, all candidate compounds showed the CDOCKER interaction energies better than P4Y (-37.6826 kcal/mol), which was used as a benchmark. Stearic acid displayed the lowest energy (-45.9276), followed by oleic acid (-44.9924 kcal/mol), ergosterol (-41.7670 kcal/mol), palmitic acid (-41.5385 kcal/mol) and linoleic acid (-40.9939 kcal/mol), respectively (Table 16).

Table 16 CDOCKER results at RNase H domain of HIV-1 RT

Ligand	CDOCKER interaction energy (kcal/mol)
Ergosterol	-41.7670
Palmitic acid	-41.5385
Linoleic acid	-40.9939
Oleic acid	-44.9924
Stearic acid	-45.9276
P4Y	-37.6826

The ligand-receptor interactions demonstrated that all candidate ligands were docked in the same pocket as the reference inhibitor. Moreover, they interacted with some amino acid residues, which were found in P4Y complex with HIV-1 RT (Table A9). For example, stearic acid bound to A: LYS540 with hydrogen and hydrophobic bonds same as PY4.



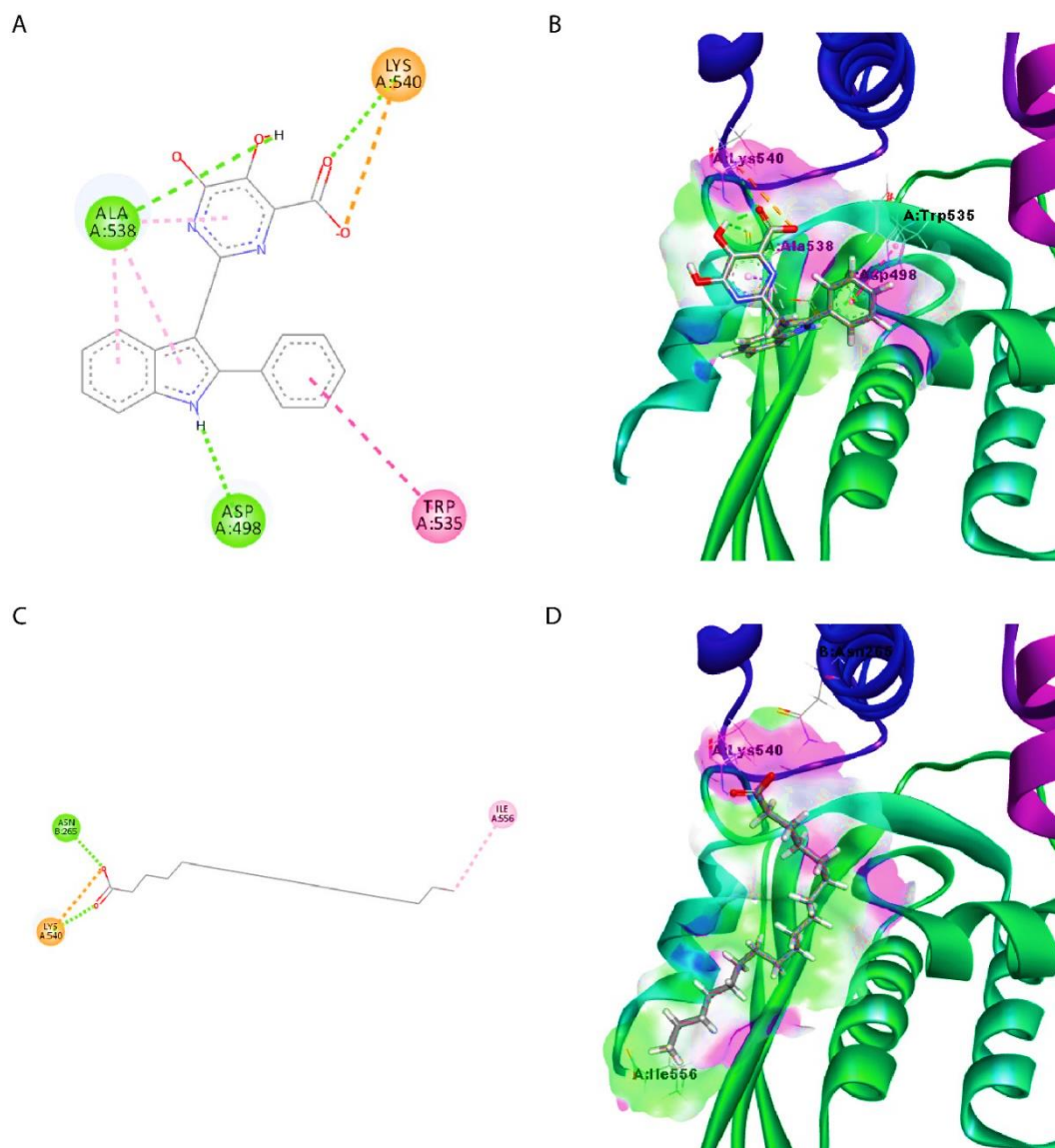


Figure 44 The interaction of candidate ligand and control at RNase H active site of HIV-1 RT.

The 2D and 3D interactions of P4Y (A and B) and stearic acid (C and D) at RNase H domain of HIV-1 RT obtained from CDOCKER

4.11 Cytotoxicity of APH Identified Compounds Against MOLT-4 Cells

All the identified compounds: ergosterol, palmitic acid, linoleic acid, oleic acid and stearic acid showed the CC_{50} greater than or equal to $2 \mu\text{M}$ at 24, 48 and 72 hours (Table 17). Linoleic and oleic acid did not exhibited noticeable toxicity on MOLT-4 cells. While ergosterol ($1 \mu\text{M}$), stearic acid ($1 \mu\text{M}$) and palmitic acid ($0.13 \mu\text{M}$) significantly reduced

MOLT-4 cell viabilities. However, all compounds did not harm the MOLT-4 cells greater than 50% (Figure 45A to 45E). Therefore, identified compounds at 2 μ M were used in further experiments.

Table 17 The fifty percent cytotoxic concentration (CC_{50}) of APH identified compounds after 24, 48 and 72 hours treatment

Compound	CC_{50} (μ M)		
	24 hours	48 hours	72 hours
Ergosterol	> 2.00	> 2.00	> 2.00
Palmitic acid	> 2.00	> 2.00	> 2.00
Linoleic acid	> 2.00	> 2.00	> 2.00
Oleic acid	> 2.00	> 2.00	> 2.00
Stearic acid	> 2.00	> 2.00	> 2.00

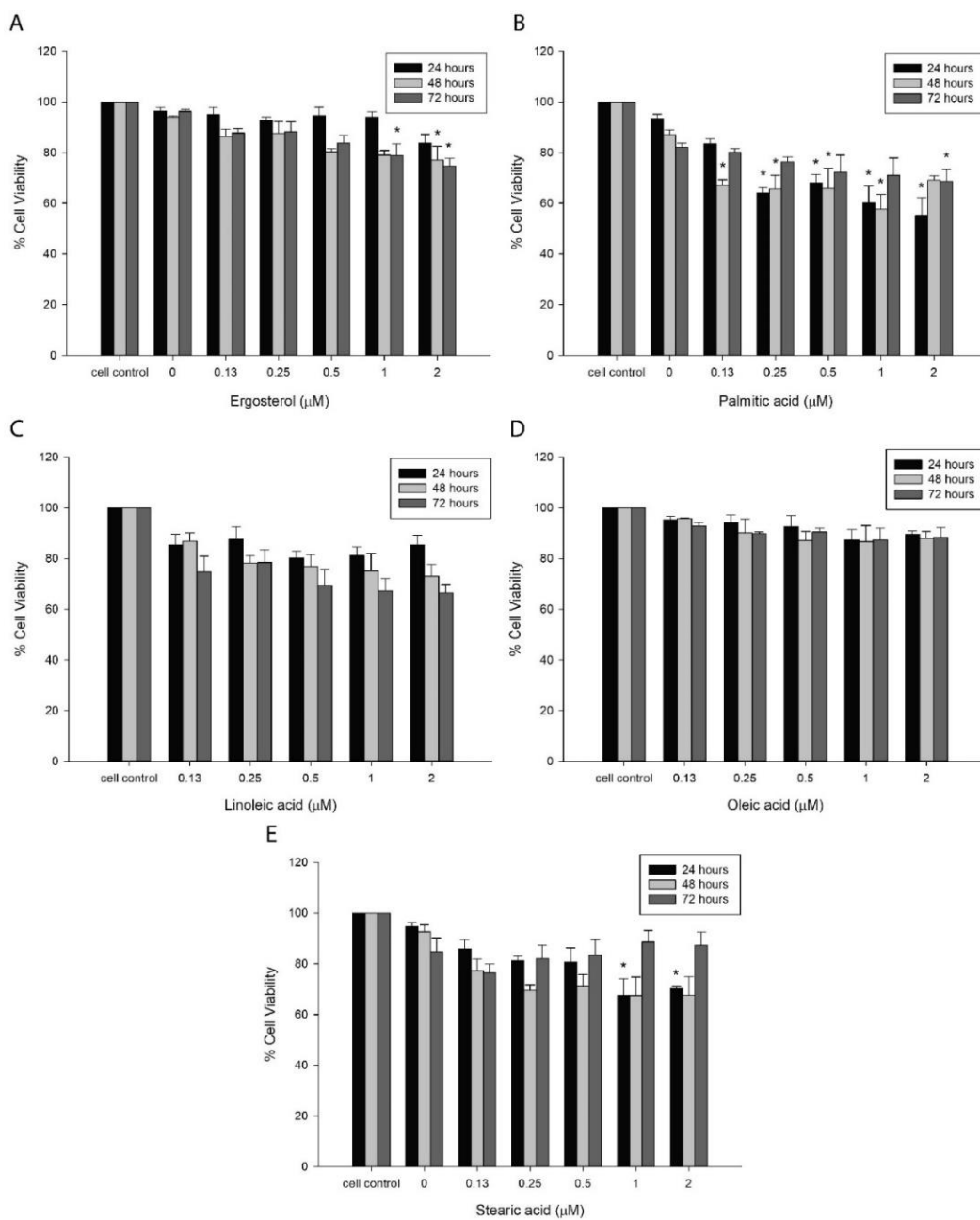


Figure 45 The cytotoxicity at various concentrations of ergosterol, palmitic acid, linoleic acid, oleic acid and stearic acid on MOLT-4 cells after 24, 48 and 72 hours of treatments. All data are shown as the mean \pm SEM of triplicate values. Statistical significance was analyzed by one-way ANOVA, Dunnett's test. * indicates $P < 0.001$, versus the vehicle control.

4.12 Anti-HIV-1 PR Activity of APH Identified Compounds in HIV-1 Infected MOLT-4 Cells

The results displayed that ergosterol, linoleic acid, oleic acid and palmitic acid significantly decreased p24 levels with percentages of relative inhibition at 28.29 ± 5.91 , 27.46 ± 6.93 , 33.35 ± 1.99 and 27.82 ± 1.11 , respectively, versus untreated cell control. In contrast, stearic acid exhibited insignificant inhibition of p24 at $24.08 \pm 8.80\%$ level (Figure 46).

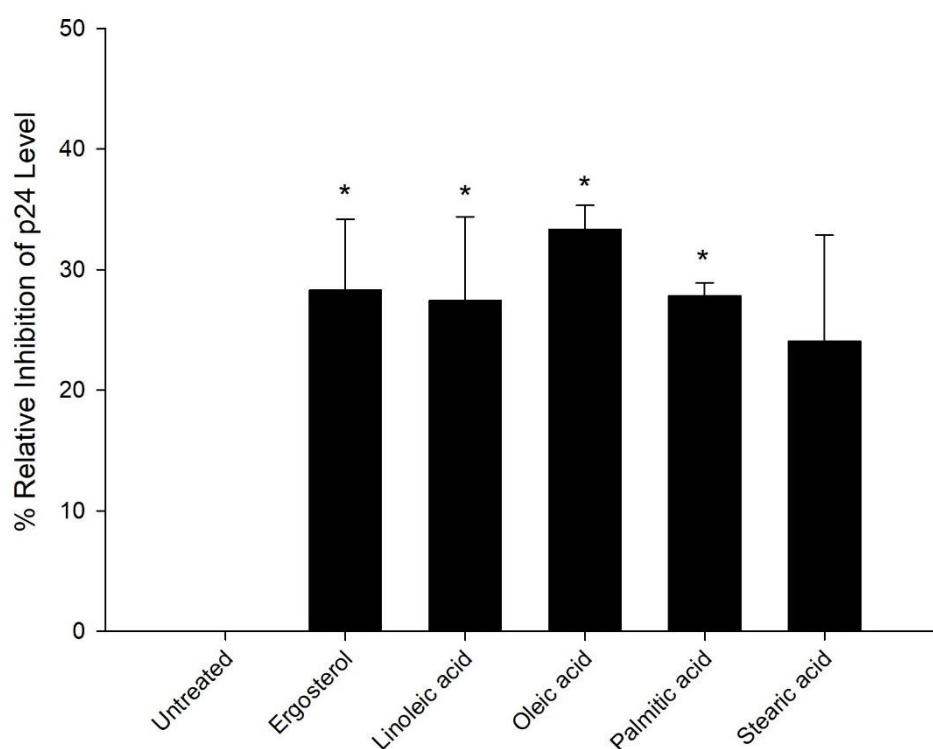


Figure 46 Inhibitory effect on p24 production in HIV-1 infected MOLT-4 cells of APH isolated compounds.

All data are shown as the mean \pm SEM of triplicate values. Statistical significance was analyzed by one-way ANOVA, Dunnett's test. * indicates $P < 0.05$, versus the vehicle control.

4.13 Anti-HIV-1 RT Activity of APH Identified Compounds in HIV-1 Infected MOLT-4 Cells

To determine the activity of identified compounds on anti-HIV-1 RT in HIV-1 infected MOLT-4 cells, the cells were treated with 2 μ M of each compounds for 24 hours, then measure HIV-1 DNAs: -sssDNA and fDNA expression by real-time PCR. Unfortunately, all identified compounds did not show significant inhibition on both -sssDNA and fDNA levels compared to untreated cell control (Figure 47A and 47B).

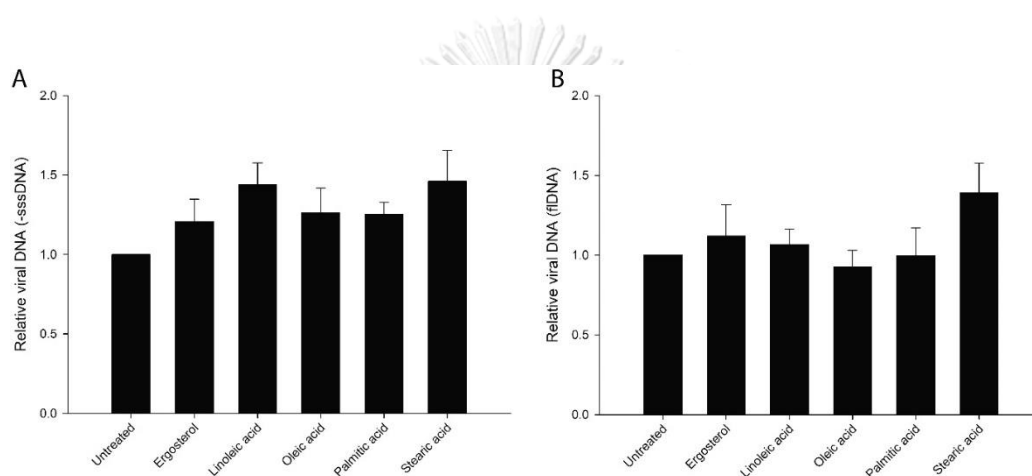


Figure 47 Real-time PCR analysis of HIV-1 DNAs expression.

(A) -sssDNA and (B) fDNA expression in APH isolated compounds treated HIV-1 infected MOLT-4 cell line. All data are shown as the mean \pm SEM of triplicate values. Statistical significance was analyzed by one-way ANOVA, Dunnett's test.

CHAPTER V

DISCUSSION

HIV-1 infected patients cannot completely eradicate all of the viruses from their body. Taking antiretroviral drugs is necessary to control the virus in the body. At present, a considerable number of effective antiretroviral drugs are available. However, there are some limitations such as drug resistance (4) and adverse effects of the antiretroviral drugs. Many side effects from antiretroviral medications have been reported including mitochondrial toxicity of long-term treatment with nucleotide reverse transcriptase inhibitors (NRTIs) (5), hepatotoxicity of NVP administration (6), hypersensitivity and lipodystrophy (8). Therefore, the discovery of antiretroviral drugs with better efficacy and lower side effect has been attracted much attention. Researchers found that several active compounds exhibiting anti-HIV-1 property isolated from mushrooms such as *Pleurotus nebrodensis* (34), Velleratretraol from *Lactarius vellereus* (35) and melanin-glucan complex from *Fomes fomentarius* (36). Although AH, LR and AP have been studied for several medicinal properties, information on anti-HIV-1 activity is yet to discovered. In this study, we are interested in the inhibitory activity of those mushrooms against the two HIV-1 enzymes which are HIV-1 PR and HIV-1 RT.

For AH crude extracts, all extracts exhibited significant inhibition on both HIV-1 PR and RT activities. Unfortunately, AHH and AHE displayed strong toxicity toward MOLT-4 cells which were used as a cell model. Thus, these extracts were not tested further in the infected cell-based assays. MOLT-4 cell is a lymphoblastic leukemia cell which has been generally used as a cell model for lymphoblastic leukemia researches (115, 116). These data suggest that AHH and AHE could have an anti-proliferative property against the leukemia cell. However, there should be further investigated carefully.

Besides, all LR extracts significantly inhibited HIV-1 PR activity *in vitro* screening assay as compared with vehicle control. Interestingly, among all LR extracts, LRH displayed the highest inhibition of HIV-1 PR activity. The LRH inhibitory potency was

comparable to pepstatin, a known inhibitor of HIV-1 PR. Moreover, all LR extracts also significantly inhibited p24 production in HIV-1 infected MOLT-4 cells. The percentages of p24 inhibition by LRH and LRE were in line with DRV. These results suggest that LRH inhibit HIV-1 PR activity in both *in vitro* non-cell-based and cell-based assays.

According to the results of anti-HIV-1 RT activity in infected MOLT-4 cells of LR crude extracts, detections of the viral DNAs synthesis were performed after LR crude extracts treatment. Only LRH significantly inhibited the synthesis of fDNA whereas the extract induced no change of –sssDNA level. These data suggest that LRH could interfere with the late reverse transcription of the viral life cycle by inhibiting HIV-1 RT activity in the infected cells.

Due to a limitation of reverse transcriptase inhibitor screening kit, this method detects DNA/RNA hybrid products which were synthesised by HIV-1 RT-associated DNA polymerase activity but not the HIV-1 RT-associated RNase H activity. The –sssDNA was generated by copying the viral RNA template using DNA polymerase active site. While the fDNA was synthesized by cooperating of both DNA polymerase and the RNase H active sites (3). Thus, DNA polymerase inhibitory activities in both *in vitro* non-cell based and cell-based assays of LRH were supported each other. Moreover, we found that LRH could inhibit RNase H-associated HIV-1 RT in the infected cells. In agreement with Tanese N, *et al.*, the constructed mutant moloney murine leukemia viruses exhibited reverse transcriptase but lacked of RNase H activities were generated –sssDNA synthesis but not fDNA (117). These are relevant to our results that LRH treated infected cells synthesized –sssDNA but not fDNA. Our data suggest that LRH could inhibit HIV-1 RT activity by blocking the RNase H active site.

In the present finding, LRE and LRW showed no significant inhibition on HIV-1 RT in the HIV-1 infected MOLT-4 cells. In contrast, both extracts significantly inhibited the RT activity in the screening assay. In the HIV-1 life cycle, reverse transcription occurs in the cytoplasm of the host cells (29). In order to inhibit the HIV-1 RT activity, the enzyme inhibitor needed to be passed into the cells. Lacking property to access the cells could

be a reason of candidate compounds from LRE and LRW unable to induce any inhibition. In addition, modification and biodegradation of the compounds inside the cells could lead to the non-functional substances that might reduce the inhibitory activity of the compounds.

For anti-HIV-1 activities of AP crude extracts, we demonstrated that APH and APE significantly inhibited HIV-1 PR in the screening assay. Conversely, in the HIV-1 infected MOLT-4 model, only APH showed significant inhibition on this enzyme by suppressing p24 production. Interestingly, APH significantly inhibited HIV-1 PR activity not only in the non-cell based but also cell-based assays. These results indicate that APH could inhibit HIV-1 replication by blocking HIV-1 PR activity.

From HIV-1 RT inhibition results by AP crude extracts; all extracts significantly inhibited HIV-1 RT in the non-cell-based assay. In the HIV-1 infected MOLT-4 cells, all extracts did not show inhibition of -sssDNA levels. In contrast, APH and APE displayed a significant reduction of fDNA production. These data suggest that APH and APE could inhibit HIV-1 RT at late reverse transcription by blocking RNase H domain.

Herein, we studied only the chemical constituents of APH because it has shown significant inhibitory activities on both HIV-1 PR and RT. We found that APH was composed of three triacylglycerols (F1A, F1B and F2), linoleic acid (F3) and ergosterol (F4). These results agreed with the previous studies whether fungi are source of fatty acids, the major fatty acids were palmitic, stearic, oleic and linoleic acid (118). Moreover, Ruess L, *et al.* reported that many edible mushroom species had a high proportion of unsaturated fatty acid, especially linoleic acid (119). Besides, linoleic acid is a precursor of 1-octen-3-ol, the aromatic compound might give mushroom its flavour (120).

Barreira J.C.M., *et al* found that triacylglycerols were chemical fingerprint of mushroom species, each mushroom species has different composition of triacylglycerol (121). These data supported our finding about triacylglycerols of APH. Furthermore, it could be a beneficial data for mushroom species identification using triacylglycerol profile.

Ergosterol was a common sterol detected in fungi (118), it is a cell membrane component of fungi. Moreover, it is also a provitamin of vitamin D₂, called ergocalciferol. Vitamin D₂ is a form of vitamin D was produced in fungi and yeast by a UVB-exposure of ergosterol. Another form of vitamin D is vitamin D₃, it is produced by UVB-exposure of 7-dehydrocholesterol (provitamin D₃) in the skin. Previous studies indicated that vitamin D₂ and vitamin D₃ acts equally in maintaining vitamin D status. Food sources of vitamin D₂ are very limited and wild mushrooms are one of the only significant sources of vitamin D₂ (122). Moreover, Campbell GR., *et al* reported that vitamin D could inhibit HIV-1 replication in macrophages via the induction of autophagy (123).

In vitro cell based assay demonstrated that ergosterol, linoleic acid, oleic acid and palmitic acid significantly inhibited HIV-1 PR activity in the HIV-1 infected MOLT-4 cells by reducing p24 levels. These compounds could be active substances of APH that provided HIV-1 PR inhibition effect. Based on the chemical structure of ergosterol, it is classified as triterpenoid. Interestingly, from previous reports found that several triterpenoids such as oleanolic acid, uvaol, ursolic acid, maslinic acid and 2 α , 19 α -dihydroxy-3-oxo-12-ursen-28-oic acid exhibited anti-HIV-1 PR (124-126). Moreover, Lee DY-W, *et al.* demonstrated that palmitic acid could inhibit viral entry by directly blocking gp120-CD4 complex formation (127). Besides, Linoleic and Oleic acid could inhibit HIV-1 RT activity in non-cell based determination (128).

Computer-aid molecular docking has provided three dimensional understanding of possible molecular interactions between studied compounds and the target proteins. Ergosterol, linoleic acid, oleic acid and palmitic acid were shown to bind to the specific site of HIV-1 PR. These results support that those compounds could be active constituents of APH that inhibit HIV-1 replication by blocking the catalytic activity of HIV-1 PR.

Unfortunately, no identified compounds of APH displayed significant results of anti-HIV-1 RT activity in HIV-1 infected MOLT-4 cells. In contrast, APH, the mixture of these identified compounds significantly inhibited HIV-1 RT activity at late reverse transcription by suppressing fDNA synthesis. These results indicate that a single identified compound

could not provide an inhibitory effect on HIV-1 RT, but the crude extract could inhibit HIV-1 RT function. From the previous report, Kametani S, *et al.* studied on the synergistic effect of chemical constituents from dichloromethane crude extract of *Aloe ferox* Miller for Ehrlich ascites tumour cell growth inhibition. They suggested that the inhibitory effect of crude extract did not depend on an isolated compound alone, but on the synergistic effect from the combination of the compounds (129). Therefore, the synergistic effect of our identified compounds should be evaluated further as a potential HIV-1 inhibitor.



CHAPTER VI

CONCLUSION

In the screening approaches, AH, LR and AP crude extracts exhibited anti-HIV-1 activities on both HIV-1 PR and RT. In addition to the HIV-1 infected cell-based assays, LR and AP crude extracts showed HIV-1 inhibitory activities. In addition, the HIV-1 infected cell-based assays showed that LR and AP crude extracts could inhibit HIV-1 activities. Especially, LRH and APH showed strong inhibition effects on not only HIV-1 PR but also RT. Herein, we studied specifically the phytochemical constituents of APH. Four major compounds were successfully isolated from APH. The chemical analysis of these four compounds by various analytical methods, confirm their identity to be contain two triacylglycerols, linoleic acid and ergosterol. For triacylglycerols, they comprised of four corresponding fatty acids: palmitic acid, linoleic acid, oleic acid and stearic acid. Quantitative of fatty acids composition showed a higher proportion of unsaturated fatty acids than saturated fatty acids. *In vitro*, cell-based assays exhibited that ergosterol, linoleic acid, oleic acid and palmitic acid significantly inhibited p24 production in the infected MOLT-4 cells. Besides, *in silico* approach supported that the identified compounds showed affinities to bind with specific sites of HIV-1 PR, in line with APV. Unfortunately, single identified compounds could not inhibit HIV-1 RT in the infected MOLT-4 cells. These results suggested that AP could be a good source of therapeutic fatty acids and ergosterol which have the anti-HIV-1 property. Furthermore, our results provided useful data for HIV-1 PR and RT drugs development.

REFERENCES



จุฬาลงกรณ์มหาวิทยาลัย
CHULALONGKORN UNIVERSITY

1. Smith T, Srinivasan A, Schochetman G, Marcus M, Myers G. The phylogenetic history of immunodeficiency viruses. *Nature*. 1988;333(6173):573.
2. Barré-Sinoussi F, Ross AL, Delfraissy J-F. Past, present and future: 30 years of HIV research. *Nature Reviews Microbiology*. 2013;11(12):877.
3. Sarafianos SG, Marchand B, Das K, Himmel DM, Parniak MA, Hughes SH, et al. Structure and function of HIV-1 reverse transcriptase: molecular mechanisms of polymerization and inhibition. *Journal of molecular biology*. 2009;385(3):693-713.
4. Apisarnthanarak A, Jirayasethpong T, Sa-nguansilp C, Thongprapai H, Kittihanukul C, Kamudamas A, et al. Antiretroviral drug resistance among antiretroviral-naïve persons with recent HIV infection in Thailand. *HIV medicine*. 2008;9(5):322-5.
5. Brinkman K, ter Hofstede HJ, Burger DM, Smeitink JA, Koopmans PP. Adverse effects of reverse transcriptase inhibitors: mitochondrial toxicity as common pathway. *Aids*. 1998;12(14):1735-44.
6. Wongtrakul J, Paemanee A, Wintachai P, Thepparit C, Roytrakul S, Thongtan T, et al. Nevirapine induces apoptosis in liver (HepG2) cells. *Asian Pacific journal of tropical medicine*. 2016;9(6):547-53.
7. Ammassari A, Murri R, Pezzotti P, Trotta MP, Ravasio L, De PL, et al. Self-reported symptoms and medication side effects influence adherence to highly active antiretroviral therapy in persons with HIV infection. *Journal of acquired immune deficiency syndromes*. 2001;28(5):445-9.
8. Carr A, Cooper DA. Adverse effects of antiretroviral therapy. *The Lancet*. 2000;356(9239):1423-30.
9. Montessori V, Press N, Harris M, Akagi L, Montaner JS. Adverse effects of antiretroviral therapy for HIV infection. *Canadian Medical Association Journal*. 2004;170(2):229-38.

10. Arora S, Goyal S, Balani J, Tandon S. Enhanced antiproliferative effects of aqueous extracts of some medicinal mushrooms on colon cancer cells. *International journal of medicinal mushrooms*. 2013;15(3).
11. Yu J, Sun R, Zhao Z, Wang Y. *Auricularia polytricha* polysaccharides induce cell cycle arrest and apoptosis in human lung cancer A549 cells. *International journal of biological macromolecules*. 2014;68:67-71.
12. K Chellappan D, Ganasen S, Batumalai S, Candasamy M, Krishnappa P, Dua K, et al. The protective action of the aqueous extract of *Auricularia polytricha* in paracetamol induced hepatotoxicity in rats. *Recent patents on drug delivery & formulation*. 2016;10(1):72-6.
13. Park KM, Kwon KM, Lee SH. Evaluation of the antioxidant activities and tyrosinase inhibitory property from mycelium culture extracts. *Evidence-based complementary and alternative medicine*. 2015;2015:616298
14. Teoh HL, Ahmad IS, Johari NMK, Aminudin N, Abdullah N. Antioxidant Properties and Yield of Wood Ear Mushroom, *Auricularia polytricha* (Agaricomycetes), Cultivated on Rubberwood Sawdust. *International Journal of Medicinal Mushrooms*. 2018;20(4):369-380.
15. Chen Y, Xue Y. Purification, chemical characterization and antioxidant activities of a novel polysaccharide from *Auricularia polytricha*. *International journal of biological macromolecules*. 2018;120:1087-92.
16. Gu J. Hypolipidaemic foods in China. *Asia Pacific journal of clinical nutrition*. 1996;5(4):249-53.
17. Zhao S, Rong C, Liu Y, Xu F, Wang S, Duan C, et al. Extraction of a soluble polysaccharide from *Auricularia polytricha* and evaluation of its anti-hypercholesterolemic effect in rats. *Carbohydrate polymers*. 2015;122:39-45.

18. Wu N-J, Chiou F-J, Weng Y-M, Yu Z-R, Wang B-J. In vitro hypoglycemic effects of hot water extract from *Auricularia polytricha* (wood ear mushroom). International journal of food sciences and nutrition. 2014;65(4):502-6.
19. Johnathan M, Gan S, Ezumi MW, Faezahtul A, Nurul A. Phytochemical profiles and inhibitory effects of Tiger Milk mushroom (*Lignosus rhinocerus*) extract on ovalbumin-induced airway inflammation in a rodent model of asthma. BMC complementary and alternative medicine. 2016;16(1):167.
20. Lee M, Tan N, Fung S, Tan C, Ng S. The antiproliferative activity of sclerotia of *Lignosus rhinocerus* (Tiger Milk Mushroom). Evidence-based complementary and alternative medicine. 2012;2012:697603.
21. Yap YH, Tan N, Fung S, Aziz AA, Tan C, Ng S. Nutrient composition, antioxidant properties, and anti-proliferative activity of *Lignosus rhinocerus* Cooke sclerotium. Journal of the Science of Food and Agriculture. 2013;93(12):2945-52.
22. Lau BF, Abdullah N, Aminudin N, Lee HB, Tan PJ. Ethnomedicinal uses, pharmacological activities, and cultivation of *Lignosus* spp.(tiger' s milk mushrooms) in Malaysia–A review. Journal of ethnopharmacology. 2015;169:441-58.
23. Mallick S, Maiti S, Bhutia S, Maiti T. Antitumor properties of a heteroglucan isolated from *Astraeus hygrometricus* on Dalton's lymphoma bearing mouse. Food and Chemical Toxicology. 2010;48(8-9):2115-21.
24. Mallick S, Dey S, Mandal S, Dutta A, Mukherjee D, Biswas G, et al. A novel triterpene from *Astraeus hygrometricus* induces reactive oxygen species leading to death in *Leishmania donovani*. Future microbiology. 2015;10(5):763-89.
25. Mallick SK, Maiti S, Bhutia SK, Maiti TK. Immunostimulatory properties of a polysaccharide isolated from *Astraeus hygrometricus*. Journal of medicinal food. 2010;13(3):665-72.

26. Laskey SB, Siliciano RF. A mechanistic theory to explain the efficacy of antiretroviral therapy. *Nature Reviews Microbiology*. 2014;12(11):772.
27. De Clercq E. Anti-HIV drugs: 25 compounds approved within 25 years after the discovery of HIV. *International journal of antimicrobial agents*. 2009;33(4):307-20.
28. De Clercq E. Emerging anti-HIV drugs. *Expert opinion on emerging drugs*. 2005;10(2):241-74.
29. Engelman A, Cherepanov P. The structural biology of HIV-1: mechanistic and therapeutic insights. *Nature Reviews Microbiology*. 2012;10(4):279.
30. Esposito F, Corona A, Tramontano E. HIV-1 reverse transcriptase still remains a new drug target: structure, function, classical inhibitors, and new inhibitors with innovative mechanisms of actions. *Molecular biology international*. 2012;2012:586401.
31. Bai R, Zhang X-J, Li Y-L, Liu J-P, Zhang H-B, Xiao W-L, et al. SJP-L-5, a novel small-molecule compound, inhibits HIV-1 infection by blocking viral DNA nuclear entry. *BMC microbiology*. 2015;15(1):274.
32. Onafuwa-Nuga A, Telesnitsky A. The remarkable frequency of human immunodeficiency virus type 1 genetic recombination. *Microbiology and Molecular Biology Reviews*. 2009;73(3):451-80.
33. Lv Z, Chu Y, Wang Y. HIV protease inhibitors: a review of molecular selectivity and toxicity. *HIV/AIDS (Auckland, NZ)*. 2015;7:95.
34. Lv H, Kong Y, Yao Q, Zhang B, Leng F-w, Bian H-j, et al. Nebrodeolysin, a novel hemolytic protein from mushroom *Pleurotus nebrodensis* with apoptosis-inducing and anti-HIV-1 effects. *Phytomedicine*. 2009;16(2-3):198-205.

35. Luo D-Q, Zhao L-Y, Shi Y-L, Tang H-L, Li Y-Y, Yang L-M, et al. Velleratretraol, an unusual highly functionalized lactarane sesquiterpene from *Lactarius vellereus*. *The Journal of antibiotics*. 2009;62(3):129.
36. Seniuk OF, Gorovoj LF, Beketova GV, Savichuk HO, Rytik PG, Kucherov II, et al. Anti-infective properties of the melanin-glucan complex obtained from medicinal tinder bracket mushroom, *Fomes fomentarius* (L.: Fr.) Fr.(Aphyllorphomycetideae). *International journal of medicinal mushrooms*. 2011;13(1):7-18.
37. Wang H, Ng T. Examination of lectins, polysaccharopeptide, polysaccharide, alkaloid, coumarin and trypsin inhibitors for inhibitory activity against human immunodeficiency virus reverse transcriptase and glycohydrolases. *Planta medica*. 2001;67(07):669-72.
38. Sun J, Chen Q-J, Cao Q-Q, Wu Y-Y, Xu L-J, Zhu M-J, et al. A laccase with antiproliferative and HIV-I reverse transcriptase inhibitory activities from the mycorrhizal fungus *Agaricus placomyces*. *BioMed Research International*. 2012;2012:736472.
39. Hu D, Zhang R, Zhang G, Wang H, Ng T. A laccase with antiproliferative activity against tumor cells from an edible mushroom, white common *Agrocybe cylindracea*. *Phytomedicine*. 2011;18(5):374-9.
40. Ngai PH, Zhao Z, Ng T. Agrocybin, an antifungal peptide from the edible mushroom *Agrocybe cylindracea*. *Peptides*. 2005;26(2):191-6.
41. Sekete M, Ma D, Wang B, Wang H, Ng T. First biochemical characterization of a novel ribonuclease from wild mushroom *Amanita hemibapha*. *SpringerPlus*. 2012;1(1):1.
42. Singh SS, Wang H, Chan YS, Pan W, Dan X, Yin CM, et al. Lectins from edible mushrooms. *Molecules*. 2014;20(1):446-69.

43. Sun J, Ng T-B, Wang H, Zhang G. A Novel Hemagglutinin with Antiproliferative Activity against Tumor Cells from the Hallucinogenic Mushroom *Boletus speciosus*. *BioMed research international*. 2014;2014:340467.
44. Wong JH, Ng TB, Wang H, Sze SCW, Zhang KY, Li Q, et al. Cordymin, an antifungal peptide from the medicinal fungus *Cordyceps militaris*. *Phytomedicine*. 2011;18(5):387-92.
45. Wong JH, Wang H, Ng TB. A haemagglutinin from the medicinal fungus *Cordyceps militaris*. *Bioscience reports*. 2009;29(5):321-7.
46. Wang S-X, Liu Y, Zhang G-Q, Zhao S, Xu F, Geng X-L, et al. Cordysobin, a novel alkaline serine protease with HIV-1 reverse transcriptase inhibitory activity from the medicinal mushroom *Cordyceps sobolifera*. *Journal of bioscience and bioengineering*. 2012;113(1):42-7.
47. Collins RA, Ng TB. Polysaccharopeptide from *Coriolus versicolor* has potential for use against human immunodeficiency virus type 1 infection. *Life Sciences*. 1997;60(25):PL383-PL7.
48. Wang H, Ng TB. Isolation and characterization of velutin, a novel low-molecular-weight ribosome-inactivating protein from winter mushroom (*Flammulina velutipes*) fruiting bodies. *Life Sciences*. 2001;68(18):2151-8.
49. Wang H, Ng T. A laccase from the medicinal mushroom *Ganoderma lucidum*. *Applied microbiology and biotechnology*. 2006;72(3):508-13.
50. Zou Y-J, Wang H-X, Ng T-B, Huang C-Y, Zhang J-X. Purification and characterization of a novel laccase from the edible mushroom *Hericium coralloides*. *The Journal of Microbiology*. 2012;50(1):72-8.
51. Wang H, Ng T. A new laccase from dried fruiting bodies of the monkey head mushroom *Hericium erinaceum*. *Biochemical and biophysical research communications*. 2004;322(1):17-21.

52. Li Y, Zhang G, Ng TB, Wang H. A novel lectin with antiproliferative and HIV-1 reverse transcriptase inhibitory activities from dried fruiting bodies of the monkey head mushroom *Hericium erinaceum*. *BioMed Research International*. 2010;2010.
53. Zhang R, Zhao L, Wang H, Ng TB. A novel ribonuclease with antiproliferative activity toward leukemia and lymphoma cells and HIV-1 reverse transcriptase inhibitory activity from the mushroom, *Hohenbuehelia serotina*. *International journal of molecular medicine*. 2014;33(1):209-14.
54. Zhu M, Xu L, Chen X, Ma Z, Wang H, Ng T. A novel ribonuclease with HIV-1 reverse transcriptase inhibitory activity from the edible mushroom *Hygrophorus russula*. *Applied biochemistry and biotechnology*. 2013;170(1):219-30.
55. Wong JH, Wang H, Ng T. Marmorin, a new ribosome inactivating protein with antiproliferative and HIV-1 reverse transcriptase inhibitory activities from the mushroom *Hypsizigus marmoreus*. *Applied microbiology and biotechnology*. 2008;81(4):669-74.
56. Lam S, Ng T. Hyspin, a novel thermostable ribosome-inactivating protein with antifungal and antiproliferative activities from fruiting bodies of the edible mushroom *Hypsizigus marmoreus*. *Biochemical and biophysical research communications*. 2001;285(4):1071-5.
57. Zhao J, Wang H, Ng T. Purification and characterization of a novel lectin from the toxic wild mushroom *Inocybe umbrinella*. *Toxicon*. 2009;53(3):360-6.
58. Wu Y, Wang H, Ng T. Purification and characterization of a novel RNase with antiproliferative activity from the mushroom *Lactarius flavidulus*. *The Journal of antibiotics*. 2012;65(2):67-72.
59. Wu Y, Wang H, Ng TB. Purification and characterization of a lectin with antiproliferative activity toward cancer cells from the dried fruit bodies of *Lactarius flavidulus*. *Carbohydrate research*. 2011;346(16):2576-81.

60. Sun J, Wang H, Ng TB. Isolation of a laccase with HIV-1 reverse transcriptase inhibitory activity from fresh fruiting bodies of the *Lentinus edodes* (Shiitake mushroom). 2011; 48(2):88-94.
61. Ngai PH, Ng T. Lentin, a novel and potent antifungal protein from shitake mushroom with inhibitory effects on activity of human immunodeficiency virus-1 reverse transcriptase and proliferation of leukemia cells. Life Sciences. 2003;73(26):3363-74.
62. Xu L, Wang H, Ng T. A laccase with HIV-1 reverse transcriptase inhibitory activity from the broth of mycelial culture of the mushroom *Lentinus tigrinus*. BioMed Research International. 2012;2012:536725.
63. Wu Y, Ng T. A novel metalloprotease from the wild basidiomycete mushroom *Lepista nuda*. Journal of microbiology and biotechnology. 2011;21(3):256-62.
64. Zhu M, Zhang G, Meng L, Wang H, Gao K, Ng T. Purification and Characterization of a White Laccase with Pronounced Dye Decolorizing Ability and HIV-1 Reverse Transcriptase Inhibitory Activity from *Lepista nuda*. Molecules. 2016;21(4):415.
65. Zhang R, Zhang G, Hu D, Wang H, Ng T. A novel ribonuclease with antiproliferative activity from fresh fruiting bodies of the edible mushroom *Lyophyllum shimeiji*. Biochemical genetics. 2010;48(7-8):658-68.
66. Lam S, Ng T. First simultaneous isolation of a ribosome inactivating protein and an antifungal protein from a mushroom (*Lyophyllum shimeiji*) together with evidence for synergism of their antifungal effects. Archives of Biochemistry and Biophysics. 2001;393(2):271-80.
67. Wang SX, Zhang GQ, Zhao S, Xu F, Zhou Y, Li Geng X, et al. Purification and characterization of a novel lectin with antiphytovirus activities from the wild mushroom *Paxillus involutus*. Protein and peptide letters. 2013;20(7):767-74.

68. Wang CR, Zhou R, Ng TB, Wong JH, Qiao WT, Liu F. First report on isolation of methyl gallate with antioxidant, anti-HIV-1 and HIV-1 enzyme inhibitory activities from a mushroom (*Pholiota adiposa*). *Environmental toxicology and pharmacology*. 2014;37(2):626-37.
69. Zhang G, Sun J, Wang H, Ng T. A novel lectin with antiproliferative activity from the medicinal mushroom *Pholiota adiposa*. *Acta Biochim Pol*. 2009;56(3):415-21.
70. Wang CR, Ng TB, Li L, Fang JC, Jiang Y, Wen TY, et al. Isolation of a polysaccharide with antiproliferative, hypoglycemic, antioxidant and HIV-1 reverse transcriptase inhibitory activities from the fruiting bodies of the abalone mushroom *Pleurotus abalonus*. *Journal of Pharmacy and Pharmacology*. 2011;63(6):825-32.
71. Li Y, Liu Q, Wang H, Ng T. A novel lectin with potent antitumor, mitogenic and HIV-1 reverse transcriptase inhibitory activities from the edible mushroom *Pleurotus citrinopileatus*. *Biochimica et Biophysica Acta (BBA)-General Subjects*. 2008;1780(1):51-7.
72. Ho Wong J, Bun Ng T, Jiang Y, Liu F, Cho Wing Sze S, Yanbo Zhang K. Purification and characterization of a laccase with inhibitory activity toward HIV-1 reverse transcriptase and tumor cells from an edible mushroom (*Pleurotus cornucopiae*). *Protein and peptide letters*. 2010;17(8):1040-7.
73. Wang H, Ng T. Purification of a laccase from fruiting bodies of the mushroom *Pleurotus eryngii*. *Applied Microbiology and Biotechnology*. 2006;69(5):521-5.
74. Wang H, Ng T. Pleureryn, a novel protease from fresh fruiting bodies of the edible mushroom *Pleurotus eryngii*. *Biochemical and biophysical research communications*. 2001;289(3):750-5.
75. Wang H, Ng T. Isolation of a novel ubiquitin-like protein from *Pleurotus ostreatus* mushroom with anti-human immunodeficiency virus, translation-inhibitory, and

- ribonuclease activities. *Biochemical and Biophysical Research Communications*. 2000;276(2):587-93.
76. Zhao S, Zhao Y, Li S, Zhao J, Zhang G, Wang H, et al. A novel lectin with highly potent antiproliferative and HIV-1 reverse transcriptase inhibitory activities from the edible wild mushroom *Russula delica*. *Glycoconjugate journal*. 2010;27(2):259-65.
77. Wang J, Wang H, Ng T. A peptide with HIV-1 reverse transcriptase inhibitory activity from the medicinal mushroom *Russula paludosa*. *Peptides*. 2007;28(3):560-5.
78. Zhao Y-C, Zhang G-Q, Ng T-B, Wang H-X. A novel ribonuclease with potent HIV-1 reverse transcriptase inhibitory activity from cultured mushroom *Schizophyllum commune*. *The Journal of Microbiology*. 2011;49(5):803-8.
79. Han C-H, Zhang G-Q, Wang H-X, Ng TB. Schizolysin, a hemolysin from the split gill mushroom *Schizophyllum commune*. *FEMS microbiology letters*. 2010;309(2):115-21.
80. Han C, Liu Q, Ng T, Wang H. A novel homodimeric lactose-binding lectin from the edible split gill medicinal mushroom *Schizophyllum commune*. *Biochemical and biophysical research communications*. 2005;336(1):252-7.
81. Zhang W, Tian G, Geng X, Zhao Y, Ng TB, Zhao L, et al. Isolation and characterization of a novel lectin from the edible mushroom *Stropharia rugosoannulata*. *Molecules*. 2014;19(12):19880-91.
82. Wang H, Ng T. Purification of a novel ribonuclease from dried fruiting bodies of the edible wild mushroom *Thelephora ganbajun*. *Biochemical and biophysical research communications*. 2004;324(2):855-9.
83. Guo Y, Wang H, Ng T. Isolation of trichogin, an antifungal protein from fresh fruiting bodies of the edible mushroom *Tricholoma giganteum*. *Peptides*. 2005;26(4):575-80.

84. Wang H, Ng T. Purification of a novel low-molecular-mass laccase with HIV-1 reverse transcriptase inhibitory activity from the mushroom *Tricholoma giganteum*. *Biochemical and biophysical research communications*. 2004;315(2):450-4.
85. Li M, Zhang G, Wang H, Ng T. Purification and characterization of a laccase from the edible wild mushroom *Tricholoma mongolicum*. *Journal of microbiology and biotechnology*. 2010;20(7):1069-76.
86. Hu Q-X, Zhang G-Q, Zhang R-Y, Hu D-D, Wang H-X, Ng TB. A novel aspartic protease with HIV-1 reverse transcriptase inhibitory activity from fresh fruiting bodies of the wild mushroom *Xylaria hypoxylon*. *BioMed Research International*. 2012;2012:728975.
87. Ichimura T, Watanabe O, Maruyama S. Inhibition of HIV-1 protease by water-soluble lignin-like substance from an edible mushroom, *Fuscoporia obliqua*. *Bioscience, biotechnology, and biochemistry*. 1998;62(3):575-7.
88. El Dine RS, El Halawany AM, Ma C-M, Hattori M. Inhibition of the dimerization and active site of HIV-1 protease by secondary metabolites from the Vietnamese mushroom *Ganoderma colossum*. *Journal of natural products*. 2009;72(11):2019-23.
89. El Dine RS, El Halawany AM, Ma C-M, Hattori M. Anti-HIV-1 protease activity of lanostane triterpenes from the vietnamese mushroom *Ganoderma colossum*. *Journal of natural products*. 2008;71(6):1022-6.
90. Ma B, Ren W, Zhou Y, Ma J, Ruan Y, Wen C-N. Triterpenoids from the spores of *Ganoderma lucidum*. *North American journal of medical sciences*. 2011;3(11):495.
91. Teke N, Kinge T, Bechem E, Nji T, Ndam L, Mih A. Ethnomycological study in the Kilum-Ijim mountain forest, Northwest Region, Cameroon. *Journal of ethnobiology and ethnomedicine*. 2018;14(1):25.

92. Song G, Du Q. Isolation of a polysaccharide with anticancer activity from *Auricularia polytricha* using high-speed countercurrent chromatography with an aqueous two-phase system. *Journal of Chromatography A*. 2010;1217(38):5930-4.
93. Zhou J, Chen Y, Xin M, Luo Q, Gu J, Zhao M, et al. Structure analysis and antimutagenic activity of a novel salt-soluble polysaccharide from *Auricularia polytricha*. *Journal of the Science of Food and Agriculture*. 2013;93(13):3225-30.
94. Arora S, Tandon C, Tandon S. Evaluation of the cytotoxic effects of CAM therapies: an in vitro study in normal kidney cell lines. *The Scientific World Journal*. 2014; 2014:452892.
95. Chiu W-C, Yang H-H, Chiang S-C, Chou Y-X, Yang H-T. *Auricularia polytricha* aqueous extract supplementation decreases hepatic lipid accumulation and improves antioxidative status in animal model of nonalcoholic fatty liver. *BioMedicine*. 2014;4(2).
96. Hossen M, Billah Prince M, Tanvir E, Chowdhury M, Rahman M, Alam F, et al. *Ganoderma lucidum* and *Auricularia polytricha* Mushrooms Protect against Carbofuran-Induced Toxicity in Rats. *Evidence-Based Complementary and Alternative Medicine*. 2018; 2018:6254929.
97. Koyama K, Akiba M, Imaizumi T, Kinoshita K, Takahashi K, Suzuki A, et al. Antinociceptive constituents of *Auricularia polytricha*. *Planta medica*. 2002;68(03):284-5.
98. Eik L-F, Naidu M, David P, Wong K-H, Tan Y-S, Sabaratnam V. *Lignosus rhinocerus* (Cooke) Ryvarden: A medicinal mushroom that stimulates neurite outgrowth in PC-12 cells. *Evidence-based Complementary and Alternative Medicine*. 2012; 2012:320308.

99. Lee SS, Tan NH, Fung SY, Pailoor J, Sim SM. Evaluation of the sub-acute toxicity of the sclerotium of *Lignosus rhinocerus* (Cooke), the Tiger Milk mushroom. *Journal of ethnopharmacology*. 2011;138(1):192-200.
100. Lai TK, Biswas G, Chatterjee S, Dutta A, Pal C, Banerji J, et al. Leishmanicidal and anticandidal activity of constituents of Indian edible mushroom *Astraeus hygrometricus*. *Chemistry & biodiversity*. 2012;9(8):1517-24.
101. Mallick S, Dutta A, Dey S, Ghosh J, Mukherjee D, Sultana SS, et al. Selective inhibition of *Leishmania donovani* by active extracts of wild mushrooms used by the tribal population of India: an in vitro exploration for new leads against parasitic protozoans. *Experimental parasitology*. 2014;138:9-17.
102. Ballester PJ, Mitchell JB. A machine learning approach to predicting protein–ligand binding affinity with applications to molecular docking. *Bioinformatics*. 2010;26(9):1169-75.
103. Brooks BR, Bruccoleri RE, Olafson BD, States DJ, Swaminathan Sa, Karplus M. CHARMM: a program for macromolecular energy, minimization, and dynamics calculations. *Journal of computational chemistry*. 1983;4(2):187-217.
104. Vicenzi E, Poli G. Infection of CD4+ primary T cells and cell lines, generation of chronically infected cell lines, and induction of HIV expression. *Current protocols in immunology*. 2005;69(1):12.3. 1-.3. 8.
105. Harada S. The broad anti-viral agent glycyrrhizin directly modulates the fluidity of plasma membrane and HIV-1 envelope. *Biochemical Journal*. 2005;392(1):191-9.
106. Reiser K, Mathys L, Curbo S, Pannecouque C, Noppen S, Liekens S, et al. The Cellular Thioredoxin-1/Thioredoxin Reductase-1 Driven Oxidoreduction Represents a Chemotherapeutic Target for HIV-1 Entry Inhibition. *PloS one*. 2016;11(1):e0147773.

107. Koup RA, Ho DD, Poli G, Fauci AS. Isolation and quantitation of HIV in peripheral blood. *Current protocols in immunology*. 1993;5(1):12.2.
108. Liu Z, Pan Q, Ding S, Qian J, Xu F, Zhou J, et al. The interferon-inducible MxB protein inhibits HIV-1 infection. *Cell host & microbe*. 2013;14(4):398-410.
109. Liu Z, Huang X, Hu L, Pham L, Poole KM, Tang Y, et al. Effects of Hinge Region Natural Polymorphisms on Human Immunodeficiency Virus-1 Protease Structure, Dynamics and Drug-Pressure Evolution. *Journal of Biological Chemistry*. 2016;291(43):22741-56.
110. Lansdon EB, Liu Q, Leavitt SA, Balakrishnan M, Perry JK, Lancaster-Moyer C, et al. Structural and binding analysis of pyrimidinol carboxylic acid and N-hydroxy quinazolinone HIV-1 RNase H inhibitors. *Antimicrobial agents and chemotherapy*. 2011;55(6):2905-15.
111. Tirado-Rives J, Jorgensen WL. Contribution of conformer focusing to the uncertainty in predicting free energies for protein-ligand binding. *Journal of medicinal chemistry*. 2006;49(20):5880-4.
112. Chira N-A, Todasca M-C, Nicolescu A, Rosu A, Nicolae M, Rosca S-I. Evaluation of the computational methods for determining vegetable oils composition using ¹H-NMR spectroscopy. *Rev Chim*. 2011;1:42-6.
113. Tao R, Wang C-Z, Kong Z-W. Antibacterial/antifungal activity and synergistic interactions between polyprenols and other lipids isolated from *Ginkgo Biloba* L. leaves. *Molecules*. 2013;18(2):2166-82.
114. Wu G, Robertson DH, Brooks III CL, Vieth M. Detailed analysis of grid-based molecular docking: A case study of CDOCKER- A CHARMM-based MD docking algorithm. *Journal of computational chemistry*. 2003;24(13):1549-62.

115. Wu W, Nie L, Zhang L, Li Y. The notch pathway promotes NF- κ B activation through Asb2 in T cell acute lymphoblastic leukemia cells. Cellular & molecular biology letters. 2018;23(1):37.
116. dos Santos DMC, Eilers J, Vizcaino AS, Orlova E, Zimmermann M, Stanulla M, et al. MAP3K7 is recurrently deleted in pediatric T-lymphoblastic leukemia and affects cell proliferation independently of NF- κ B. BMC cancer. 2018;18(1):663.
117. Tanese N, Telesnitsky A, Goff S. Abortive reverse transcription by mutants of Moloney murine leukemia virus deficient in the reverse transcriptase-associated RNase H function. Journal of virology. 1991;65(8):4387-97.
118. Van Etten JL, Gottlieb D. Biochemical changes during the growth of fungi II. Ergosterol and fatty acids in *Penicillium atrovirens*. Journal of bacteriology. 1965;89(2):409-14.
119. Ruess L, Häggblom MM, Zapata EJGa, Dighton J. Fatty acids of fungi and nematodes-possible biomarkers in the soil food chain? Soil Biology and Biochemistry. 2002;34(6):745-56.
120. Maga JA. Mushroom flavor. Journal of Agricultural and Food Chemistry. 1981;29(1):1-4.
121. Barreira JC, Ferreira IC, Oliveira MB. Triacylglycerol profile as a chemical fingerprint of mushroom species: Evaluation by principal component and linear discriminant analyses. Journal of agricultural and food chemistry. 2012 Oct 12;60(42):10592-9.
122. Jäpelt RB, Jakobsen J. Vitamin D in plants: a review of occurrence, analysis, and biosynthesis. Frontiers in plant science. 2013 May 13;4:136.
123. Campbell GR, Spector SA. Vitamin D inhibits human immunodeficiency virus type 1 and Mycobacterium tuberculosis infection in macrophages through the induction of autophagy. PLoS pathogens. 2012 May 10;8(5):e1002689.

124. Mengoni F, Lichtner M, Battinelli L, Marzi M, Mastroianni CM, Vullo V, et al. In vitro anti-HIV activity of oleanolic acid on infected human mononuclear cells. *Planta medica*. 2002;68(02):111-4.
125. Min BS, Jung HJ, Lee JS, Kim YH, Bok SH, Ma CM, et al. Inhibitory effect of triterpenes from *Crataegus pinatifida* on HIV-I protease. *Planta medica*. 1999;65(04):374-5.
126. Xu H-X, Zeng F-Q, Wan M, Sim K-Y. Anti-HIV triterpene acids from *Geum japonicum*. *Journal of natural products*. 1996;59(7):643-5.
127. Lee DY-W, Lin X, Paskaleva EE, Liu Y, Puttamadappa SS, Thornber C, et al. Palmitic acid is a novel CD4 fusion inhibitor that blocks HIV entry and infection. *AIDS research and human retroviruses*. 2009;25(12):1231-41.
128. Lee DY-W, Canki M. Methods and compositions for the use of sargassum fusiforme for the inhibition of hiv-1 infection. United States patent application US 12/601,072. 2010 Sep 30.
129. Kametani S, Kojima-Yuasa A, Kikuzaki H, Kennedy DO, Honzawa M, Matsui-Yuasa I. Chemical constituents of cape aloe and their synergistic growth-inhibiting effect on Ehrlich ascites tumor cells. *Bioscience, biotechnology, and biochemistry*. 2007;71(5):1220-9.



Table A 1 Nucleotide sequences of AP

Nucleotide region	Nucleotide sequence (5' -> 3')
ITS1	GGCTTGGATTTTGGGCTTTTACCCGATCGTTCAGCTGTGCGCCCTTC ACAGGGCTGCACGCTGGAGCAAGACCCACACCTGTGCACCTTTT CGGTTGCGGCTTCGGTCGCTGCCGCTTTCAAATGCAACAACCTCAGT CTCGAATGTTAACAAAACCATAAAAAGTAACAACCTTTCAACAACGGA TCTCTTGGCTCTCGCATCGATGAAGAACGCAGCGAAATGCGATAAG TAATGTGAATTGCAGAATTCAGTGAATCATCGAATCTTTGAACGCAT CTTGCGCTCCTTGGTATTCCATGGAGCATGCCTGTTTGAGTGTACAG TAAACCCTCACCTTGGCATGTAACAGTCGCCCGTGGTGGACTTGG ACTGTGCCGTAACCGGCTCGTCTTGAAATGCATTAGCTGGCGCTTTT AGAGTGCTGGGCGACGGTGTGATAATTATCTGCGCCAATGCCTTAG GCCTCTTCAGCGGTGCTTGCTTACAGCCGTCCTCTGTGGACACATT ATTTTAAAGCTTTGGCCTCAAATCAGGTAGGACTACCCGCTGAACT TAAGCATATCAATAGCCGGGAGGAAAA
ITS4	GGACTGGCTGTCTACCTGATTTGAGGCCAAGCTTTAAAATAATGTG TCCACAGAGGGACGGCTGTAAGCAGCACCGCTGAAGAGGCCTAAG GCATTGGCGCAGATAATTATCACACCGTCGCCAGCACTCTAAAAG CGCCAGCTAATGCATTTCAAGACGAGCCGGTTACGGCACAGTCCAA GTCCACCACGGGCGACTGTTACATCGCAAGGGTGAGGGTTTACGT GAACTCAAACAGGCATGCTCCATGGAATACCAAGGAGCGCAAGA TCGTTCAAAGATTTCGATGATTCACTGAATTCTGCAATTCACATTACT TATCGCATTTCGCTGCGTTCTTCATCGATGCGAGAGCCAAGAGATC CGTTGTTGAAAGTTGTTACTTTTTATGGTTTTGTTAACATTTCGAGACTG AGTTGTTGCATTTGAAAGCGGCAGCGACCGAAGCCGCAACCGAAA AGGTGCACAGGTGTGGGGTCTTGCTCCAGCGTGCAGCCCTGTGAA GGGCGCACAGCTGAACGATCGGGTTAAAAGCCCAAAATCTTTAATG ATCCTTCCGAGGTACCCTACCGGAAAGA

Table A 2 Comparison of nucleotide sequences of AP at ITS1 region with GenBank database

#	Description	Max score	Total score	Query cover	Ident	Accession
1	<i>Auricularia polytricha</i> strain 4328 18S ribosomal RNA gene, partial sequence; internal transcribed spacer 1, 5.8S ribosomal RNA gene, and internal transcribed spacer 2, complete sequence; and 28S ribosomal RNA gene, partial sequence	1048	1048	98%	99%	KY345416.1
2	<i>Auricularia polytricha</i> cultivar Kangjian 18S ribosomal RNA gene, partial sequence; internal transcribed spacer 1, 5.8S ribosomal RNA gene, and internal transcribed spacer 2, complete sequence; and 28S ribosomal RNA gene, partial sequence	1044	1044	98%	99%	KJ627785.1

#	Description	Max score	Total score	Query cover	Ident	Accession
3	<i>Auricularia polytricha</i> cultivar ZH 18S ribosomal RNA gene, partial sequence; internal transcribed spacer 1, 5.8S ribosomal RNA gene, and internal transcribed spacer 2, complete sequence; and 28S ribosomal RNA gene, partial sequence	1042	1042	98%	99%	HM448450.1
4	<i>Auricularia polytricha</i> cultivar 951 18S ribosomal RNA gene, partial sequence; internal transcribed spacer 1, 5.8S ribosomal RNA gene, and internal transcribed spacer 2, complete sequence; and 28S ribosomal RNA gene, partial sequence	1042	1042	98%	99%	HM448453.1

#	Description	Max score	Total score	Query cover	Ident	Accession
5	<i>Auricularia polytricha</i> voucher Cui6115 internal transcribed spacer 1, partial sequence; 5.8S ribosomal RNA gene and internal transcribed spacer 2, complete sequence; and 28S ribosomal RNA gene, partial sequence	1042	1042	98%	99%	FJ617292.1

Table A 3 Comparison of nucleotide sequences of AP at ITS4 region with GenBank database

#	Description	Max score	Total score	Query cover	Ident	Accession
1	<i>Auricularia polytricha</i> strain 610723MF0009 small subunit ribosomal RNA gene, partial sequence; internal transcribed spacer 1, 5.8S ribosomal RNA gene, and internal transcribed spacer 2, complete sequence; and large subunit ribosomal RNA gene, partial sequence	1026	1026	97%	99%	KY950445.1

#	Description	Max score	Total score	Query cover	Ident	Accession
2	<i>Auricularia polytricha</i> cultivar Kangjian 18S ribosomal RNA gene, partial sequence; internal transcribed spacer 1, 5.8S ribosomal RNA gene, and internal transcribed spacer 2, complete sequence; and 28S ribosomal RNA gene, partial sequence	1026	1026	96%	99%	KJ627785.1
3	<i>Auricularia polytricha</i> strain HBME 18S ribosomal RNA gene, partial sequence; internal transcribed spacer 1, 5.8S ribosomal RNA gene, and internal transcribed spacer 2, complete sequence; and 28S ribosomal RNA gene, partial sequence	1026	1026	96%	99%	KF297976.1

#	Description	Max score	Total score	Query cover	Ident	Accession
4	<i>Auricularia polytricha</i> cultivar ZH 18S ribosomal RNA gene, partial sequence; internal transcribed spacer 1, 5.8S ribosomal RNA gene, and internal transcribed spacer 2, complete sequence; and 28S ribosomal RNA gene, partial sequence	1026	1026	97%	99%	HM448450.1
5	<i>Auricularia polytricha</i> cultivar Huang er10 18S ribosomal RNA gene, partial sequence; internal transcribed spacer 1, 5.8S ribosomal RNA gene, and internal transcribed spacer 2, complete sequence; and 28S ribosomal RNA gene, partial sequence	1026	1026	97%	99%	HM448471.1

Table A 4 The results of TLC analysis in gradient of hexane/ethyl acetate system

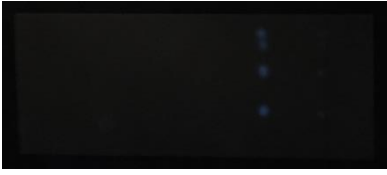
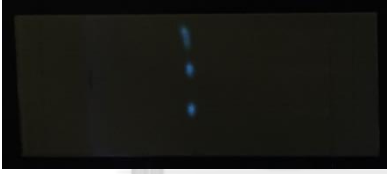
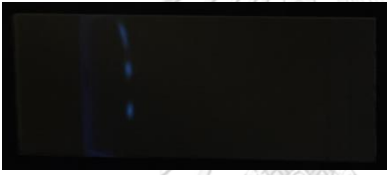



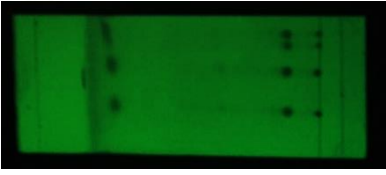
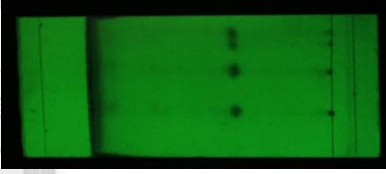
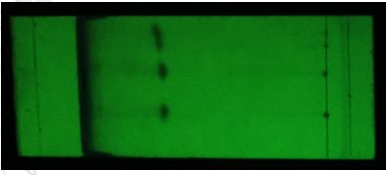
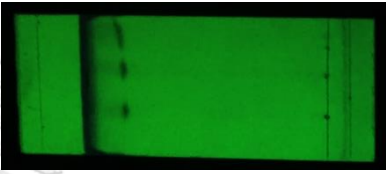


UV Wavelength (nm)	Mobile phase system (hexane: ethyl acetate)	100 : 0	90 : 10	80 : 20	70 : 30	60 : 40	50 : 50
254	Non move						
365	Non move						

Table A 5 The association between time and absorbance at 490 nm of different cell concentration by MTS assay

Amount of cell (cells)	Absorbance at 490 nm		
	24 hours	48 hours	72 hours
5.0×10^3	0.126 ± 0.011	0.258 ± 0.037	0.574 ± 0.026
1.0×10^4	0.287 ± 0.015	0.519 ± 0.055	1.023 ± 0.006
1.5×10^4	0.453 ± 0.023	0.740 ± 0.073	1.214 ± 0.044
2.0×10^4	0.656 ± 0.024	0.893 ± 0.096	1.485 ± 0.092
2.5×10^4	0.818 ± 0.060	1.163 ± 0.080	1.786 ± 0.178
3.0×10^4	0.943 ± 0.018	1.284 ± 0.042	1.827 ± 0.116

Table A 6 The R-square value from linear regression test between time of incubation and absorbance at different cell concentration by MTS assay

Amount of cell (cells)	R-square
5.0×10^3	0.9468
1.0×10^4	0.9565
1.5×10^4	0.9803
2.0×10^4	0.9424
2.5×10^4	0.9732
3.0×10^4	0.9829

Table A 7 Amino acid interaction of ligands with HIV-1 PR obtained by CDOCKER

Amino acid	APV	ERG	PA	LA	OA	SA
A: ARG8	-	-	H/ E	H/ E	E	E
A: ASN25	H	-	-	-	-	-
A: GLY27	H	-	-	-	-	-
A: ALA28	H	HP	-	HP	-	HP
A: VAL32	-	-	-	HP	-	-
A: ILE47	-	HP	HP	HP	HP	HP
A: GLY49	H	-	-	-	-	-
A: ILE50	HP	-	-	-	-	-
A: PRO81	HP	-	-	-	-	-
A: VAL82	HP	-	-	-	-	-
B: LEU23	HP	-	-	-	-	-
B: GLY27	H	-	-	-	-	-
B: ALA28	H	HP	-	-	-	-
B: ASP30	H	-	-	-	-	-
B: VAL32	-	HP	-	-	-	-
B: ILE47	HP	HP	-	-	-	-
B: GLY48	H	-	-	-	-	-
B: GLY49	H	-	-	-	-	-
B: ILE50	-	HP	-	-	-	-
B: VAL82	HP	-	-	-	-	-
B: ILE84	HP	HP	-	-	-	-

ERG: Ergosterol, PA: Palmitic acid, LA: Linoleic acid, OA: Oleic acid, SA: Stearic acid,

H: Hydrogen bond, HP: Hydrophobic bond, E: Electrostatic bond

Table A 8 Amino acid interaction of ligands with HIV-1 RT at DNA polymerase domain obtained by CDOCKER

Amino acid	NVP	PA	LA	OA	SA
A: LEU100	HP	-	HP	-	-
A: LYS101	H	H/ E	-	E	-
A: LYS103	HP	-	-	H/ E	E
A: VAL106	HP	-	HP	HP	-
A: VAL179	HP	-	-	-	-
A: TYR181	HP	HP	-	-	HP
A: TRY188	H	HP	-	-	-
A: PHE227	-	-	-	HP	-
A: TRP229	HP	HP	-	-	HP
A: LEU234	HP	HP	-	HP	HP
A: TYR318	HP	-	HP	-	-

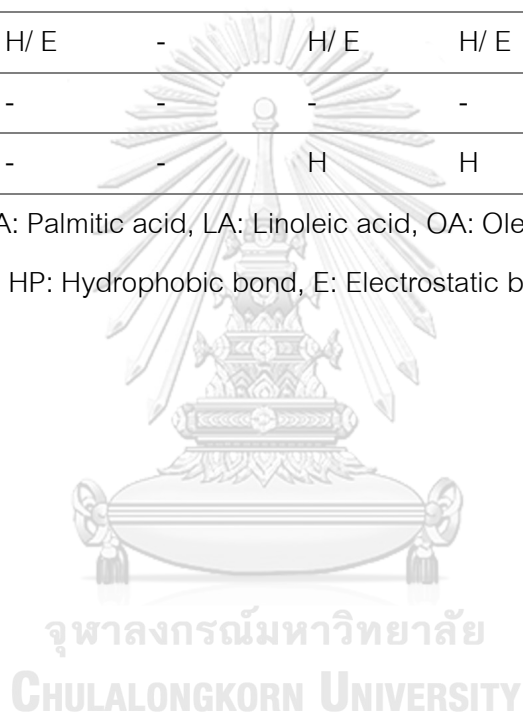
PA: Palmitic acid, LA: Linoleic acid, OA: Oleic acid, SA: Stearic acid, H: Hydrogen bond, HP: Hydrophobic bond, E: Electrostatic bond

Table A 9 Amino acid interaction of ligands with HIV-1 RT at RNase H domain obtained by CDOCKER

Amino acid	P4Y	ERG	PA	LA	OA	SA
A: ALA445	-	HP	HP	-	HP	-
A: ASP498	H	-	-	-	-	-
A: TRP535	HP	-	-	-	-	-
A: ALA538	H/ HP	HP	-	-	-	-
A: HIS539	-	-	-	HP	-	-
A: LYS540	H/ E	-	H/ E	H/ E	H/ E	H/ E
A: ILE556	-	-	-	-	HP	HP
B: ASN265	-	-	H	H	-	H

ERG: Ergosterol, PA: Palmitic acid, LA: Linoleic acid, OA: Oleic acid, SA: Stearic acid,

H: Hydrogen bond, HP: Hydrophobic bond, E: Electrostatic bond



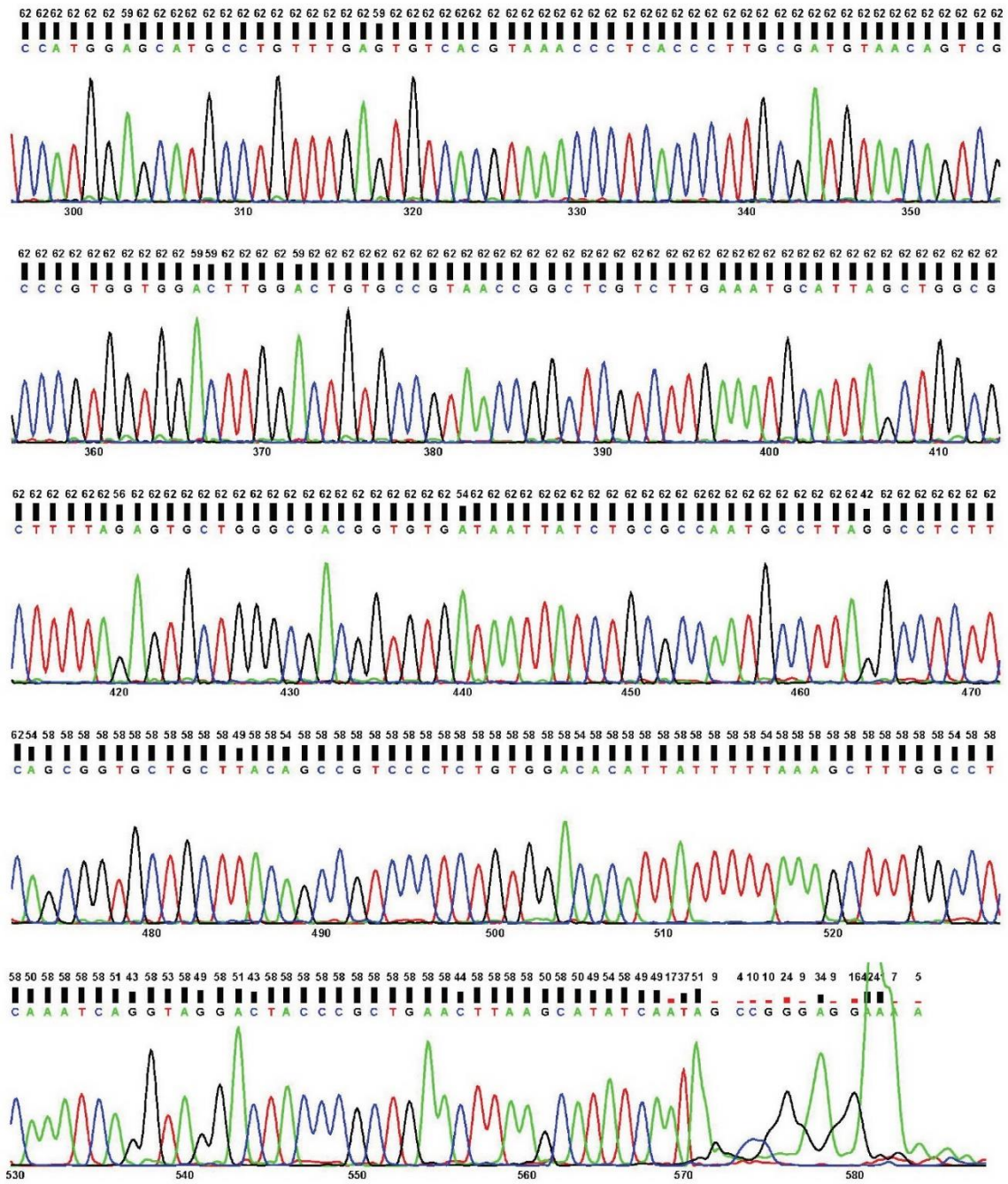


Figure A 1 (continue) Electropherogram of nucleotide sequence of AP at ITS1 region

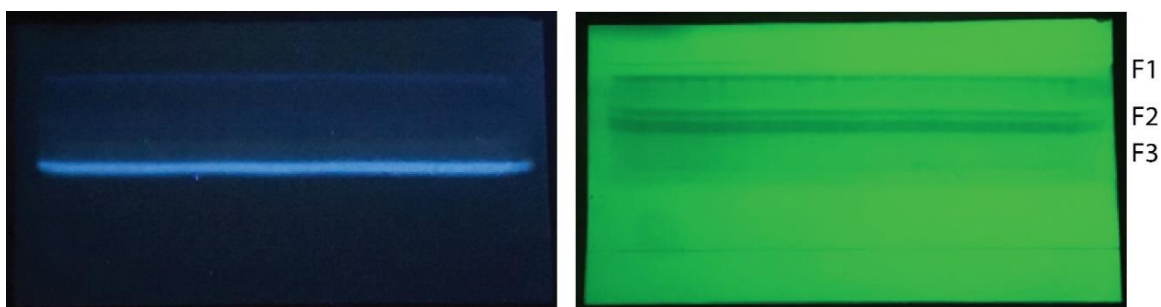


Figure A 3 preparative TLC of the APH mixture of F1, F2 and F3 under UV at 254 nm (left) and 365 nm (right)

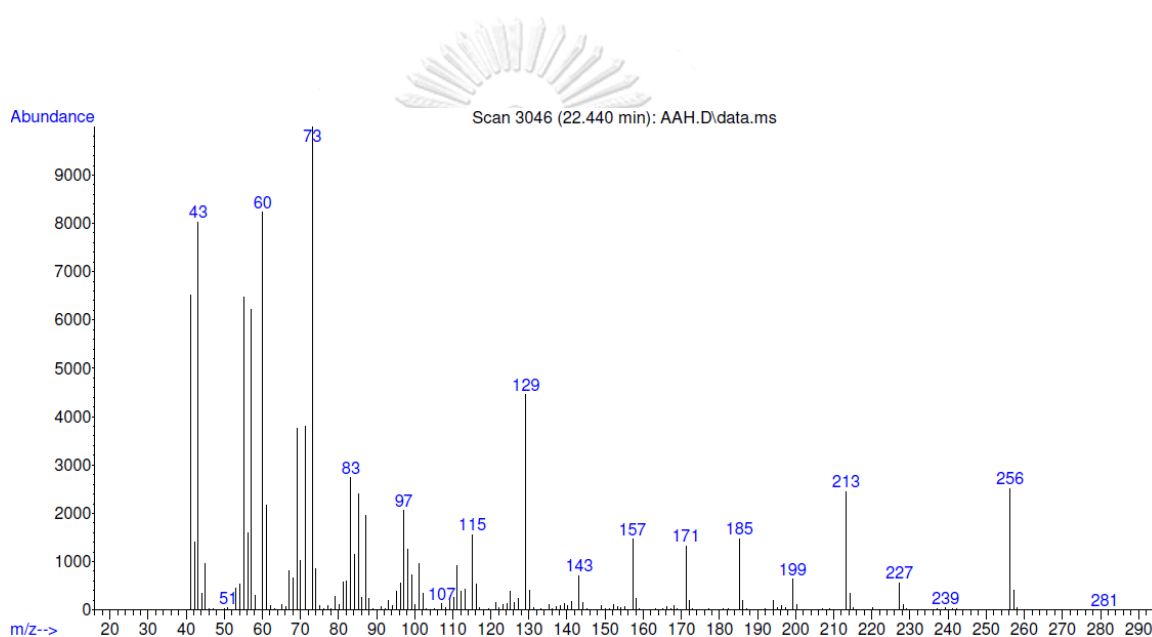


Figure A 4 Mass spectrum from GC-MS analysis of APH at retention time of 22.440 min, represent m/z of palmitic acid

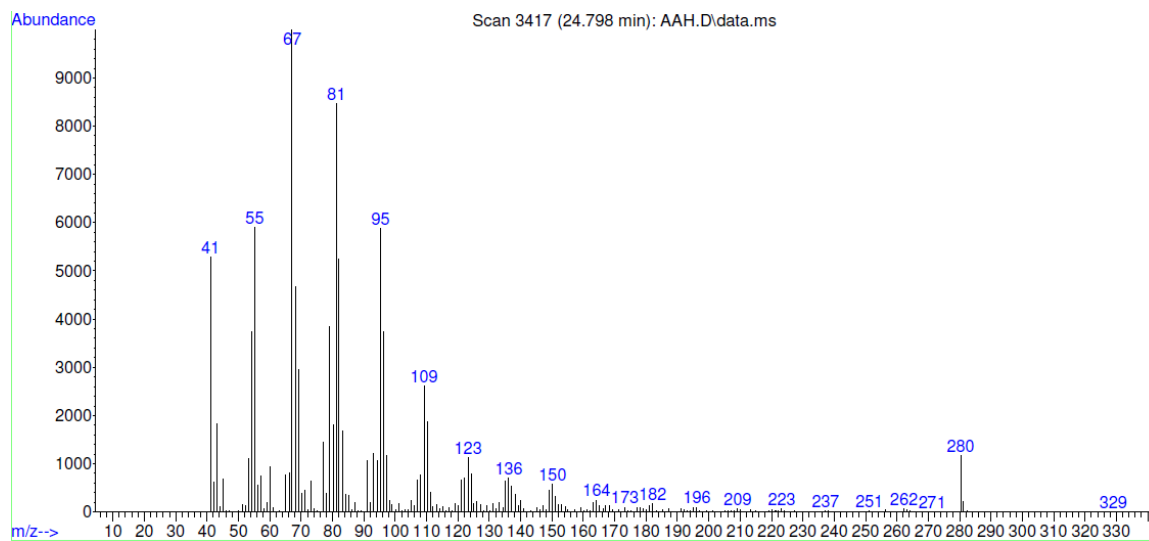


Figure A 5 Mass spectrum from GC-MS analysis of APH at retention time of 24.798 min,
represent m/z of linoleic acid

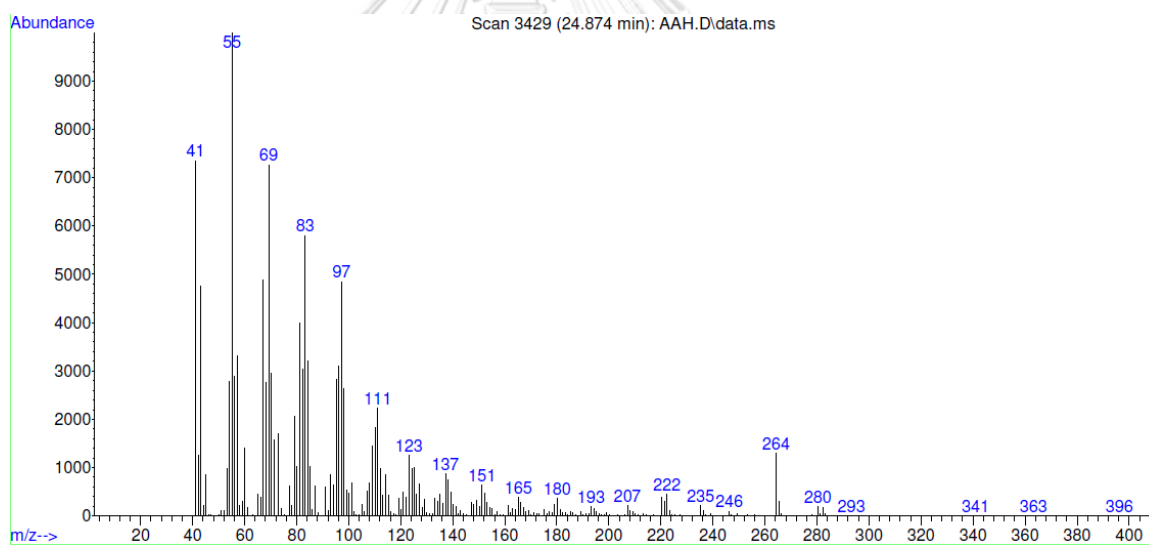


Figure A 6 Mass spectrum from GC-MS analysis of APH at retention time of 24.878 min,
represent m/z of oleic acid

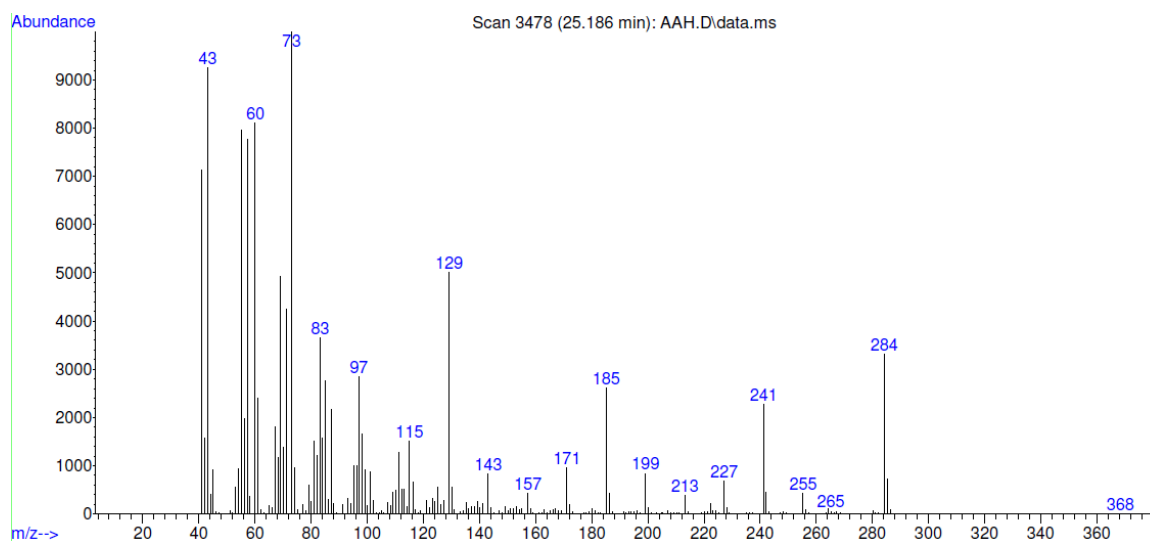


Figure A 7 Mass spectrum from GC-MS analysis of APH at retention time of 25.186 min,
represent m/z of stearic acid

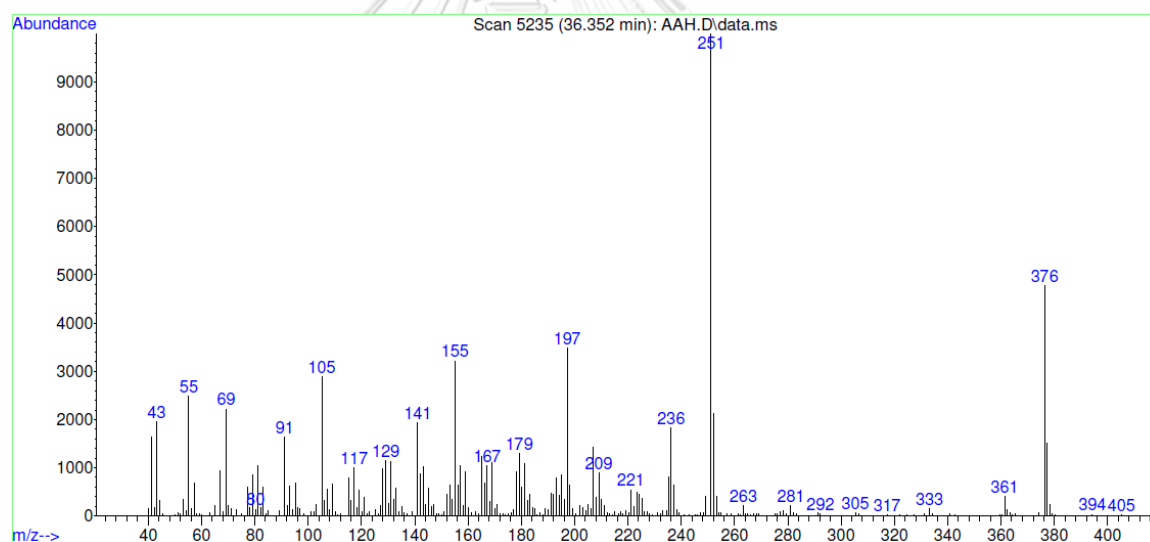


Figure A 8 Mass spectrum from GC-MS analysis of APH at retention time of 36.352 min,
represent m/z of anthraergostapentene

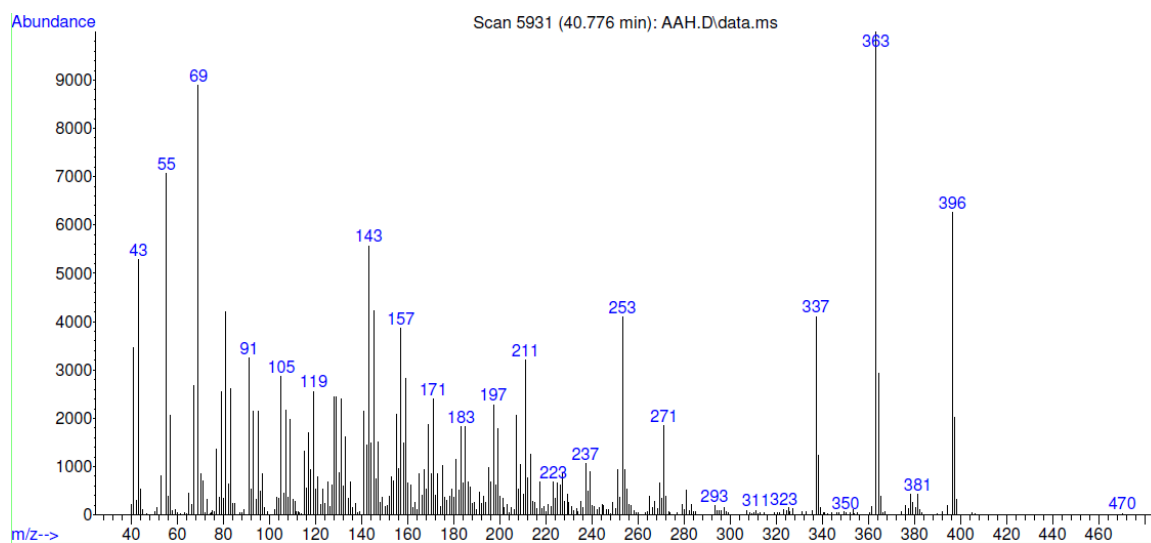


Figure A 9 Mass spectrum from GC-MS analysis of APH at retention time of 40.776 min, represent m/z of ergosterol

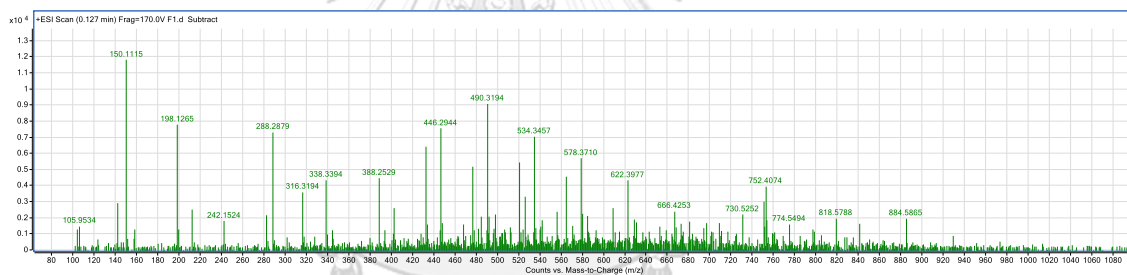


Figure A 10 Mass spectrum from HRMS analysis of F1 showed m/z 884.5865 [M]⁺

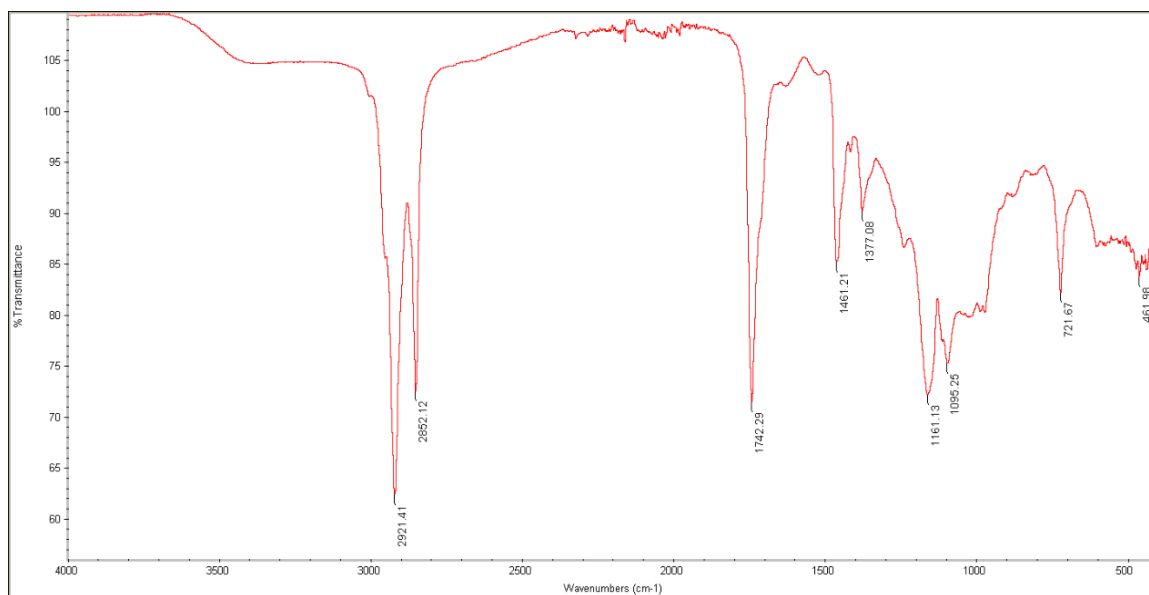
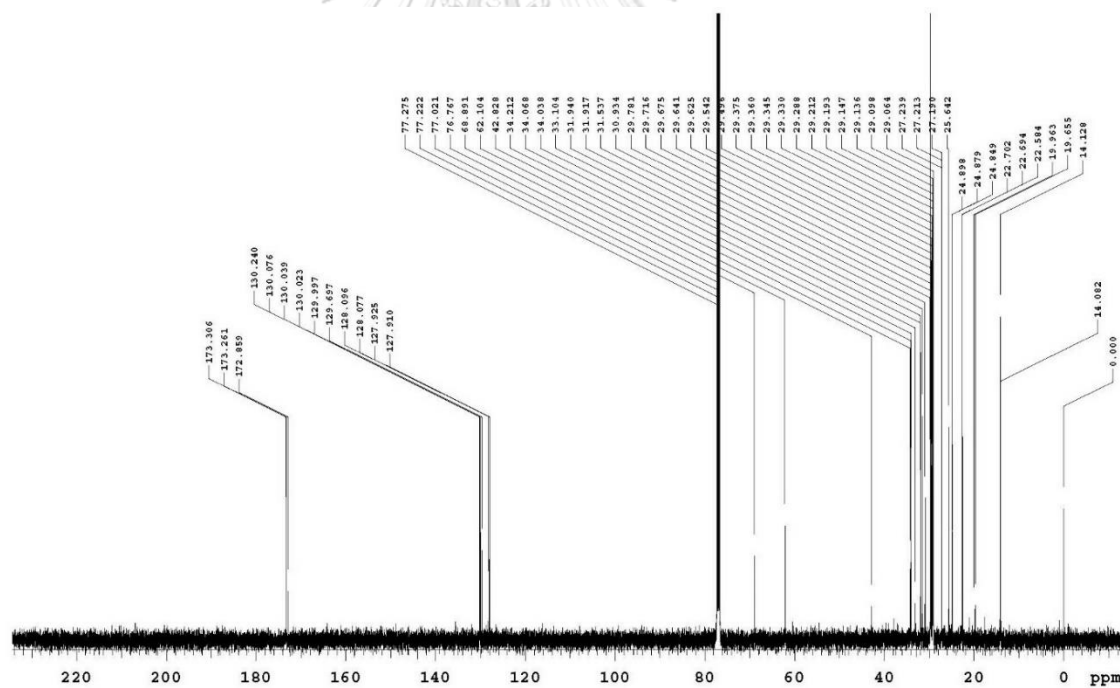


Figure A 11 FTIR spectrum of F1

Figure A 12 ^{13}C NMR spectrum of F1

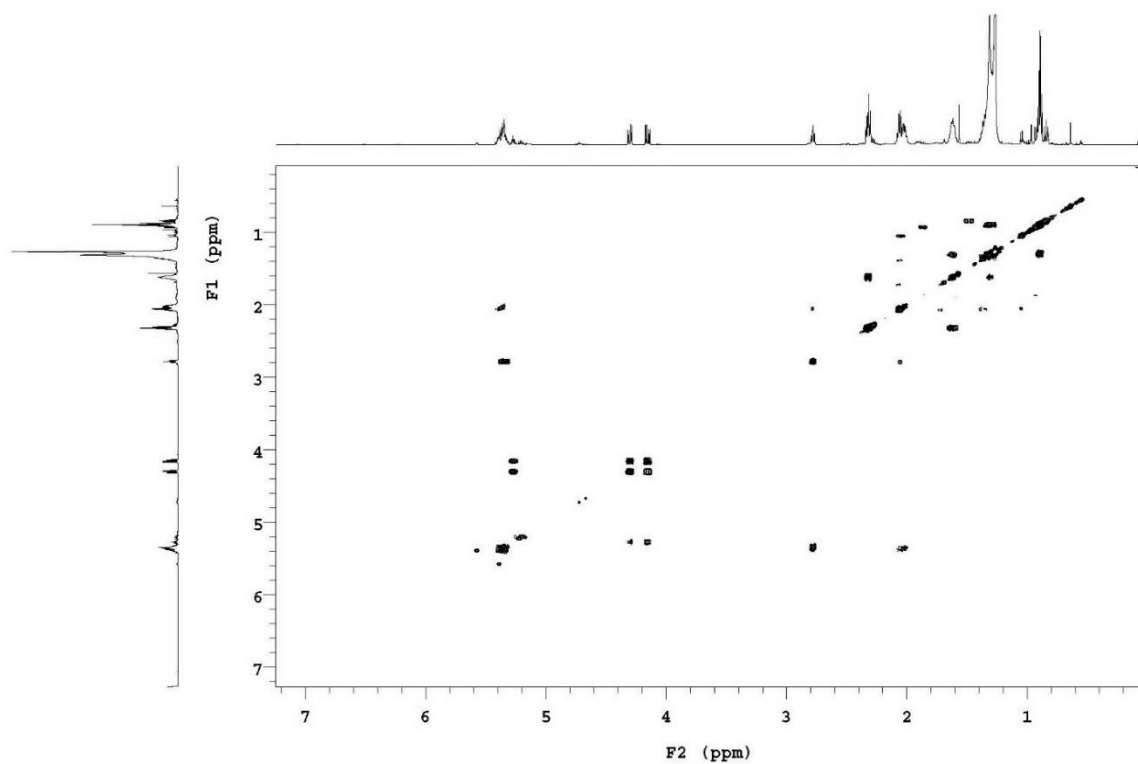


Figure A 13 COSY NMR spectrum of F1

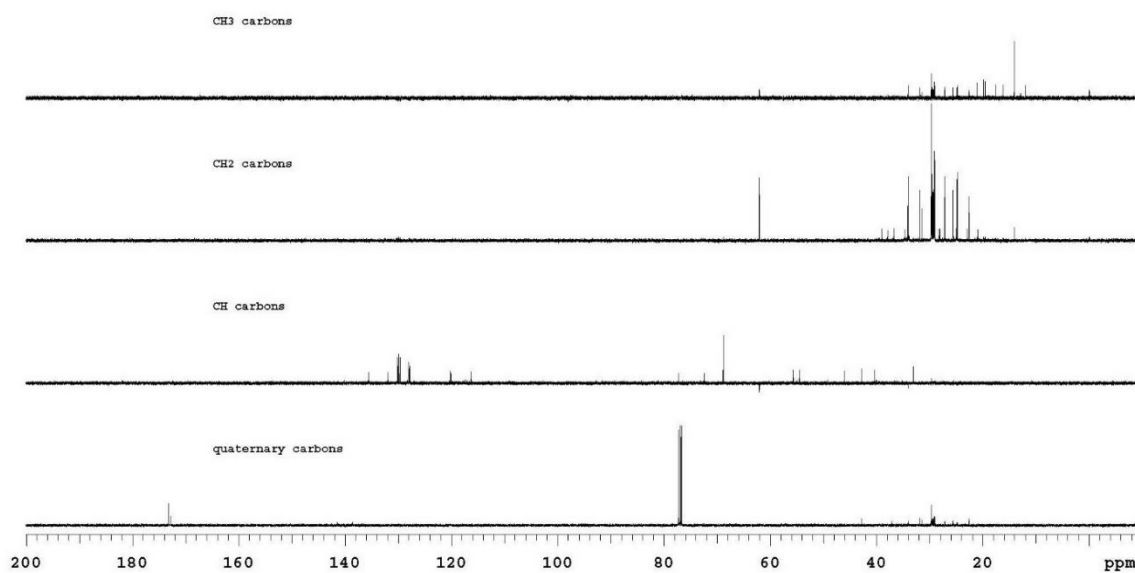


Figure A 14 DEPT NMR spectrum of F1

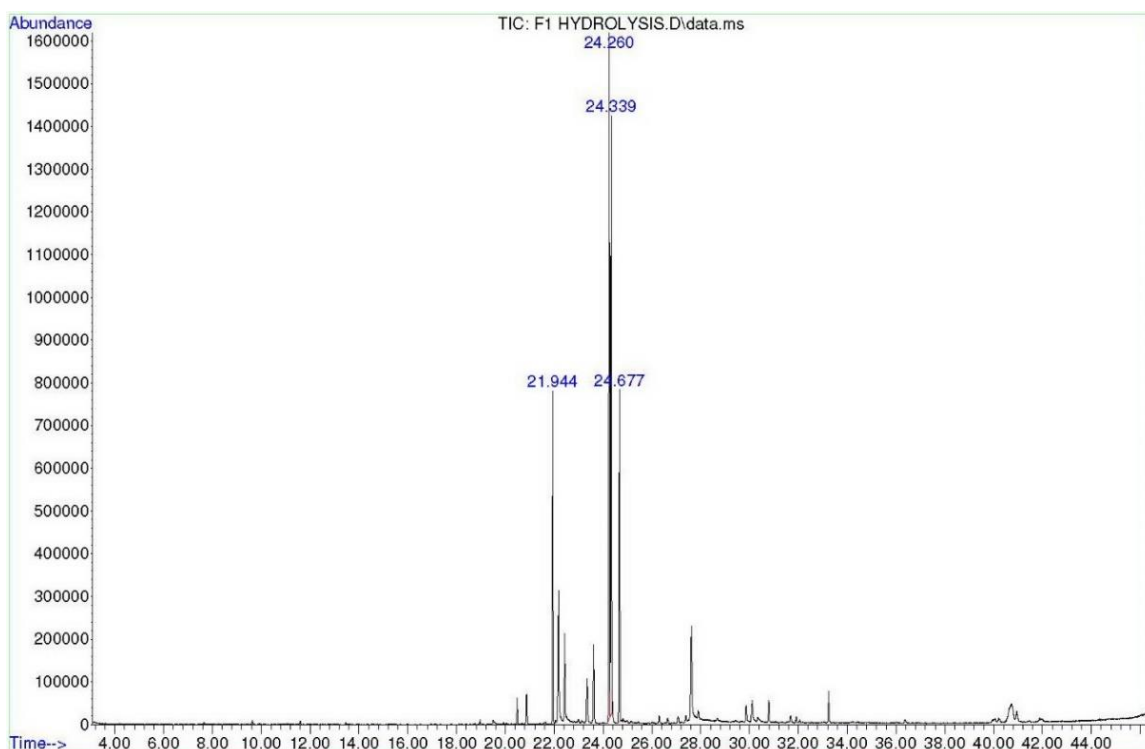


Figure A 15 Gas chromatogram of F1 hydrolysis

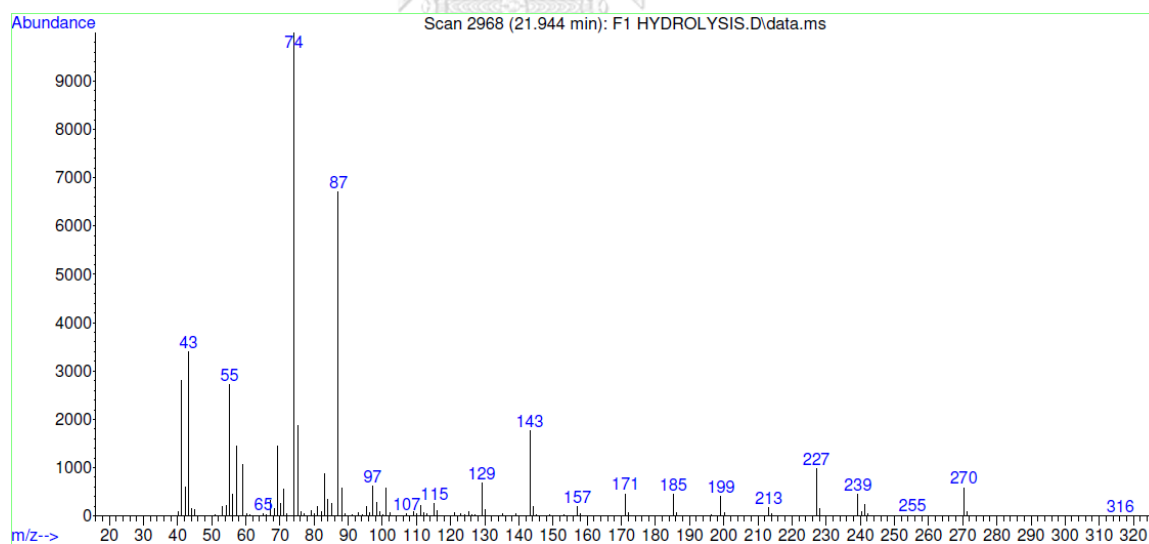


Figure A 16 Mass spectrum from GC-MS analysis of F1 hydrolysis at retention time of 21.944 min, represent m/z of palmitic acid, methyl ester

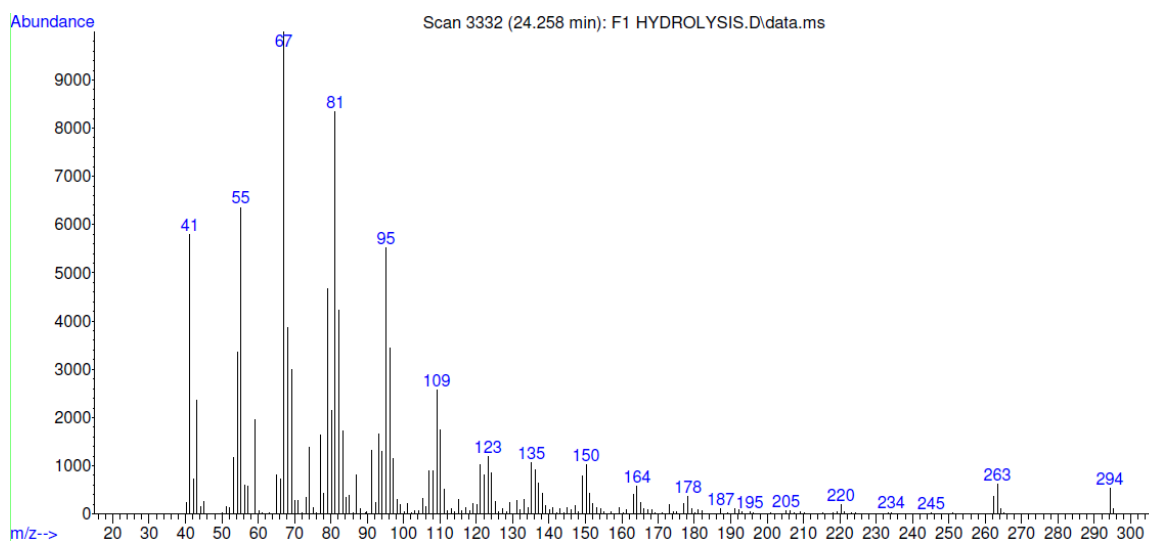


Figure A 17 Mass spectrum from GC-MS analysis of F1 hydrolysis at retention time of 24.258 min, represent m/z of linoleic acid, methyl ester

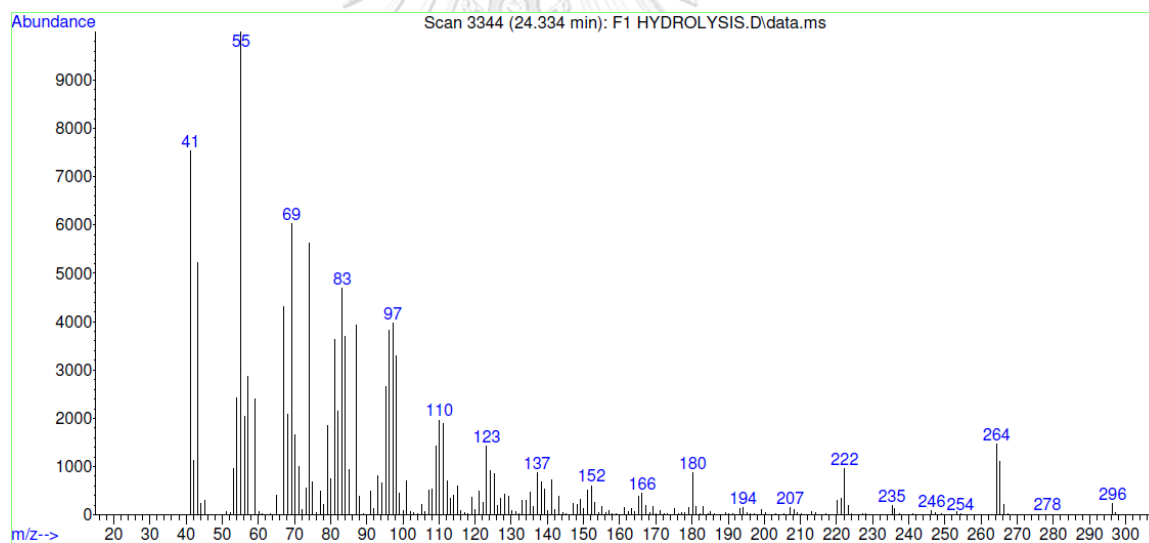


Figure A 18 Mass spectrum from GC-MS analysis of F1 hydrolysis at retention time of 24.334 min, represent m/z of oleic acid, methyl ester

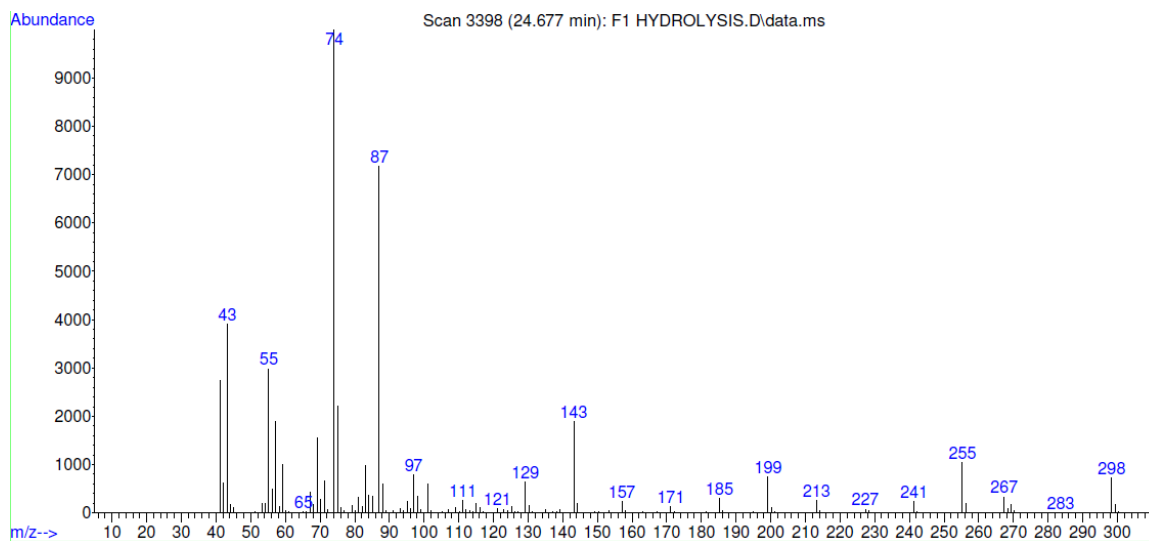


Figure A 19 Mass spectrum from GC-MS analysis of F1 hydrolysis at retention time of 24.677 min, represent m/z of stearic acid, methyl ester

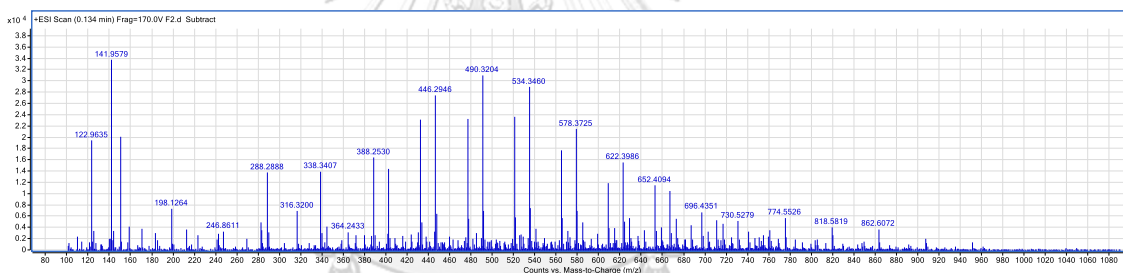
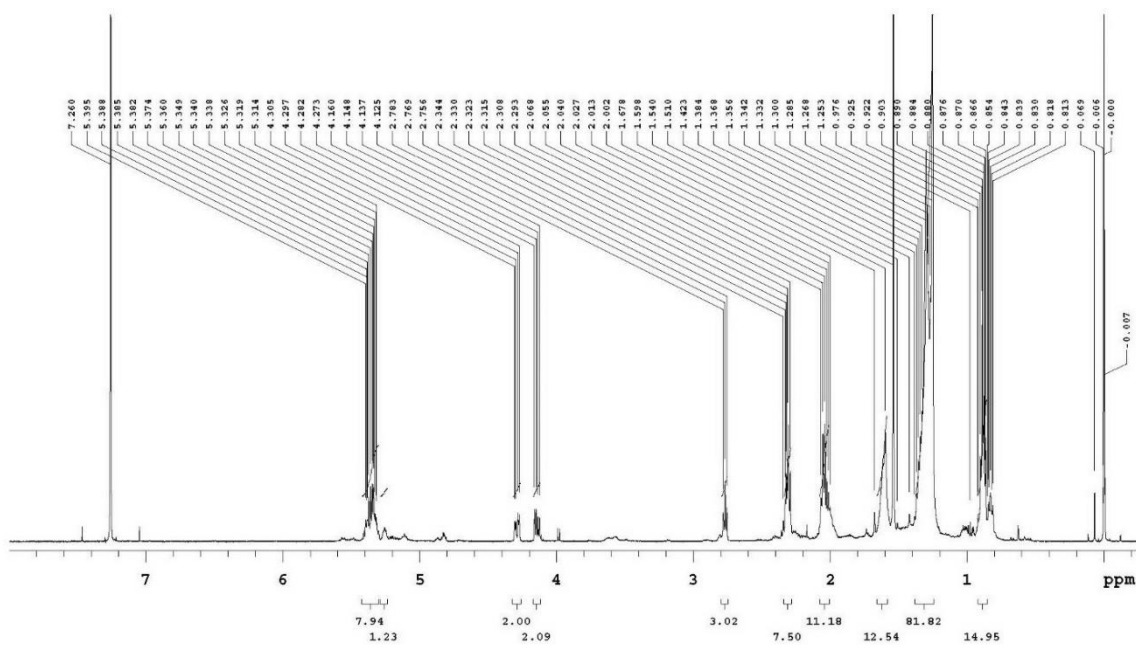
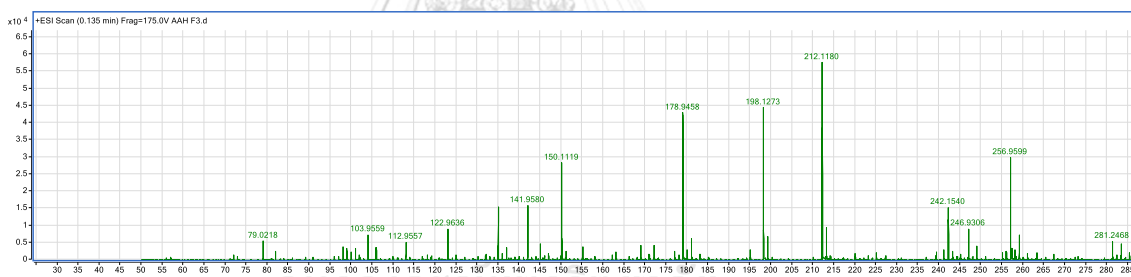


Figure A 20 Mass spectrum from HRMS analysis of F2 showed m/z 862.6072 [M]⁺

Figure A 21 ^1H NMR spectrum of F2Figure A 22 Mass spectrum from HRMS analysis of F3 showed m/z 281.2468 $[\text{M}+\text{H}]^+$

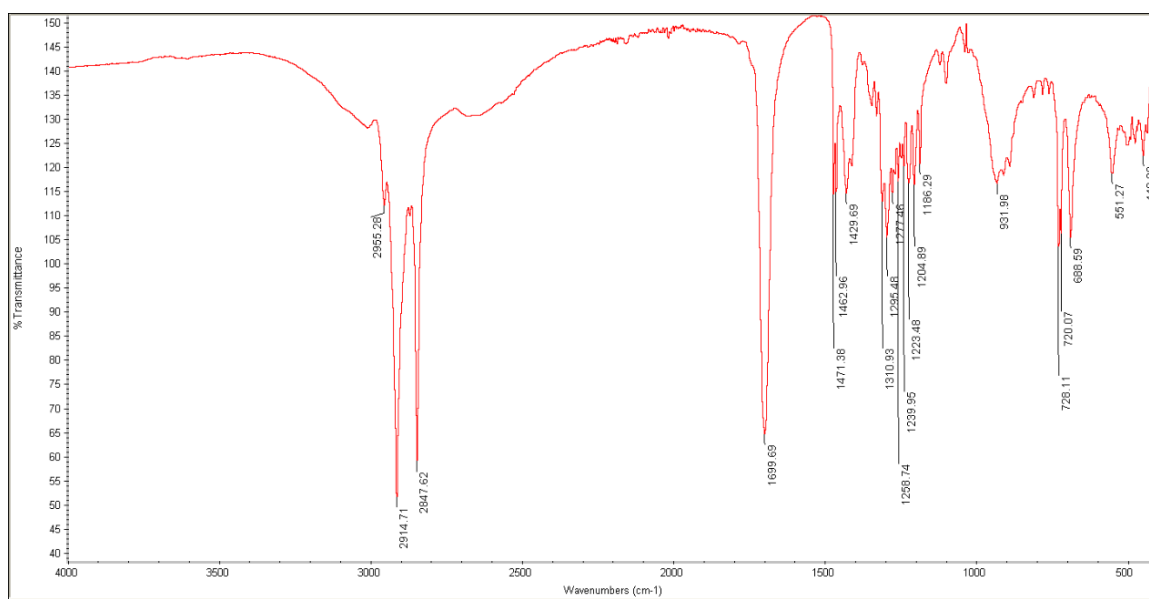
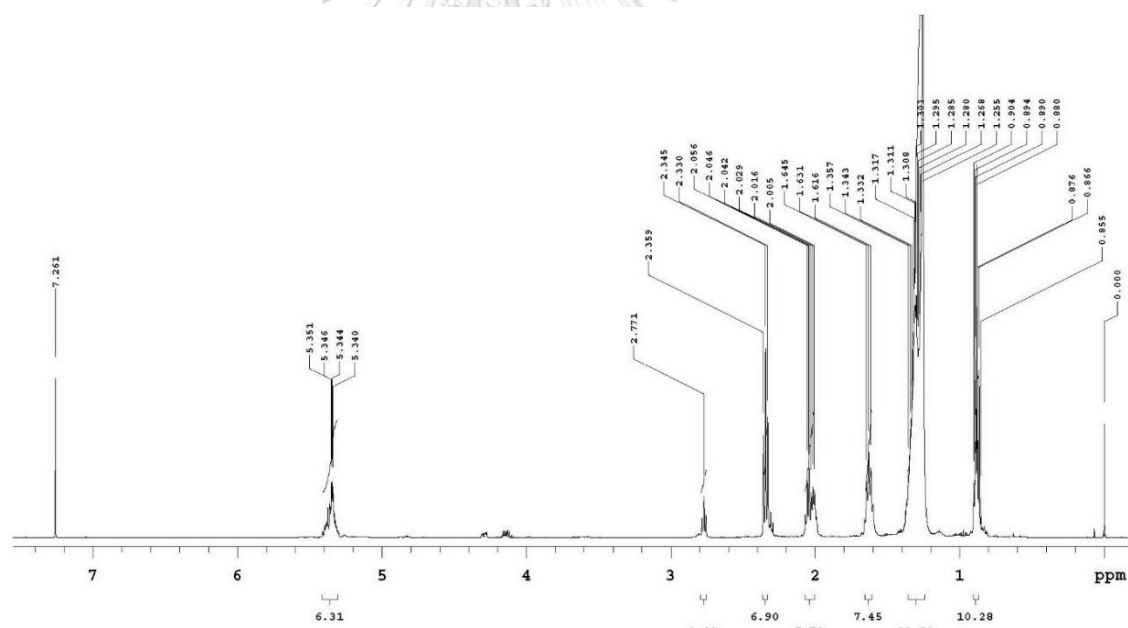


Figure A 23 FTIR spectrum of F3

Figure A 24 ¹H NMR spectrum of F3

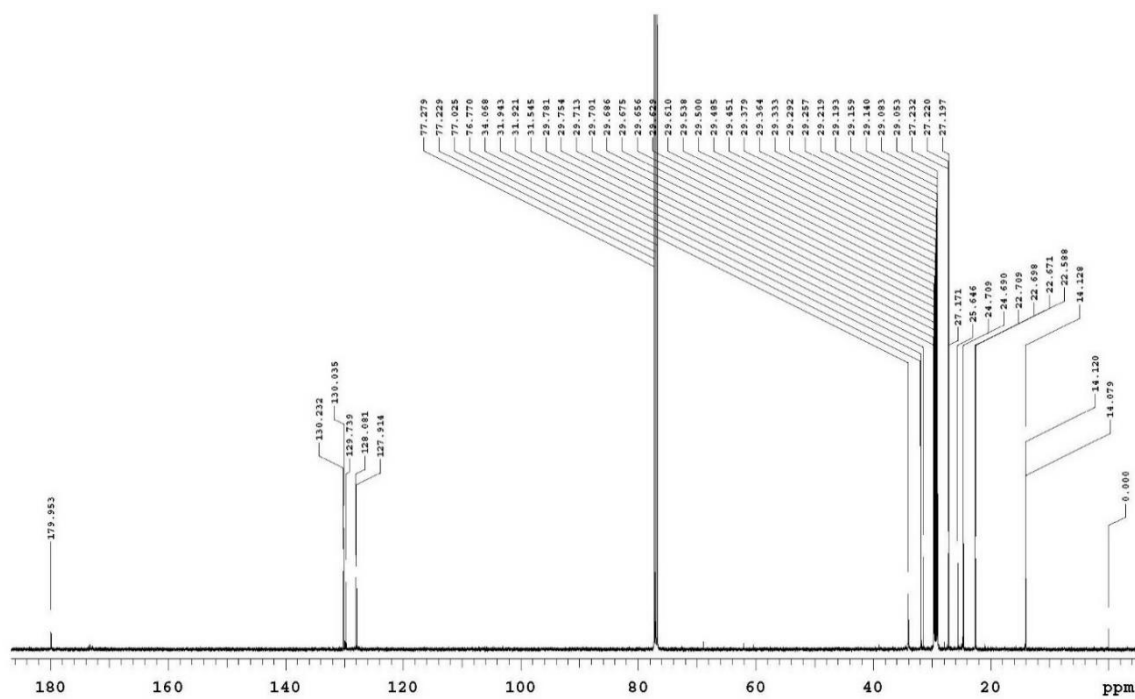
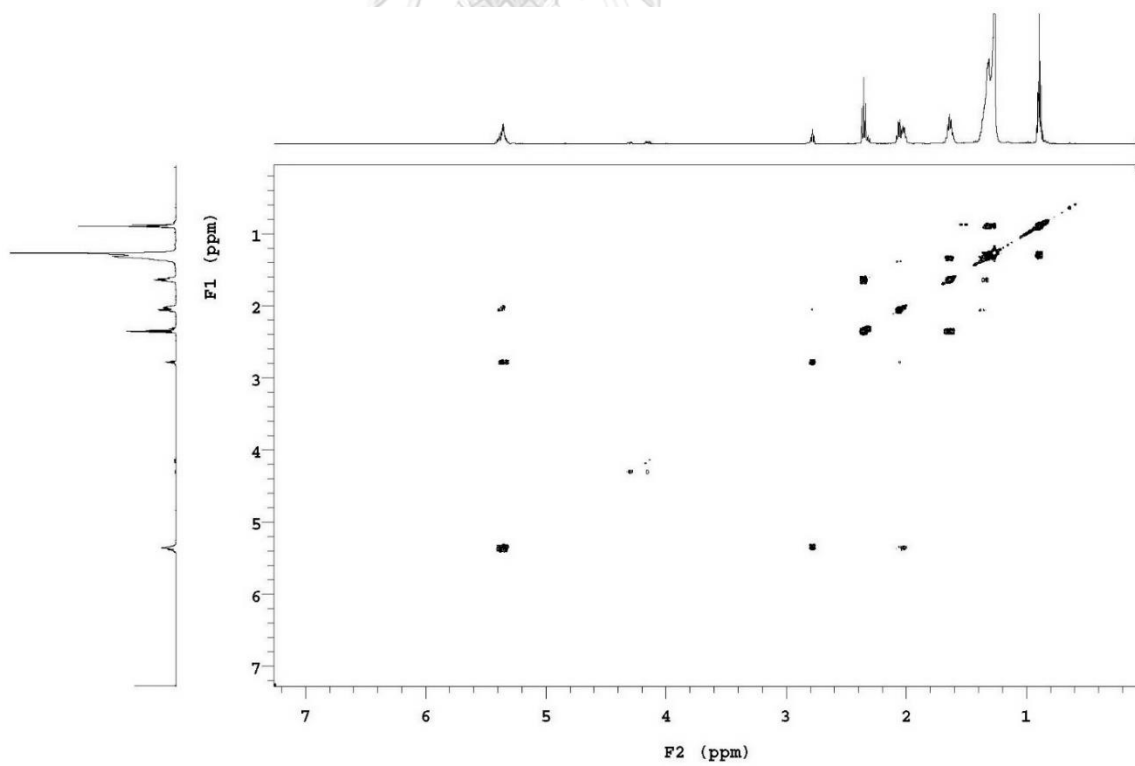
Figure A 25 ^{13}C NMR spectrum of F3

Figure A 26 COSY NMR spectrum of F3

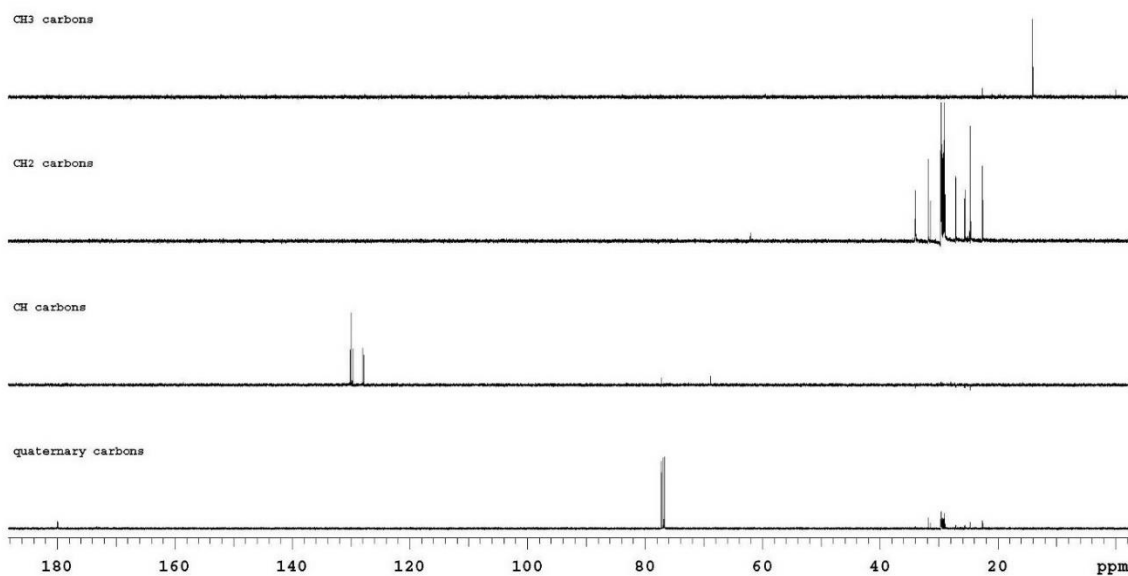
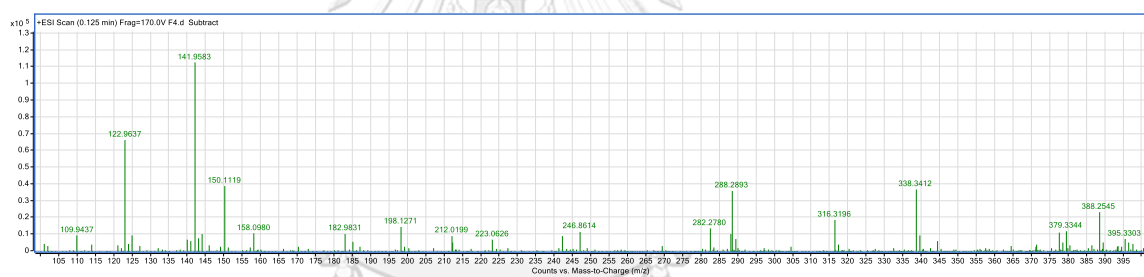


Figure A 27 DEPT NMR spectrum of F3

Figure A 28 Mass spectrum from HRMS analysis of F4 showed m/z 395.3303 [M-H]⁺

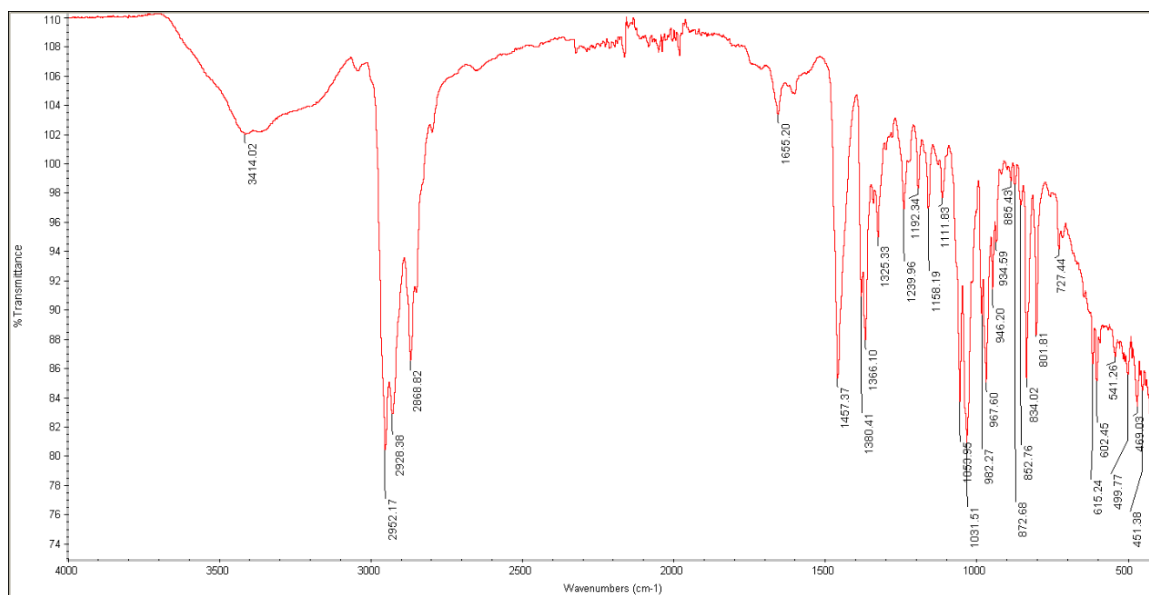
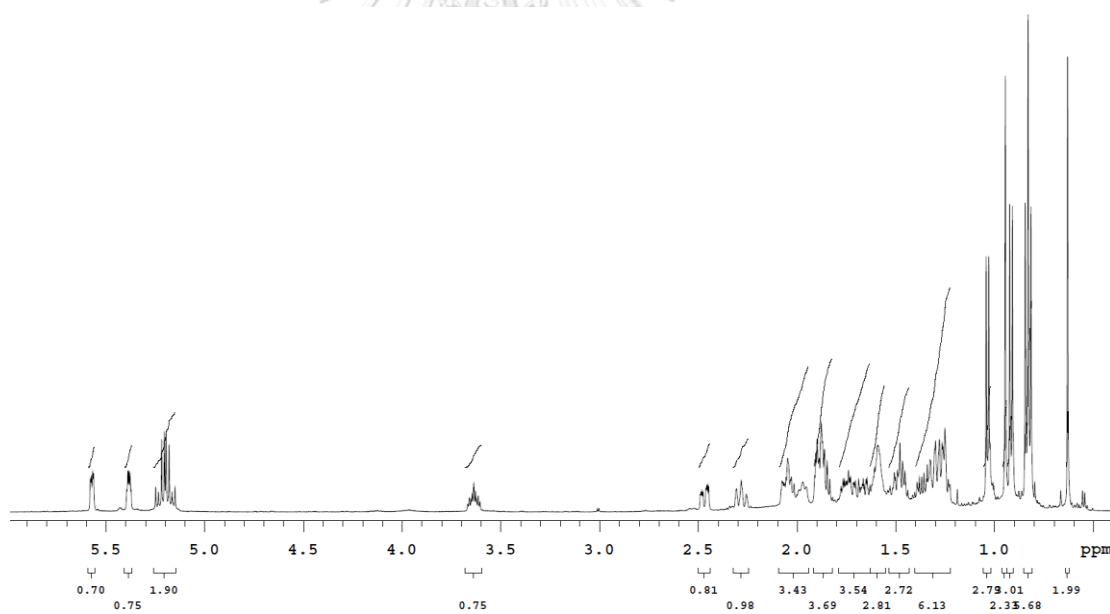


Figure A 29 FTIR spectrum of F4

Figure A 30 ¹H NMR spectrum of F4

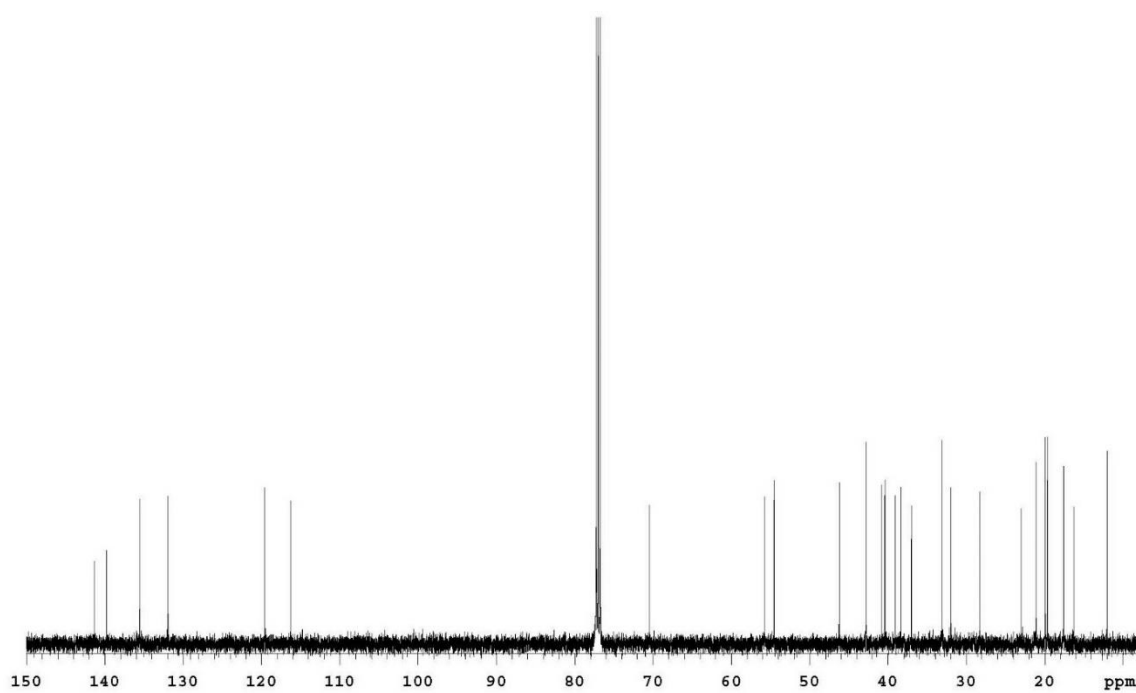
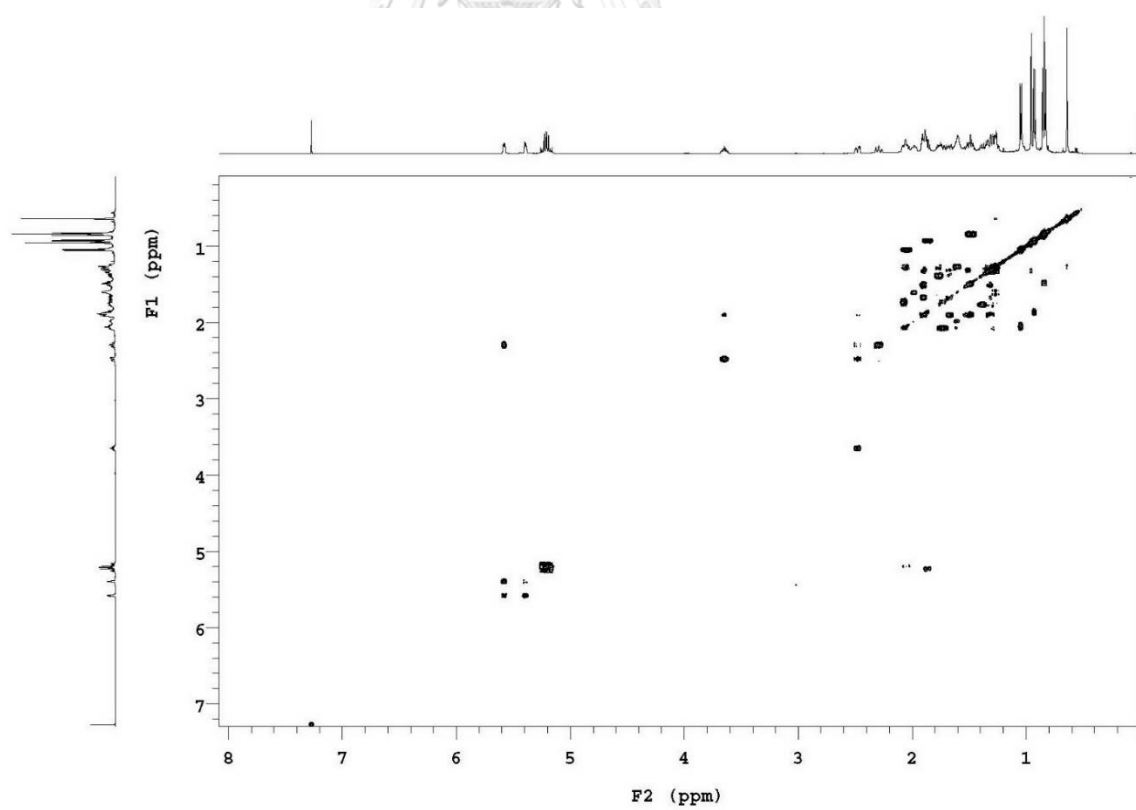
Figure A 31 ^{13}C NMR spectrum of F4

Figure A 32 COSY NMR spectrum of F4

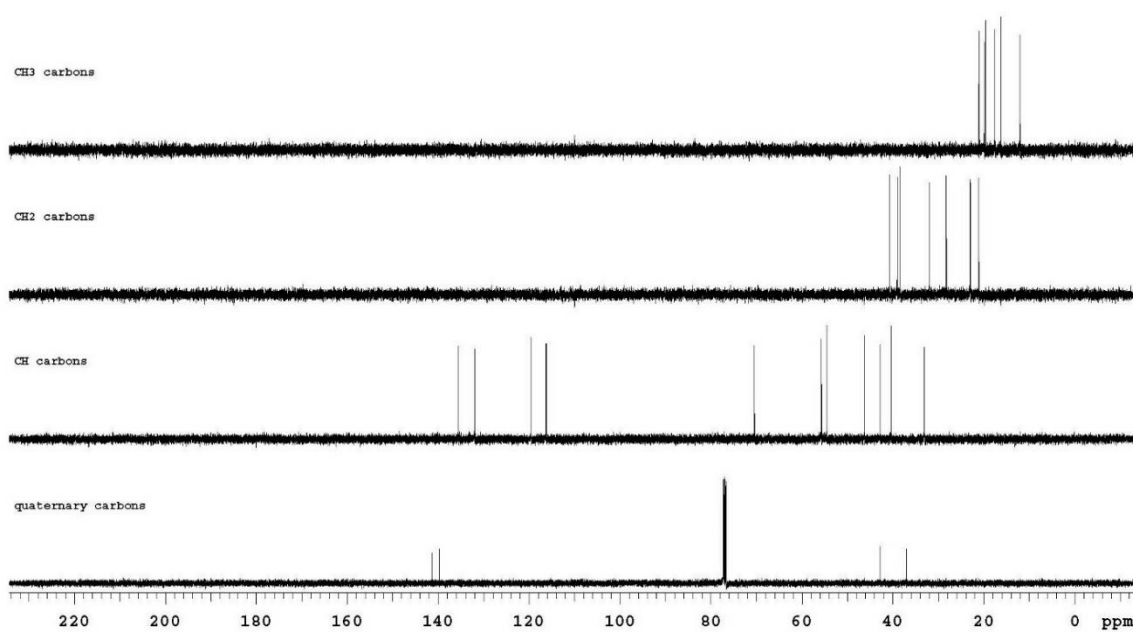
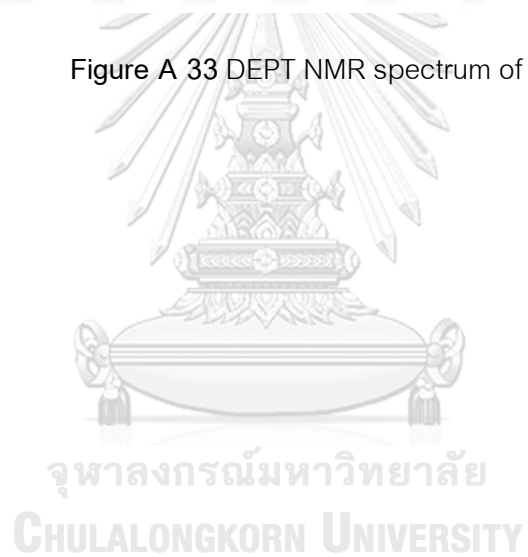


Figure A 33 DEPT NMR spectrum of F4



VITA

NAME Chanin Sillapachaiyaporn

DATE OF BIRTH 11 October 1992

PLACE OF BIRTH Chonburi

INSTITUTIONS ATTENDED 2015 - Bachelor of Sciences (Medical Technology), Second Class Honors
Faculty of Allied Health Sciences, Chulalongkorn University, Bangkok, Thailand

HOME ADDRESS 24 M.2, Samed, Muang Choburi, Chonburi

PUBLICATION Ahmad R, Sahidin I, Taher M, Low C, Noor NM, Sillapachaiyaporn C, Chuchawankul S, Sarachana T, Tencomnao T, Iskandar F, Rajab NF. Polygonumins A, a newly isolated compound from the stem of Polygonum minus Huds with potential medicinal activities. Scientific reports. 2018 Mar 9;8(1):4202.